POLITECNICO DI MILANO

School of Industrial and Information Engineering

Master of Science in Electrical Engineering

OPERATION OF HVDC CONVERTERS CONTROLLED AS VIRTUAL SYNCHRONOUS MACHINES UNDER UNBALANCED CONDITIONS

Supervisor: Prof. Luigi Piegari

Co-supervisor: Prof. Jon Are Suul

Co-supervisor: Dr. Salvatore D'Arco

Tesi di Laurea Magistrale di:

Eros Avdiaj

Matr. 913211

Anno Accademico 2020-2021

INDEX

INDEX 1
FIGURE INDEX 5
TABLE INDEX 9
ABSTRACT 10
ACKNOWLEDGMENT 11
1 INTRODUCTION 12
2 HIGH VOLTAGE DIRECT CURRENT TRANSMISSION 15
2.1 Introduction 15
2.2 Comparison of HVDC transmission over HVAC transmission 16
2.3 HVDC technologies 17
2.3.1. Line Commutated Converter 18
2.3.2. Voltage Source Converter 19
2.3.3. Comparison between LCC and VSC technology 20
2.4 HVDC configurations 22
2.4.1. Monopolar configuration 22
2.4.2. Bipolar configuration 22
2.4.3. Point-to-point configuration 23
2.4.4. Multi-terminal configuration 24
3 CONTROL SYSTEM FOR VSC AS VIRTUAL SYNCHRONOUS MACHINES 25
3.1 Introduction 25
3.2 Overview of the control 26
3.3 VSM inertia emulation 27
3.3.1. VSM swing equation 27

3.3.2. Damping Power and PLL....28
3.3.3. Active Power Droop control....31
3.4 Reactive Power Droop Control....31
3.5 Virtual impedance....33
3.6 Current control....36
3.6.1. Current controller implemented in the synchronous rotating reference frame 37
3.6.2. Current controller implemented in the stationary reference frame....38
3.7 Active damping....39
4 CONTROL STRATEGIES FOR UNBALANCED CONDITIONS....41
4.1 Introduction....41
4.2 Sequence detection and power calculations....42
4.3 Control Strategies for operating under unbalanced conditions....48
4.3.1. Control strategies for Balanced Current....49
4.3.2. Control strategies for Balance Voltage....50
4.3.3. Control strategies for Constant Active or Reactive Power....54
4.3.4. Control strategies for suppressing dc side voltage fluctuations....55
4.4 Power and current limitations....56
4.4.1. When controlling for Constant Active Power:....58
4.4.2. When controlling for Constant Reactive Power:....59
4.4.3. When controlling Balanced Currents:....60
4.4.4. When controlling with negative sequence virtual impedance or negative sequence voltage controller:....62
4.5 Simulation of VSC as VSM under unbalanced conditions....64
4.5.1. Configuration and control....65
4.5.2. Transient response under unbalanced conditions....67
4.5.3. Current and power limitation....72

4.5.4. Reducing the dc side power fluctuations 72
4.5.5. Transient response when islanding under unbalanced conditions 73
4.5.6. Inertial responses upon different perturbations 76
4.6 Conclusion 78
5 OPERATION AND CONTROL OF MODULAR MULTILEVEL CONVERTERS 80
5.1 Introduction 80
5.2 Operation 81
5.2.1. Topology 81
5.2.2. Modulation 83
5.2.3. Balancing 85
5.3 Control 85
5.3.1. Mathematical model 86
5.3.2. Circulating current 89
5.4 Simulations for MMC as VSM under unbalanced conditions 95
5.4.1. Configuration and control 95
5.4.2. The internal dynamic of the MMC controlled as VSM 98
5.4.3. The internal dynamic of the MMC controlled as VSM under grid unbalanced conditions 102
5.4.4. Transient response of the MMC when islanding under an unbalanced local load 105
5.5 Conclusions 108
6 CONCLUSIONS 109
Conclusions and contributions 109
7 REFERENCES 111
APPENDIX 116
Publication 116

FIGURE INDEX

Fig. 1.1. Share of electricity production by source in Europe 12
Fig. 2.1. Comparison between HVDC and HVAC using cost for distance 17
Fig. 2.2. LCC-HVDC convertion station[1] 18
Fig. 2.3. Two-level VSC 20
Fig. 2.4. Single-phase VSC-HVDC Modular Multilevel Converter 1) half-bridge submodule, 2) full-bridge submodule[1] 20
Fig. 2.5. HVDC configurations[1]. 23
Fig. 2.6. Multi-terminal HVDC configuration[49] 24
Fig. 3.1.VSC control scheme for a current controlled VSM. 26
Fig. 3.2.Inertia emulation of the Virtual Synchronous Machine. 28
Fig. 3.3.PLL structure while using the voltage measured across the LC filter capacitor. 29
Fig. 3.4.PLL structure while using the positive sequence voltage. 30
Fig. 3.5. Represent the frequency with respect to time, comparison between the three cases for implementing the damping power. PLL with Vo (──) , PLL with the positive sequence of Vo (──), Filtering wVSM (──) 30
Fig. 3.6 Reactive Power Droop Control 33
Fig. 3.7 Voltage controlled virtual synchronous machine 34
Fig. 3.8 Current controlled virtual synchronous machine 34
Fig. 3.9 VSC configuration 37
Fig. 3.10 PR controller 39
Fig. 4.1. Locus of voltage under unbalanced conditions. 43
Fig. 4.2. SOGI-QSG structure. 45
Fig. 4.3. Dual set of SOGI-QSGs used for sequence separation. 46
Fig. 4.4. Generated currents for controlling balanced three phase currents. 50
Fig. 4.5. Current generation with positive and negative virtual impedance. 51
Fig. 4.6. Generated currents using negative sequence voltage control 53

Fig. 4.7. Representation of the phase current limitation and vector current limitation in the SRF. 57
Fig. 4.8. Unbalanced voltage conditions and apparent power limitation.....63
Fig. 4.9. Flexible selection of control objectives for negative sequence current references. 66
Fig. 4.10. Overview of the CCVSM-based control strategy for unbalanced grid-connected and islanded operation.....66
Fig. 4.11. Simulation results in grid-connected mode showing the transient response to an unbalanced voltage sag occurring at t=0.05 a) Balanced positive sequence currents b) Constant active power c) Constant reactive power, d) Negative sequence virtual impedance e) Negative sequence voltage controller. 68
Fig. 4.12. Comparison of inertial response to an unbalanced voltage sag.....70
Fig. 4.13. Simulation results in grid-connected mode showing the transient response to an unbalanced voltage sag occurring at t=0.05 with 100% of voltage unbalanced factor a) Balanced positive sequence currents b) Constant active power c) Constant reactive power, d) Negative sequence virtual impedance e) Negative sequence voltage controller. 71
Fig. 4.14. Simulation results in grid-connected mode with 100% of voltage unbalanced factor showing the transient when passing from CAP to BPSC control strategy.....72
Fig.4.15. Control strategy results for keeping constant DC power oscillations PDC (──) *Po*(- - -) 73
Fig. 4.16. Simulation results show the transient to sudden islanding occurring at t=0.05 when connected to an unbalanced local load a) Balanced positive sequence currents b) Constant active power c) Constant reactive power, d) Negative sequence virtual impedance e) Negative sequence voltage controller. 75
Fig. 4.17. Comparison of response to the transition from grid-connected operation to islanded mode with an unbalanced load.....76
Fig. 4.18. Comparison of responses under unbalanced voltage conditions to a step: a) increase of 0.3 pu in the power reference at t= 0.1 s b) decrease of 0.1 Hz (=0.002 pu) in the grid frequency at t = 0.1 s.....77
Fig. 4.19. Response to a step increase of the load by 0.1 pu at t=0.1 s under unbalanced conditions.....78

Fig. 5.1. SM topologies, a)half-bridge, b)full-bridge, c)clamp-double, d)three-level FC, e)three-level NPC, f)five-level cross-connected 82
Fig. 5.2. Schematic of MMC 82
Fig. 5.3. Carries for MMC, a)PD, b)POD, c)APOD, d)Saw-tooth, e)phase-shifted carriers [48] 83
Fig. 5.4. Circuit diagram of the MMC 86
Fig. 5.5.Generating dc component of the circulating 92
Fig. 5.6.Generating the first harmonic component of the circulating current 92
Fig. 5.7.Generating the first harmonic component of the circulating current under unbalanced conditions 94
Fig. 5.8.Energy control and circulating current control 94
Fig. 5.9. System configuration with MMC 95
Fig. 5.10. The control structure for MMC controlled as VSM under unbalanced conditions 96
Fig. 5.11. MMC dynamic in a step perturbation from the VSM active power set-point 98
Fig. 5.12. Active power perturbation effect in the energy control, ... 100
Fig. 5.13. Frequency power perturbation effect in the energy control, ... 101
Fig. 5.14. Simulation results of MMC in grid-connected mode showing the transient response to an unbalanced voltage sag occurring at t=0.05 a) Balanced positive sequence currents b) Constant active power c) Constant reactive power, d) Negative sequence virtual impedance e) Negative sequence voltage controller. 102
Fig. 5.15. Simulation results of MMC in grid-connected mode showing the transient response of the arm voltages and circulating current for an unbalanced voltage sag occurring at t=0.05 a) Balanced positive sequence currents b) Constant active power c) Constant reactive power, d) Negative sequence virtual impedance, e) Negative sequence voltage controller. 103
Fig. 5.16.Inertia response for the MMC under unbalanced conditions 104
Fig. 5.17. Islanding operation of a MMC connected with an unbalanced local load a) Balanced positive sequence currents b) Constant active power c) Constant reactive power, d) Negative sequence virtual impedance e) Negative sequence voltage controller. 105
Fig. 5.18.Inertia response for the MMC under unbalanced conditions. 106

Fig. 5.19. MMC dynamic when islanding with an unbalanced local load 107

TABLE INDEX

Table I: Comparison between LCC and VSC.....21
Table II: Parameters of the Investigated System Configuration.....67
Table III: Parameters of the Investigated System Configuration 81
Table IV: Parameters of the MMC System Configuration and Control.....97

ABSTRACT

This thesis presents a comprehensive evaluation of control structures for HVDC converters operating as Virtual Synchronous Machines (VSM) under unbalanced conditions in both grid-connected and islanded mode. The converters taken into considerations are the two-level VSC and MMC. The obtained control for the converters is a Current Controlled VSM where a quasi-stationary virtual impedance emulates a simplified positive sequence electrical model of a synchronous machine. A Negative Sequence Current Generator is defined, which depends on the control objective for the unbalanced conditions, and for the MMC an additional energy control and circulating current controller are used. It is shown how three general strategies can be selected for controlling the negative sequence currents: i) calculation of the negative sequence current references according to the desired active and reactive power flow characteristics, ii) applying a negative sequence virtual impedance resulting in unbalanced currents as in the steady-state response of a synchronous machine, or iii) operation with a negative sequence voltage controller for eliminating unbalances in the locally measured voltages. For the first approach, four objectives for shaping the power flow characteristics can be selected: i) balanced three-phase currents, ii) constant instantaneous active power flow, iii) constant instantaneous reactive power flow, or iv) reduction of dc side voltage fluctuations. Comprehensive simulation results are presented to evaluate the performance and applicability under grid connected and islanded operation. The results demonstrate how utilization of the negative sequence currents to control the power flow characteristics is only applicable for grid connected operation, while the other two approaches can be utilized in both islanded and grid-connected modes. However, closed loop control for balancing the local voltages depends on a high equivalent grid impedance and is not suitable for operation in strong grid conditions.

ACKNOWLEDGMENT

This master thesis is the output of my internship at Sintef Energy Trondheim (Norway). And, it was supported by the project “HVDC Inertia Provision” (HVDC Pro), coordinated by Jon Are Suul (Sintef Energy), financed by the ENERGIX program of the Research Council of Norway (RCN) with project number 268053/E2, and the industry partners; Statnett, Statoil, RTE and ELIA.

This work would not be possible without the opportunity provided by Prof. Luigi Piegari and his collaboration with Prof. Jon Are Suul and Dr. Salvatore D’Arco. I want to praise these men for their dedication, and thank them for their encouragement, motivation and support.

I want to give a special thanks to Bendik Torp Hansen and Lennart Schönfelder, that were like my family during the Covid-19 Global pandemic.

Last but not least I would like to thank my grandmother, my parents, my sister Ana Avdiaj who is like a catalyzer for my endeavors, and my girlfriend Enxhi Qyra. Thank you for believing in me and help me to be the best man I can be.

1 INTRODUCTION

Electric power quality for today's society is a merit good. As such to be produced and distributed as effectively and efficiently as possible is of paramount importance. The production of clean energy is vital for the climate situation. Public and private entities have been taking actions such as decommissioning coal power plans and innovating for sustainable solutions. And for this reason, in the last years, a surge in renewable energies has been experienced. In *Fig. 1.1* is shown the share of electricity production by source in Europe and, more than 35% is produced by renewable resources from which more than 15% is produced by wind and solar technologies. There is a 400% increase in wind and solar energy production share from 2010. This increase has started to drive the market which has reduced the cost of power generation for these sources. Thus providing space for further prosperity for renewables.

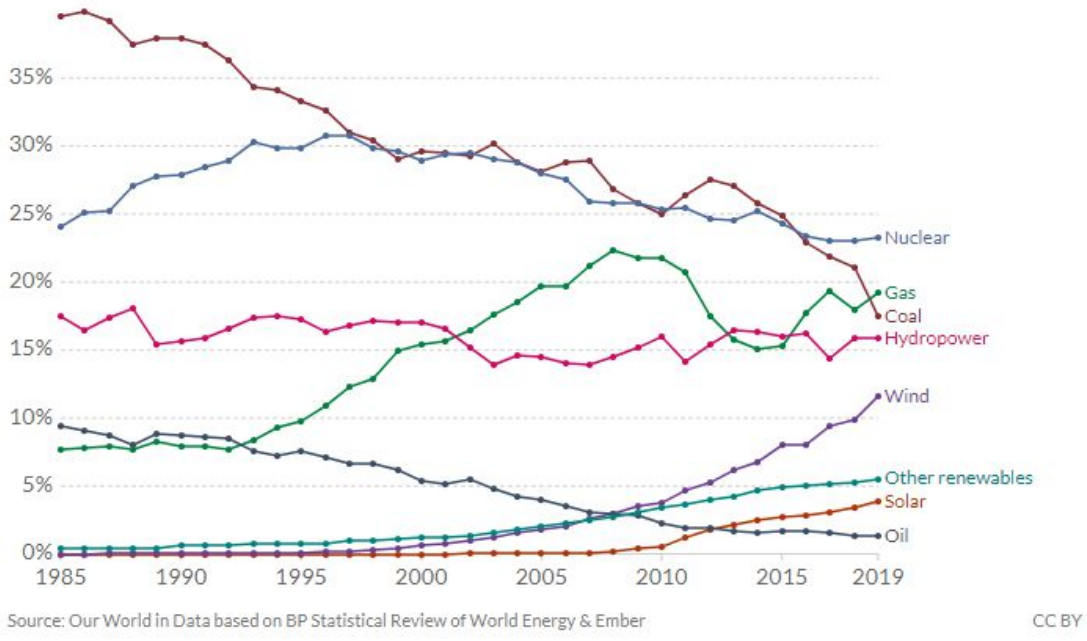

Fig. 1.1. Share of electricity production by source in Europe

Power converters are the technologies that allow efficient and flexible interconnection between the renewables and power systems. The static power electronic converters used in HVDC (High Voltage Direct Current) links allow bulk power transmission over long distances with low losses. The diffusion of power converters into the power systems makes them decisive for a stable and reliable system. Therefore, operation under adverse conditions such as unbalanced conditions should be insured for these converters.

A further concern that is related to the grid stability is the decrease in the rotating masses. As previously mentioned, the decarbonization actions reduced the number of coal power plants with their rotating generators. The place of these big synchronous generators in the new electrical grid is taken by the static electronic converters which do not have any inertia as the former. Thus reducing the total rotating inertia of the grid. The frequency in the grid is stabilized by this inertia, therefore reducing the rotating inertia brings reduced frequency stability which has a big impact on the other variables of the grid. To solve this problem, solutions are presented by controlling the power electronic converters not just to transfer power, but control them in such a way that provide virtual inertia (also known as synthetic inertia). This can be realized using frequency-derivative-based inertia emulation by grid following control. The drawback if this control is the need to be connected all the time with the grid. Another approach to solve this problem is by using grid forming control. For such control the converter behaves like a generator. Virtual Synchronous Machines also known as Virtual Synchronous Generators are the most diffused grid forming control approaches with virtual inertia.

In this thesis are considered HVDC converters that are controlled as Virtual Synchronous Machines which can operate and control the grid under balanced condition and also under unbalanced condition. The unbalanced condition may be related to unbalanced three phase local load or unbalanced grid. Furthermore, operation in islanded mode is considered.

Firstly, the main characteristics of HVDC transmission are highlighted and its advantages and disadvantages are compared to HVAC transmission. In the first chapter are also shown the HVDC configurations and topologies. Moreover, explanations are given for the main technologies such as Line Commutated Converters and Voltage Source Converters.

Where the Voltage Source Converter has the ability to control voltage magnitude and angles and for this reason is chosen to be used as a Virtual Synchronous Generator.

In the second chapter is shown how to control the two-level Voltage Source Converters so that they can behave as the Virtual Synchronous Generators. Details are given how the synthetic inertia is provided and how additional functions such as the Governor or the Automatic Voltage Regulator are modeled. Additionally, two different current controllers are considered, one of which allows the converter to work under unbalanced conditions.

As previously mentioned insuring operation under unbalanced condition is important therefore in the 3rd chapter are shown the changes made to the control so that the Virtual Synchronous Machine can operate properly. Furthermore, strategies are considered to control unbalanced conditions. The proposed strategies that control the power flow are, balanced three phase currents, constant active power, constant reactive power, and the strategies to reduce the unbalanced voltages are, negative virtual impedance, negative sequence voltage control. In addition, for this strategies, power limitations are derived so that the converter current does not surpass the threshold. To guarantee the effectiveness of these control strategies, simulations are done using MatLab/Simulink. Some of this results are presented in the 9th ICRERA conference, Glasgow, UK [50]. This publication can be find in the appendix of this thesis.

For high voltages and high powers applications, the best-suited technology is the Modular Multilevel Converter. In this thesis is shown how to operate and control this converter. And is shown how its control structure will adapt if the converter has to behave as a Virtual Synchronous Generator and ensure operation under unbalanced conditions. To validate the control structure and to explain the internal dynamic of the Modular Multilevel Converter simulations with different scenarios are done via MatLab/Simulink.

2 HIGH VOLTAGE DIRECT CURRENT TRANSMISSION

2.1 Introduction

High Voltage Direct Current (HVDC) Transmission is an alternative way of transmitting electrical energy with respect to the most well-known Alternating Current (AC) Transmission. HVDC systems in certain situations have different economical and technical advantages over the AC ones. HVDC is one of the best transmission solutions for bulk power transfer over long distances. Hence in the last decades, the Direct Current Transmission has started to spread out at a fast pace. The HVDC links play a key role in future advancement plans for the European transmission grid [1].

Several inherent capabilities with the HVDC technology provide auxiliary services, from which the power system can benefit. The use of these capabilities contributes to meeting the current and future challenges, for example, decarbonization and the large-scale penetration of Renewable Energy which is largely implemented through Power Electronic interfaces. Some typical applications for HVDC transmission are bulk power delivery in long distances, the connection of asynchronous ac system or systems with different frequencies, submarine power transmission, ancillary services, Ultra-High voltage dc links, etc. The following sections compare HVDC and HVAC transmissions and also discuss the technologies and configuration used for HVDC.

2.2 Comparison of HVDC transmission over HVAC transmission

Advantages that HVDC transmission has over HVAC transmission [2].

1. With the same conductor size and insulation level, the dc lines transfer a higher power compared to ac lines. In dc transmission the effective voltage and conductor diameter can be higher. In ac, the conductor diameter is limited due to skin effect.
2. There are lower power losses in dc transmission.
3. For overhead lines, the required ground area and support towers are smaller in HVDC. This happens because for the same power transfer HVDC transmission uses smaller cable sizes.
4. There is no need for reactive power compensation for power transmission purposes. HVDC power can be transferred over long distances with constant voltage. When using long ac lines there will be high voltage drops from the reactance of the line, thus compensating devices such as SVCs (static VAR compensators) or STATCOMs (static synchronous compensators) are required to maintain the ac voltage level. This increases the cost of HVAC over long distances.
5. HVDC allows connections between asynchronous ac grids.
6. System operations can actively control the power flow. This is because of the way that HVDC connections can quickly control the transmitted power. This might be challenging from an operational perspective, nevertheless, it will allow the system operator to utilize the existing ac system more efficiently.

Disadvantages of HVDC transmission over HVAC transmission.

1. Transformers and circuit breakers for HVAC are less complex and less expensive than HVDC. There is no zero-crossing on the current thus the dc circuit breakers have a complex design, especially at high power levels.

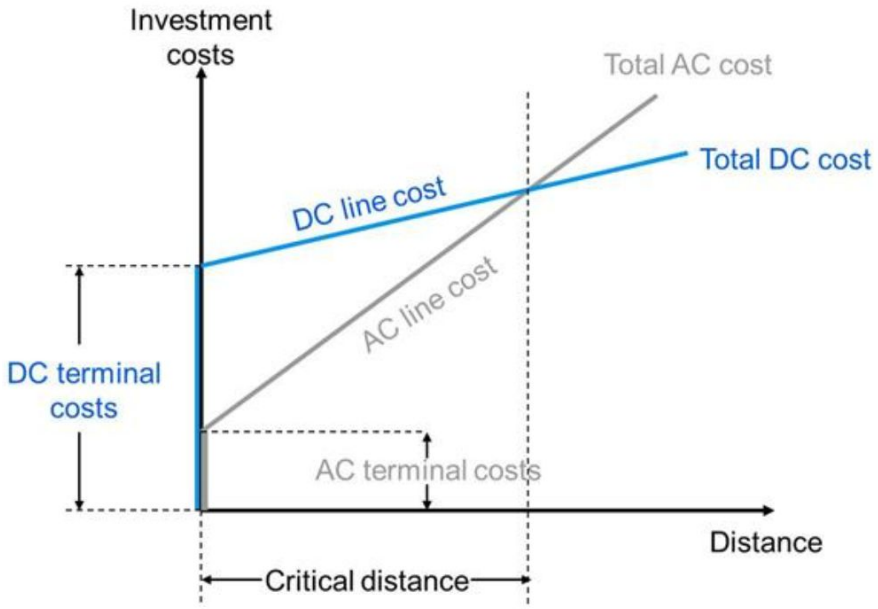

Fig. 2.1. Comparison between HVDC and HVAC using cost for distance

2. HVDC terminals have a higher cost of construction with respect to HVAC due to the power electronics and converter transformers.

This comparison helps us understand that the best solution for power transmission is strongly related to the type of project implemented. Taking into consideration the transmission distance and the initial start-up cost of the project is obtained the graph as shown in *Fig. 2.1*. From this graph can be seen that the terminal cost for dc is higher but the ratio cost/distance is higher for ac transmission. Therefore, there is a critical distance called the break-even distance, from this point on utilizing the dc transmission is a cost-effective solution [3].

2.3 HVDC technologies

Power electronic technology has increased rapidly over the last decades and this created the opportunity to have different types of HVDC technologies. Line- Commutated Converter for HVDC is used for more than 50 years for Bulk power transfer and has the highest power and efficiency ratings [9]. Voltage Source Converters were first commissioned for HVDC systems in 1997 with a voltage of ±10 kV and a transmission

capacity of 3 MW. Nowadays, operation with voltages above ±500 kV and 2 GW are feasible, but there has been no operating experience with them [10]. The development of Modular Multilevel Converter technology for HVDC transmission started with the need to reduce the switching losses and power, and improve the converter ac side voltage waveform to lower the filter requirements that are present in a two-level Voltage Source Converter.

2.3.1. Line Commutated Converter

Line Commutated Converter (LCC) is used mostly for the transmission of bulk power using high voltage transmission lines. LCC uses thyristor-based technology. The thyristor is a solid-state semiconductor device that turns on in a determined time instant by a gate signal and it will conduct until the thyristor is reversed in polarity and current. The breakdown voltage of the thyristors is a few kV thus to use it in HVDC applications several series-connected thyristors are needed. The AC/DC conversion is performed in the rectifier units and the DC/AC conversion is performed in the inverter units. Typically, each unit has a 12-pulse arrangement consisting of two 6-pulse thyristor bridges. The transformer for a 12-pulse bridge has a star-star-delta three-winding configuration and typically has a leakage reactance to limit the current during a short-circuit fault of the bridge arm.

The LCC technology as a line-commutated thyristor valve converter which relies on a stable AC system for a reliable commutation. If the converter unit is located in a weak ac

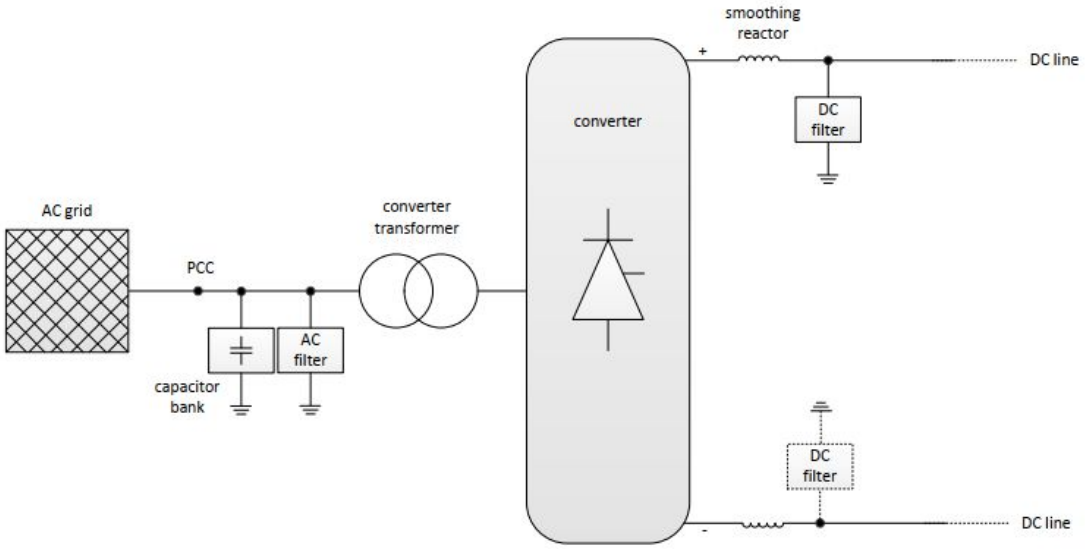

Fig. 2.2. LCC-HVDC convertion station[1]

grid it may be needed to install Synchronous Condensers to increase the short circuit level, a typical short circuit ratio (SCR) is SCR>2-3. LCC-HVDC link has a high reactive power demand that varies with the DC power. Typically, the required reactive power is up to 60% of the dc power rating and is provided by filter banks, capacitor banks, or static converters such as STATCOM or SVC.

2.3.2. Voltage Source Converter

Voltage Source Converter (VSC) is an transistor-based technology where for high power HVDC application is mostly used IGBT(Isolated Gate Bipolar Transistor). The IGBT capability of turning on and off allows the generation of the ac side voltage with a specific amplitude and phase angle. These parameters are derived by the set-points provided to the control by the system operator. Since the voltage magnitudes and angles can be controlled separately, the active and reactive power can be controlled separately as well. VSC-HVDC systems can be easily connected with a weak grid and even energize a dead network. Energizing a dead network is also known as black-start [11]. This is a strong point of VSCs therefore it makes them very suitable for distributed energy resources such as photovoltaic power stations or wind power plans.

VSCs usually have been based on two-level or three-level converters which provide switching respectively with two or three different voltage levels to the ac side. Therefore, the ac side voltage has high harmonic content, that is why an LC or LCL filter is used between the converter and the grid. A two-level VSC is represented in *Fig. 2.3*.

The newest generation of converters applies a modular concept which increases the arbitrary number of voltage levels which leads to reduced losses and improved harmonic content. This modular concept with many series connected submodules (mostly half-bridge or full-bridge modules) in each arm *Fig. 2.4*, enables the generation of an almost perfect sinusoidal voltage on the ac side of the converter. The modular concept is known as Modular Multilevel Converter (MMC) and more about it is discussed in the fourth chapter of this thesis.

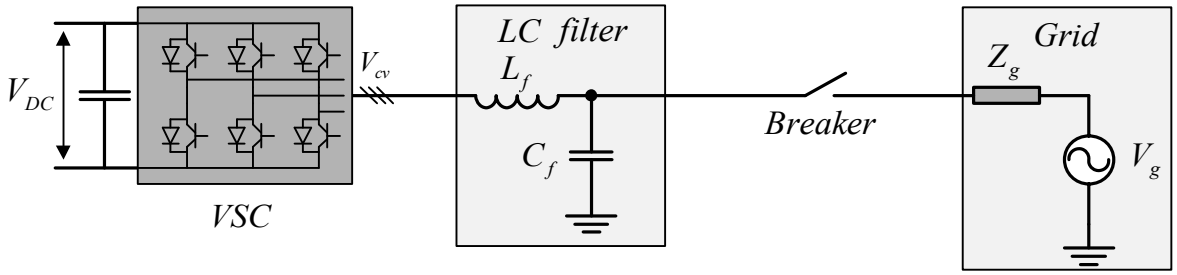

Fig. 2.3. Two-level VSC

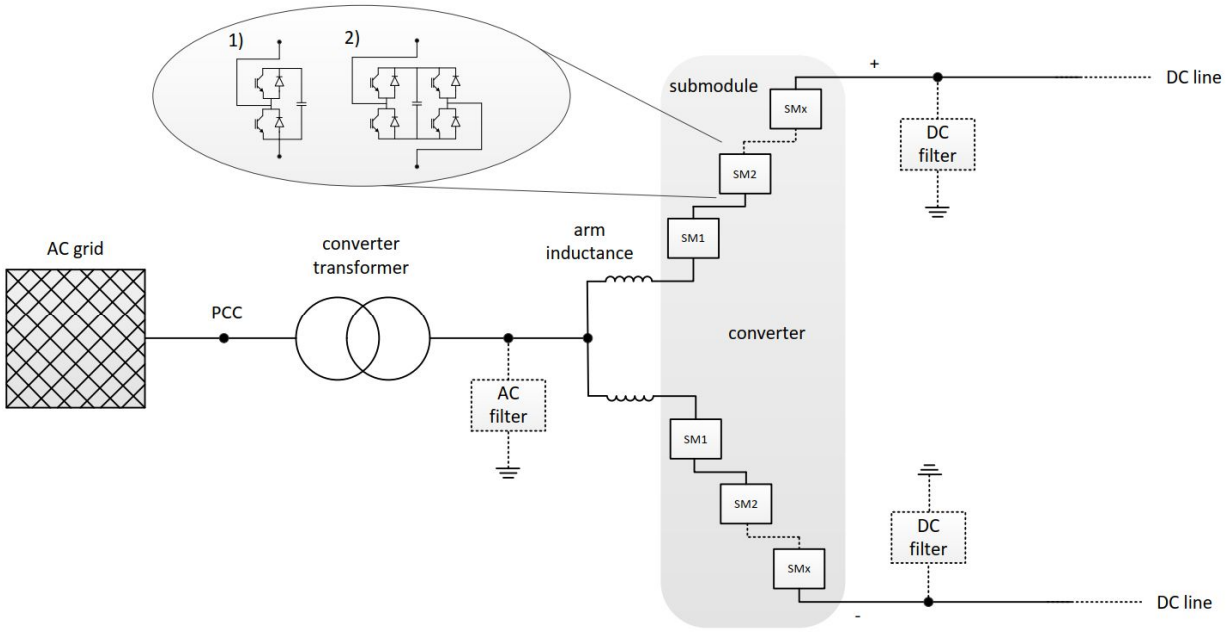

Fig. 2.4. Single-phase VSC-HVDC Modular Multilevel Converter 1) half-bridge submodule, 2) full-bridge submodule[1]

2.3.3. Comparison between LCC and VSC technology

In [1] is extracted a comparison between LLC and VSC technologies used in HVDC. Their similarities and differences are shown in Table I.

Table I: Comparison between LCC and VSC

LCC	VSC
Thyristor-based technology	IGBT-based technology
The semiconductor can withstand voltage in either polarity	Can withstand current in either direction
Constant current direction (power reversal by changing voltage polarity)	Current direction changes with power
Energy is stored inductively	Capacitive energy storage
Turned on by a gate pulse but relies on an external circuit for its turn off	Both turn on and off are carried out without the help of an external circuit
High power capability per converter	Lower power capability per converter
Strong overload capability	Weak overload capability
Requires stronger AC systems for excellent performance	Operates well in weak AC systems
Requires additional equipment for black start operation such as a synchronous condenser	Possesses black start capability
Requires AC and DC harmonic filters for removal of distortion and harmonics	Requires no filters because it generates an insignificant level of harmonics (MMC)
Limited in reactive power control (filters may be needed for operation)	Good reactive power control
Large site area, dominated by harmonic filters	A more compact site area
Requires converter transformer	A conventional transformer is used
Lower station losses (approx. 0.7%)	Higher station losses (approx. 1%)
More mature long-existing technology	Technology still relatively new
Higher voltage capability of over 1000 kV	Lower voltage capability of around 600 kV
The inverter side suffers commutation failures (active power = 0 for a few hundred ms) as a result of a sudden drop in the amplitude or phase shift in the AC voltage, which results in a temporal DC overcurrent This happens even if the voltage drop is small, and even if it occurs on one phase, and therefore also occurs as a result of AC single-phase faults far from the HVDC. The commutation failure could be a significant problem for the AC system when the transmitted DC power is very high compared to the total demand of the interconnected AC networks	Ability to be turned on as well as off, makes it immune to any voltage dips or transient AC disturbances; therefore, it does not suffer commutation failures
A low number of LCC in multi-terminal systems	A high number of VSC in a multi-terminal system possible (needs to be investigated)
During short circuits on the DC line, control of the firing angle of the thyristor valves stops the increase of the DC fault current. This converter control prevents the damage caused by the fault current. During overhead line faults, power transmission is stopped for arc deionization, after which power transmission is resumed. This is not a critical point	Continuous conduction in the diode of half bridge submodules will cause an increase in DC fault current even when the IGBTs are turned off. The AC circuit breakers at both ends must be opened to stop the diode conduction. The HVDC link must be restarted after the fault has been removed. This is a critical point
Need for minimum active power transmission	No need for minimum active power transmission
Need for short circuit power	Short circuit power during normal operation and/or in STATCOM operation and/or in black start operation may be required
Power reversal is critical	Power reversal is not critical

2.4 HVDC configurations

HVDC transmission systems have many different configuration topologies. They can be monopolar, bipolar. And depending on the number of converters they can be point-to-point which are back-to-back or long distances, and multi-terminal. The configuration will depend on operational requirements.

2.4.1. Monopolar configuration

The monopolar configuration can be symmetric or asymmetric. In the case of a monopolar asymmetric HVDC configuration, two converters are connected by a high-voltage cable. Depending on the case, for returning the current, a metallic low-voltage conductor line Fig. 2.5. c), or earth/sea return Fig. 2.5. d) can be used. In the recent schemes, using earth as a return conductor is becoming less common because of the environmental impact.

As for the symmetrical HVDC monopolar configuration Fig. 2.5. e), the dc side of the converter has two high-voltage cables with opposite polarity. This means that the voltage difference between the cables is twice as high as before. In case there is a failure in one of the conductors this configuration does not allow for earth returning. The monopolar symmetric configuration has a higher cost with respect to the asymmetrical configuration nevertheless the symmetrical configuration is the most used in VSC-HVDC systems.

2.4.2. Bipolar configuration

The most common configuration is bipolar configuration, with two independent poles (one positive and the other negative), which are normally balanced with no ground current. The configuration with ground electrodes is known as rigid bipole and is shown in Fig. 2.5. b). In case of fault for one of the cables, it will continue operating, using the ground as a returning path. The operation, in this case, is in monopolar-mode which allows 50% of

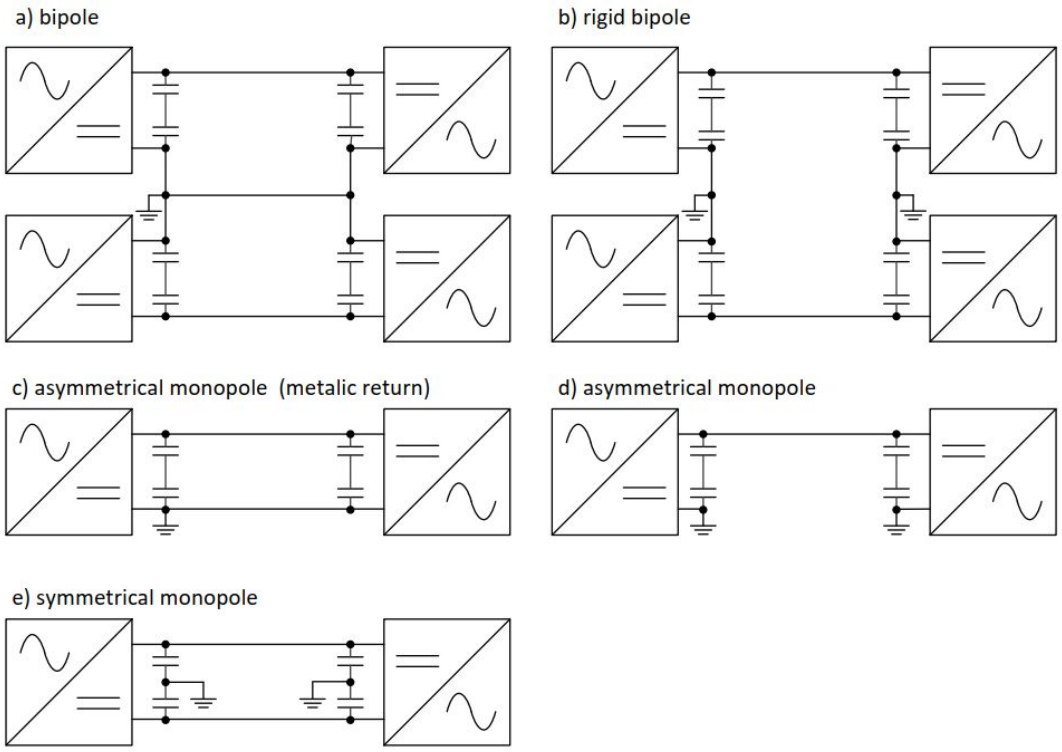

Fig. 2.5. HVDC configurations[1].

the transmission capabilities of the initial bipolar configuration. In some grid code regulations, using the ground as a return path is not allowed due to environmental impact. In this situation, a metallic return is used, although more expensive is becoming more and more common. In some cases, is possible to change the configuration from bipolar operation with no ground return to monopole operation using one of the cables as a ground return.

2.4.3. Point-to-point configuration

The simplest configuration is a *back-to-back* interconnection where two converters are in the same place with a short direct-current line or even without one. This is mainly used to interconnect lines with different frequencies or asynchronous line ac systems. As the cost of HVDC components is voltage-dependent and there is no need for dc cables, the currents usually are high while the voltages are kept low [4]. One of the advantages of this

configuration is the increasing stability of the grid which is achieved by interconnecting two asynchronous ac systems [5].

Long-distance interconnections are considered when two converters are connected by submarine, ground cables, or overhead lines. In this situation, the losses in the conductor considerable hence higher voltages are used for these types of interconnections.

2.4.4. Multi-terminal configuration

In multi-terminal HVDC (MTDC) more than two sets of converters operate independently. Each converter can operate either as a rectifier or an inverter. Using MTDC technology, multiple generators and ac grids can be connected as shown in Fig. 2.6. For MTDC, IGBT-based technologies are more suitable than thyristor-based technologies since IGBT-based technologies can change the direction of the power flow without changing the polarity of the dc voltage. Recent consideration of countries with real possibilities of building MTDC networks for large offshore windfarms and inter-regional dc grids has encouraged serious research and development efforts from manufacturers and academia[6] [7][8]. Studies have been carried out on dc switchgear, dc faults and protections, system responses during the loss of converters, and circuit topologies.

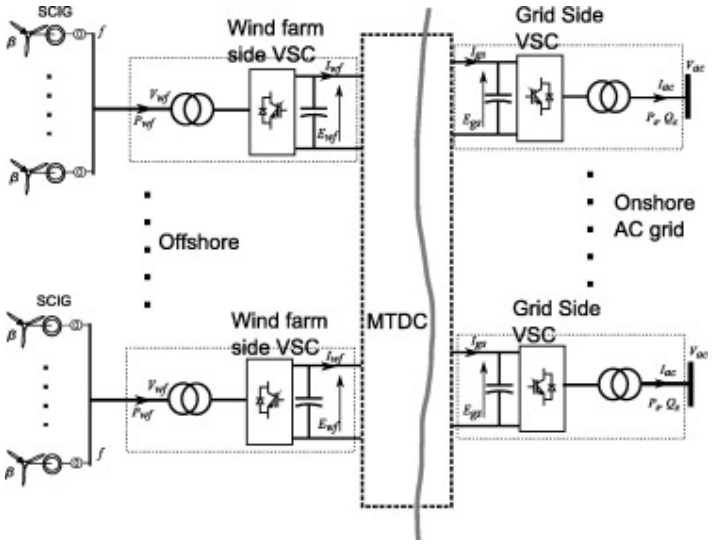

Fig. 2.6. Multi-terminal HVDC configuration[49]

3 CONTROL SYSTEM FOR VSC AS VIRTUAL SYNCHRONOUS MACHINES

3.1 Introduction

The usual strategies for VSC control try to provide a cos(φ)=1 hence providing active power transfer. By doing this they are seen as constant power and do not give any response to the grid frequency changes. As a consequence, they reduce the total inertia of the grid. If we consider a control that models the behavior of the Synchronous Machine in the grid then we increase the total inertia and the frequency regulation capabilities of the grid.

The Virtual Synchronous Machine (VSM) concept allows the converters to operate both in grid connections and islanded conditions. The inherent inertial characteristic of the VSM can provide services as frequency support and sharing of the transient power as primary control actions but it can also offer grid forming capabilities. These control strategies don't reduce the ability of the converter to operate in structures where the external references and set-points are provided by a centralized controller for optimizing the grid operation. A further advantage of VSMs approach lies in the fact that based on the physical machine, it gives an intuitive interpretation of its behavior.

Usage of the swing equation of SMs allows the modeling of inertial response and damping
that these machines have. Considering these characteristics, several control strategies have been developed to permit power electronic converters to provide synthetic or virtual inertia to the power system. Nevertheless, emulation of the inertia and damping effects requires an energy buffer that has sufficient capacity to represent the energy storage effect of the emulated rotating inertia available. Thus, the amount of virtual inertia that can be added to

the system by a single VSM unit will be limited both by the DC-side configuration and the current ratings of the converter.

3.2 **Overview of the control**

The system starts with the DC link capacitor as shown in the right of Fig. 3.1, whose voltage is fed to the DC side of VSC which is connected to the grid. Between the grid and the converter, an LC filter is implemented in order to remove the high harmonics produced by the converter.

As previously mentioned to control the converter, a VSM model is implemented. To do so there are two loops the inner and outer. The inner is the current loop which is the fastest. The outer loop gives the voltage as magnitude and angle respectively by the Reactive power controller and VSM inertia emulation. A Phase Lock Loop (PLL) is used to detect the actual frequency of the grid w_g. This last one helps the swing equation of the VSM inertia emulation to implement the damping term.

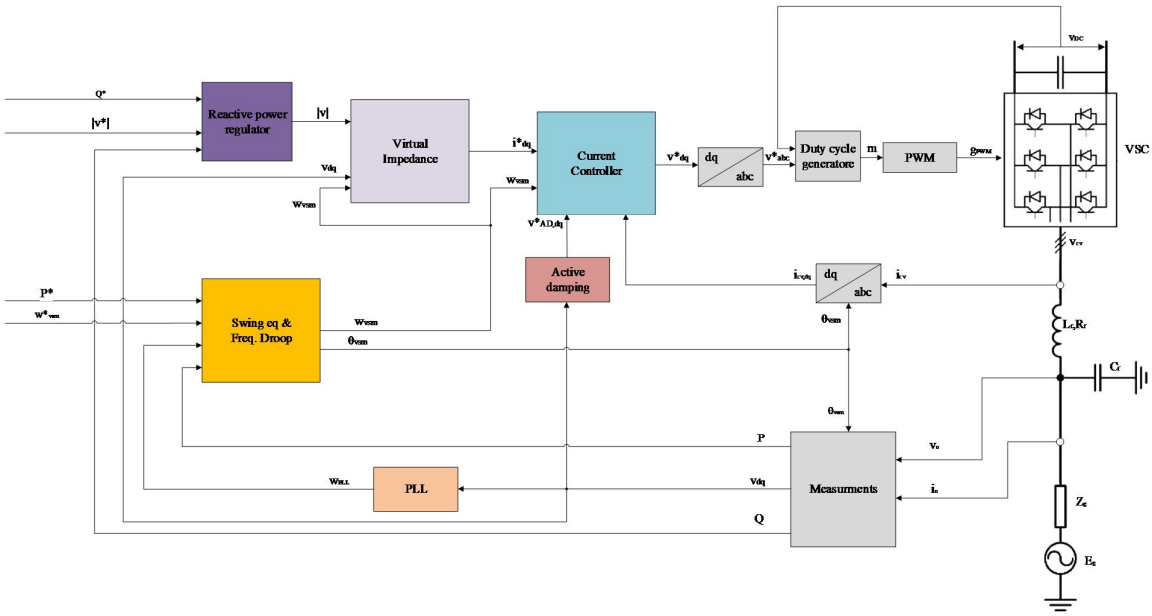

Fig. 3.1.VSC control scheme for a current controlled VSM.

The most common strategy to realize this control is the decoupled dq-vector control. This approach utilizes a linear PI controller and Pulse Width Modulation to control the VSC's switches.

3.3 VSM inertia emulation

The emulation of rotating inertia and the power-balance based synchronization mechanisms of this virtual inertia is the main difference between the considered VSM control structure and conventional control systems for VSCs. The VSM implementation is based on a conventional swing equation 3.3.1, where is considered also the damping of the traditional SMs and the frequency droop.

$$2H\frac{d\omega}{dt} = Tm - Tel \qquad 3.3.1$$

3.3.1. VSM swing equation

For this thesis is used equation 3.3.2 as presented in [12] and with a block diagram as shown in Fig. 3.2.

$$Ta\frac{d\omega_{vsm}}{dt} = p^{r*} - p - p_d \qquad 3.3.2$$

$$p_d = k_d(\omega_{vsm} - \omega_{grid}) \qquad 3.3.3$$

$$p^{r*} = p^* + k_w(\omega^*_{vsm} - \omega_{vsm}) \qquad 3.3.4$$

Where p^{r*} is the virtual input power that comes from the output of frequency droop, p is the measured electrical active power flowing from the VSC into the grid, and p_d is the damping power. While the mechanical time constant is defined as Ta (corresponding to 2H in a traditional SM). The p.u speed ω_{vsm} is then given by the integral of the power balance while the corresponding angle is given by the integral of the speed.

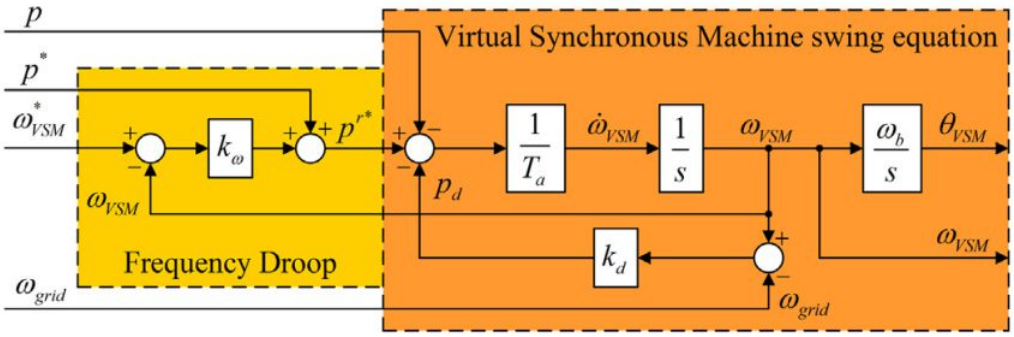

Fig. 3.2.Inertia emulation of the Virtual Synchronous Machine.

3.3.2. Damping Power and PLL

The damping power is defined by the damping coefficient k_d and the difference between ω_{vsm} and ω_{grid} (eq. 3.3.3). The grid frequency is unknown for our control, but a similar frequency can be considered. There are different methods to find this frequency.

In this part, we take into consideration 3 methods. Finding ω by:

- using a PLL with the measurement Vo (voltage across the capacitor at the LC filter)
- using a PLL with the positive sequence of Vo
- filtering ω_{VSM}.

The phase lock loop (PLL) applied in the first method is used for tracking and estimating the actual grid frequency. The structure used is shown in the figure.

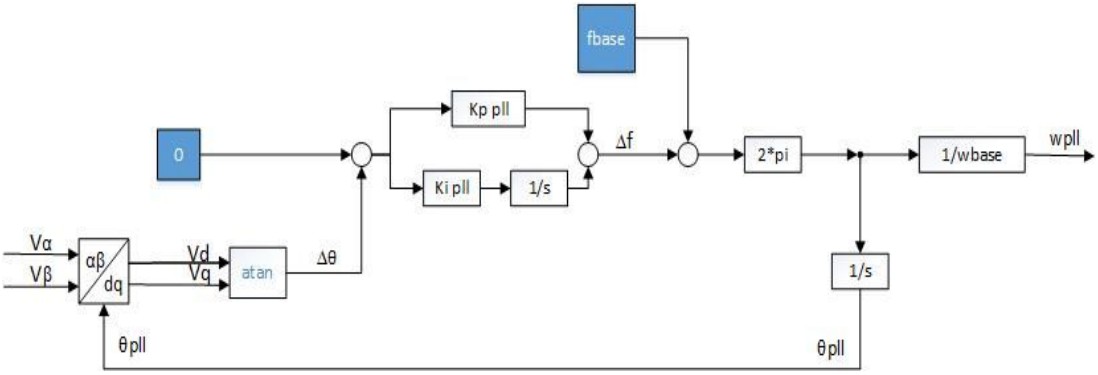

Fig. 3.3.PLL structure while using the voltage measured across the LC filter capacitor.

The structure is based after [13] where $V_{\alpha\beta}$ is the measured voltage expressed in the stationary reference frame.

To follow the grid frequency (in the Synchronous Rotating Reference Frame) the angle between the measured voltage vector and the grid vector should be zero. As a consequence, the inverse tangent is used to calculate this error. This phase error is given as an input to the PI controller in order to find δf_{PLL}.

$$\omega_{PLL} = (f_{base} + \delta f_{PLL}) * 2 * \pi \quad 3.3.5$$

$$\delta f_{PLL} = k_p * \varepsilon_{PLL} + \int k_i * \varepsilon_{PLL} * dt \quad 3.3.6$$

$$\varepsilon_{PLL} = \tan^{-1} \frac{v_{o,q}}{v_{o,d}} \quad 3.3.7$$

For the first case, Vd and Vq are found by transforming V_o from αβ to dq frame with the angle θ_{PLL}. The first and second methods are identical with the only exception being that in the second method is considered just the positive sequence of the voltage measured across the filter capacitor.

In the second method from V_o a sequence detection is done and $V^+_{o,\alpha\beta}$ is found which is used as shown in *Fig. 3.4*. Hence transforming from αβ frame to dq frame is attained V_d^+ and V_q^+.

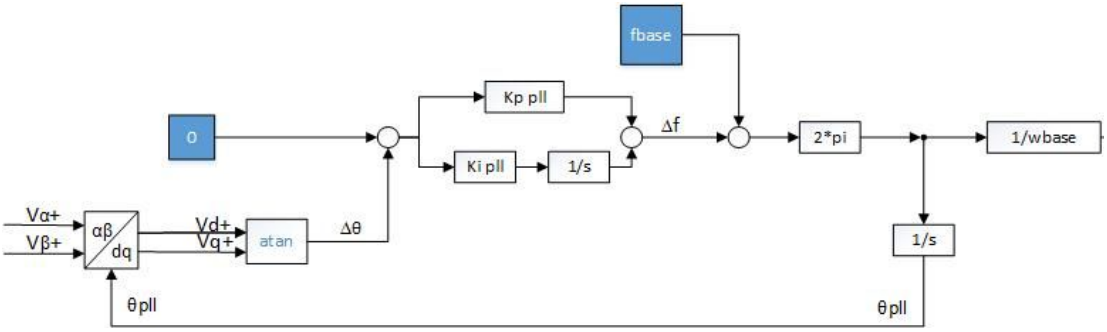

Fig. 3.4.PLL structure while using the positive sequence voltage.

In the third method for the damping are used the oscillations of ω_{VSM}. By making the difference between ω_{VSM} and $\omega_{Filtered}$ by a low pass filter gives the frequency oscillations which are needed to be damped.

The above described solutions are tested under the same model where is simulated a power reference perturbation at time t=2s, a perturbation in the local load at time t=3s, and an unbalanced condition occurring at time t=4s. The results are shown in *Fig. 3.5*

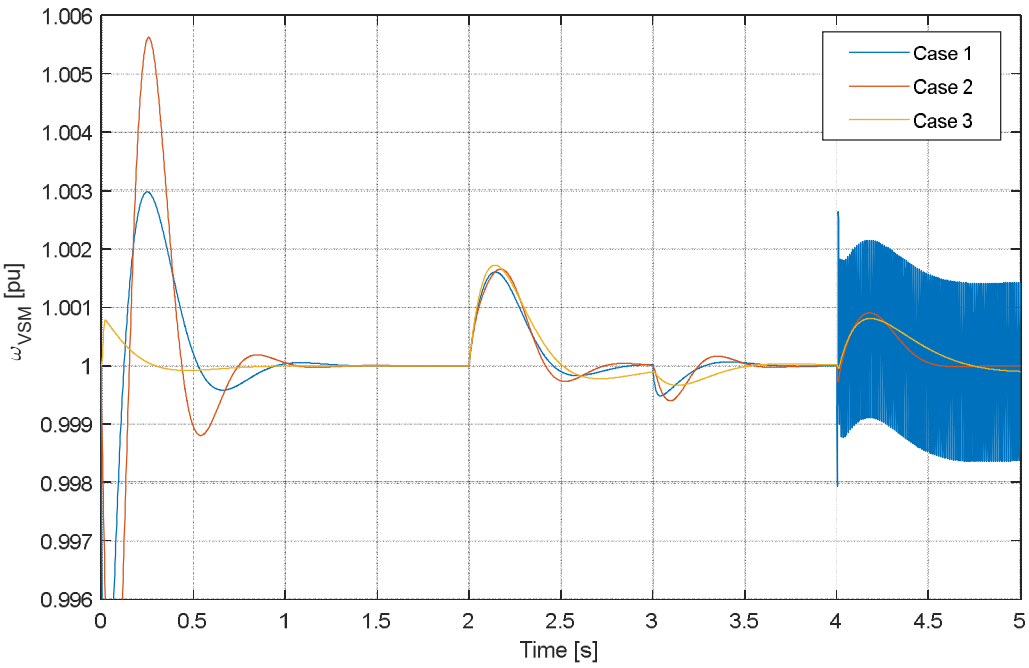

Fig. 3.5. Represent the frequency with respect to time, comparison between the three cases for implementing the damping power. PLL with Vo (—), PLL with the positive sequence of Vo (—), Filtering w_{VSM} (—)

For Case 1 where the PLL with the measurement from Vo.

Parameters: Kp=10, Ki =100, Kd=200

For Case 2 where the PLL with the positive sequence of Vo.

Parameters: Kp=2, Ki =70, Kd=200

For Case 3 where the filtered oscillations of w_{VSM} are used.

Parameters: Kd=100, wd=2

As shown in *Fig. 3.5* , case 1 (PLL with measured voltage of across LC filter capacitor, blue curve) when the system is unbalanced, ω oscillates with twice the fundamental grid frequency and it will affect negatively ω_{VSM} by introducing second harmonic rriples in it. In the second case(red) the system behaves similarly to the previous case for power and load perturbation but better behavior under unbalanced conditions. The 3rd case(yellow) it can be seen that the settling time is quite long since the low pas filter introduces delays. On the other hand it can also be seen that under grid fault ω_{VSM} is not effected as much as in the previous two cases.

3.3.3. Active Power Droop control

An external frequency droop is included in the power control of the VSM which acts as a frequency controller of the internal frequency of the VSM. This frequency droop is modeled after the steady-state characteristic of the speed governor from a traditional synchronous machine.

This power-frequency droop is characterized by the droop constant k_w acting on the difference between a frequency reference w^*_{vsm} and the actual w_{vsm}. As a consequence the virtual mechanical input power p^{r*} to the VSM swing equation is given by the sum of the external power reference set-point, p^*, and the frequency droop effect (eq. 3.3.4).

3.4 Reactive Power Droop Control

The Reactive Power Droop provides as an output the voltage amplitude reference |v*| that is needed by the Virtual Impedance. This voltage changes in such a way to keep the reactive power close to a reference (since the droop controller has just the proportional it doesn't reach error =0).

The internal voltage amplitude reference $|v|$ is calculated by equation 3.4.1 where $|v^*|$ is the external voltage amplitude reference and $q^*$is the reactive power reference. The gain k_q of the reactive power droop acts on the difference between the reactive power reference q^* and the measured reactive power q.

$$|v| = |v^*| + k_q(q^* - q) \qquad 3.4.1$$

The application of this technique is very common in microgrid systems when the compensation of a low-inertia problem is required [14].

Another way to provide the internal voltage reference is by using a Reactive Power Droop with Voltage Control which copies the behavior of the Automatic Voltage Regulator for SMs. A voltage controller regulates the amplitude of the internally induced voltage of the VSM electric model, to control the voltage amplitude at the VSC filter capacitor. A standard PI controller acts on the voltage amplitude error calculated as the difference between the amplitude reference $|v^*|$ and the measured output voltage at the filter capacitor $|v_o|$.

The controller offers the possibility to have an active droop function in the voltage reference by adopting the Reactive Power Droop Control. In this case, q∗ defines the level of reactive power at which the droop effects the voltage set-point changing it from a positive value to a negative one. Considering this type of control, the internal voltage amplitude will be given by the equation below:

$$|v| = k_{pv}\,(|v^*| - |v_o|) + \; k_q\, k_{pv}(q^* - q) \; + k_{iv}\xi + k_{ffe}\,|v_o| \qquad 3.4.2$$

$$\frac{d\xi}{dt} = \quad (|v^*| - |v_o|) + k_q(q^* - q) \qquad 3.4.3$$

Where k_{ffe} is the coefficient for the feed-forward action and ξ represents the integrator state of the PI controller. For a better and more robust behavior is advised to use a filtered q. Hence the final scheme is going to be as *Fig. 3.6*.

3.5 **Virtual impedance**

The virtual impedance is part of the VSM, it provides a interface between the Simulated SM and the control loops. The virtual impedance can be considered as an emulation of the impedance of a traditional SM in a SRRF (Synchronous rotating reference frame) as in equation 3.5.1.

$$v_s = e - r_s i_s - l_s \frac{di_s}{dt} - j\omega l_s i_s \qquad 3.5.1$$

This impedance influences both the steady-state and the dynamic operation of the VSM. It will cause a phase angle displacement between the grid and the VSM voltage, also it will reduce the sensitivity to small disturbances in the grid thus making the model more robust. In general, there are two dominating architectures, depending on whether the machine model provides a current reference or a voltage reference for controlling the converter operation. In the following are going to be expressed these 2 architectures as represented in [15].

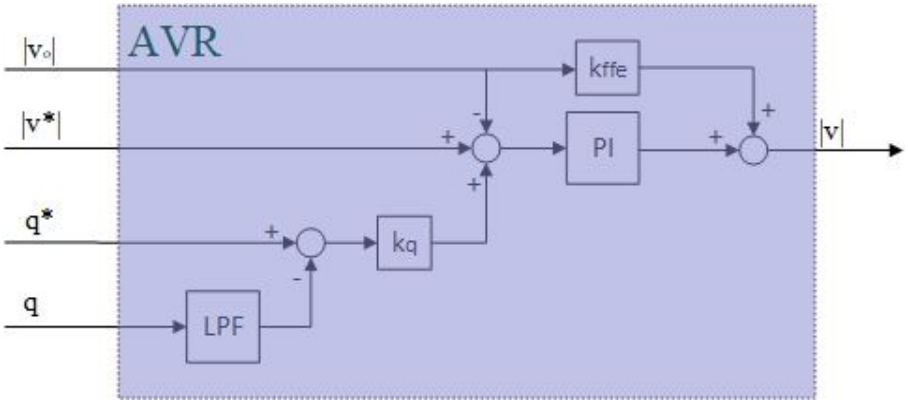

Fig. 3.6 Reactive Power Droop Control

The voltage controlled virtual synchronous machine *Fig. 3.7* or VCVSM for short has a closed loop voltage controller that provides the reference for the inner loop current controller. Its references as the terminal voltages are provided by the Virtual Impedance.

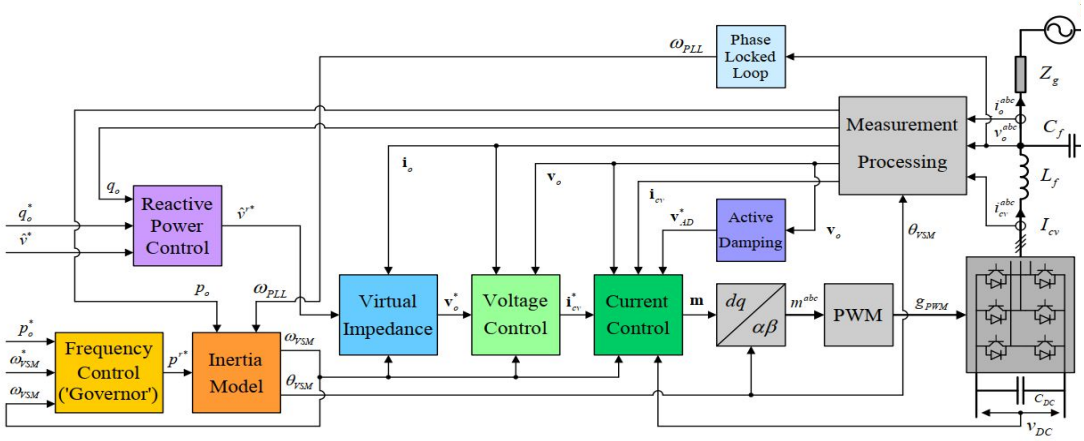

Fig. 3.7 Voltage controlled virtual synchronous machine

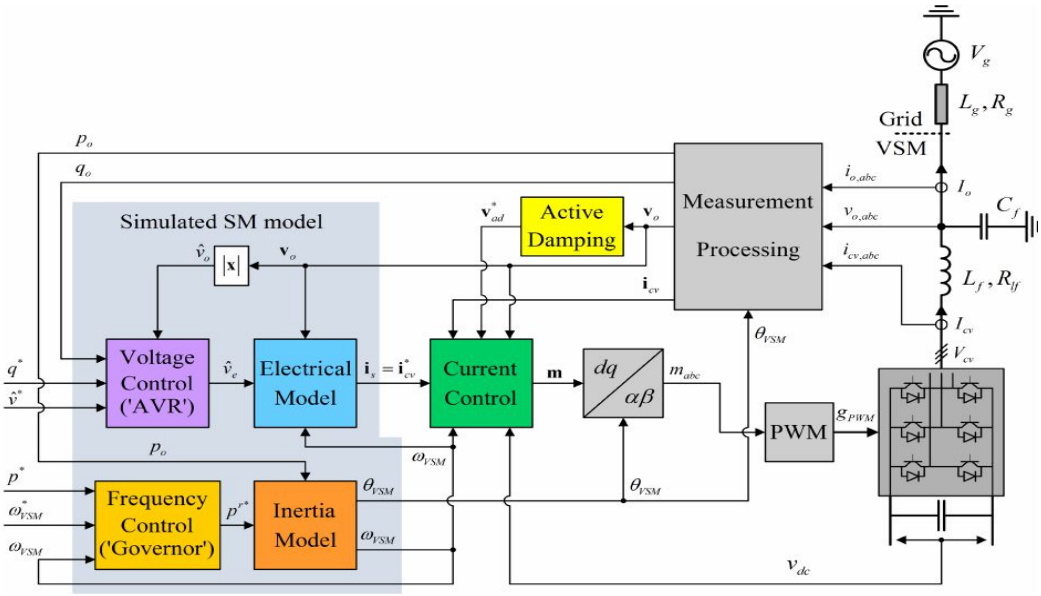

Fig. 3.8 Current controlled virtual synchronous machine

The second architecture *Fig. 3.8* is the current controller Virtual Synchronous Machine (CCVSM) which has a current controller for the inner loop and its references are provided again by the Virtual Impedance.

As before mentioned the electrical model used for the Virtual Impedance is based on (eq. 3.5.1) the stator equation of the SM and it can be represented with 2 different approaches.

The first one is a Dynamic Electrical Model (DEM).

$$v_o = v_e - r_v i_o - l_v \frac{di_o}{dt} - j\omega_{VSM} l_v i_o \quad 3.5.2$$

$$\frac{di_o{}^{DEM}}{dt} = \frac{v_e}{l_v} - \frac{v_o}{l_v} - (r_v/l_v + j\omega_{VSM}) i_o \quad 3.5.3$$

This model is relevant for CCVSM where v_e represents the internally induced voltage of a SM, in series with a dynamic representation of a RL impedance representing the virtual stator windings. The LC-filter output voltage v_o is measured and used as an input to the internally simulated electrical model. The current $i_o{}^{DEM}$, calculated by the numerical simulation of the model, are provided as references to the VSC current controllers. In equation 3.5.3 r_v, l_v are the per unit virtual stator resistance and inductance and w_{VSM} is the per unit speed of the virtual inertia.

In the second approach is a Quasi-Stationary electrical model based on [16]. The QSEM (Quasi-Stationary Electrical Model) implementation assumes a representation of the SM in the SRRF. This is done by setting the current derivative to zero, equation 3.5.5, resulting in the quasi-stationary stator current.

$$v_o = v_e - r_v i_o - l_v \frac{di_o}{dt} - j\omega_{VSM} l_v i_o \quad 3.5.4$$

$$v_o = v_e - r_v i_o - j\omega_{VSM} l_v i_o \quad 3.5.5$$

$$i_o = \frac{v_e - v_o}{r_v + j\omega_{VSM} l_v} \quad 3.5.6$$

Equation 3.5.6 is used for QSEM-based CCVSM implementation. Where v_o is the measured voltage at the filter capacitor, equivalent to the voltage measured at the terminals

of the SM, v_e is the reference voltage that comes from the outer loop control and equivalent to the back emf e of the SM, i_o is the current that should be used as a reference for the current controller of the VSC which is equivalent to the stator current of the SM.

For VCVSM is used:

$$v^*{}_o = v^* - r_v i_o - j\omega_{VSM} l_v i_o \qquad 3.5.7$$

As before v^* is the reference voltage, r_v, l_v are the per-unit virtual stator resistance and inductance and w_{VSM} is the per-unit speed of the virtual inertia. For this case i_o is the measured current after the LC filter and $v^*{}_o$ is the voltage that should be used as a reference for the voltage controller.

3.6 Current control

The current controller represents the inner loop. It provides the voltage for which the switches of the inverter will be driven *Fig. 3.9*. This current will depend on the voltage of the connection point as expressed in equation 3.6.1. This equation can be expressed both in the Stationary Reference Frame and in the Synchronous Rotating Reference Frame hence we are going to consider the current control in both the frames.

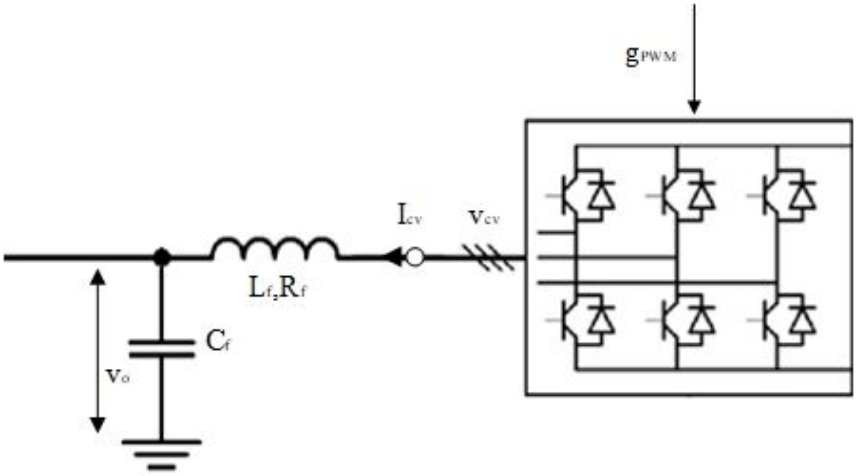

Fig. 3.9 VSC configuration

$$v_{cv}^{abc} = v_o^{abc} + R_f\, i_{cv}^{abc} + L_f \frac{di_{cv}^{abc}}{dt} \quad 3.6.1$$

$$v_{cv}^{\alpha\beta} = v_o^{\alpha\beta} + R_f\, i_{cv}^{\alpha\beta} + L_f \frac{di_{cv}^{\alpha\beta}}{dt} \quad 3.6.2$$

$$v_{cv}^{dq} = v_o^{dq} + R_f\, i_{cv}^{dq} + L_f \frac{di_{cv}^{dq}}{dt} + \mathrm{j}\,\omega\, L_f\, i_{cv}^{dq} \quad 3.6.3$$

3.6.1. Current controller implemented in the synchronous rotating reference frame

In SRRF in steady-state under balanced conditions the current and voltages are constant hence a linear PI controller will work perfectly. Presenting equation 3.6.3 from complex vector to its dq form.

$$v_{cv}^{d} = v_o^{d} + R_f\, i_{cv}^{d} + L_f \frac{di_{cv}^{d}}{dt} - \omega\, L_f\, i_{cv}^{q} \quad 3.6.4$$

$$v_{cv}^{q} = v_o^{q} + R_f\, i_{cv}^{q} + L_f \frac{di_{cv}^{q}}{dt} + \omega\, L_f\, i_{cv}^{d} \quad 3.6.5$$

In per unit

$$v_{cv}^{d} = v_{o}^{d} + r_f\, i_{cv}^{d} + \frac{l_f}{\omega_b}\frac{di_{cv}^{d}}{dt} - \omega_{pu}\, l_f\, i_{cv}^{q} \quad 3.6.6$$

$$v_{cv}^{q} = v_{o}^{q} + r_f\, i_{cv}^{q} + \frac{l_f}{\omega_b}\frac{di_{cv}^{q}}{dt} + \omega_{pu}\, l_f\, i_{cv}^{d} \quad 3.6.7$$

Considering equation 3.6.6 and equation 3.6.7 the reference voltage for the converter becomes:

$$v_{cv}^{d\,*} = v_{o}^{d} + v_{PI}^{d} - \omega_{pu}\, l_f\, i_{cv}^{q} \quad 3.6.8$$

$$v_{cv}^{dq\,*} = v_{o}^{q} + v_{PI}^{q} + \omega_{pu}\, l_f\, i_{cv}^{d} \quad 3.6.9$$

Where

$$v_{PI}^{d} = k_p\,(i_{cv}^{d\,*} - i_{cv}^{d}) + k_i \int (i_{cv}^{d\,*} - i_{cv}^{d})\, dt \quad 3.6.10$$

$$v_{PI}^{q} = k_p\,(i_{cv}^{q\,*} - i_{cv}^{q}) + k_i \int (i_{cv}^{q\,*} - i_{cv}^{q})\, dt \quad 3.6.11$$

3.6.2. Current controller implemented in the stationary reference frame

As before can be presented, equation 3.6.2, from complex vectors to its αβ form and after in per unit and we get:

$$v_{cv}^{\alpha} = v_{o}^{\alpha} + R_f\, i_{cv}^{\alpha} + L_f \frac{di_{cv}^{\alpha}}{dt} \quad 3.6.12$$

$$v_{cv}^{\beta} = v_{o}^{\beta} + R_f\, i_{cv}^{\beta} + L_f \frac{di_{cv}^{\beta}}{dt} \quad 3.6.13$$

In SRF the current reference changes in time with frequency $\omega = \omega_{VSM}$, by doing so the PI controllers are not the most suitable solutions hence the PR (proportional resonance) controllers are used for the inner loop *Fig. 3.10*. These controllers are SOGI-based structures. The SOGI (Second Order Generalized Integrator) is resonant term that oscilates with the frequency of the VSM. In the frequency domain the SOGI provides a gain theroretically infinite for the resonant frequency and zero for the other ones [17].

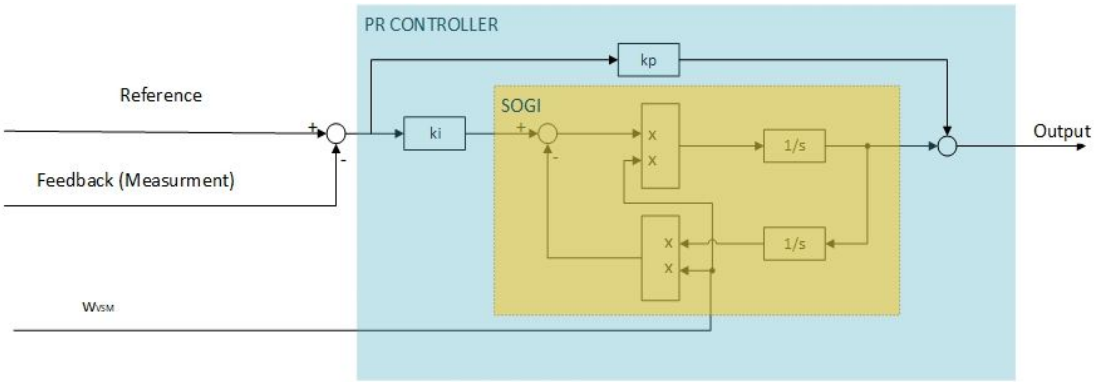

Fig. 3.10 PR controller

Considering the RL as the object under regulation the voltage on which the VSC is controlled as follows.

$$v_{cv}^{\alpha\ *} = v_o^{\alpha} + v_{PR}^{\alpha} \quad 3.6.14$$

$$v_{cv}^{\beta\ *} = v_o^{\beta} + v_{PR}^{\beta} \quad 3.6.15$$

The frequency adaptation for this two integrator scheme is of paramount importance. There is a high peak gain on the needed frequency and thus allow a zero steady-state error. The frequency of the integral part should be the same with the frequency of the virtual machine which is also the changing frequency of the reference.

$$H_{PR}(w) = k_p + \frac{k_i * \omega_0 * s}{s^2 + \omega_0^2} \quad 3.6.16$$

$$v_{PR} = H_{PR}(i^* - i_{cv}) \quad 3.6.17$$

Where v_{PR} is the controller output voltage, i^* is the reference current provided by the virtual impedance, i_{cv} is the current measured at the output of the converter. Tuning the PR controller parameters can be done similarly to the PI controller as presented in [17].

3.7 **Active damping**

The LC filter creates oscillations in the voltage. To suppress the oscillations an active damping term is needed. Firstly, we find these oscillations by filtering the voltage v_o measured across the LC filter capacitor and by subtracting from the measured voltage the filtered one we get the oscillations. Secondly, the oscillations are reduced by an active damping coefficient k_{AD} and feed negatively to the voltage that comes as a reference from the current controller. Hence we get the formula:

$$v_{AD}^{*} = k_{AD}(v_o - \varphi) \qquad 3.7.1$$

Where φ is the filtered signal. In case the current controller is in SRRF the voltage references are in dq and v_{AD}^{*} is in dq as well. In this case v_o^{dq} is filtered by a low pass filter.

In case the current controller is in SRF the voltage references are in αβ. In this case $v_o^{\alpha\beta}$ changes with the frequency of the grid hence a Band Pass Filter with adaptive capabilities is needed. For this reason, SOGI can be used as BPF.

4 CONTROL STRATEGIES FOR UNBALANCED CONDITIONS

4.1 Introduction

The electrical network is a dynamical system, whose behavior depends upon many factors thus the grid-connected power converters should guarantee proper operation under normal conditions and ensure a robust and safe performance under abnormal grid conditions. Nonlinear loads and occurrence of grid faults may give rise to distortion and/or unbalanced grid voltages at the point of common coupling (PCC) of the converter. Being subject to unbalanced conditions and also the unbalanced currents, and the interaction between unbalanced voltages and currents create oscillations in the active and reactive power delivered to the grid. The proper operation of the power converter under such conditions is a challenging control issue.

Controlling the unbalanced current injections under unbalanced grid voltage conditions allows attenuating power oscillations, maximizing the power delivery, or even having balanced grid voltages at the point of connection. With VSM implementation (see chapter 2) these control strategies are useful also in islanded mode.

Ideally, power converters used for HVDC should stay actively connected, supporting the grid services (voltage/frequency) but, under unbalanced conditions, this is not always fulfilled. The currents injected by the power converter into the phases of the grid should always be under control, even though the grid voltage may experience variations. Therefore, the control algorithms should estimate the instantaneous performance of these currents at any time, even during transient faults, in order to avoid any overcurrent tripping. Thus, considerations should be made, for the calculation of the maximum power that can be delivered to the grid, without overpassing the current limits of the power converter.

4.2 Sequence detection and power calculations

In this section, it is shown how to acquire the positive and negative sequences of the voltage and current from the three phase measurement.

Under generic grid conditions the voltage at PCC is as follows:

$$v_{abc} = v_{abc}^{+} + v_{abc}^{-} + v_{abc}^{0} \qquad 4.2.1$$

Where:

$$v_{abc}^{+} = V^{+}\begin{bmatrix} \cos(wt + \theta^{+}) \\ \cos(wt - \frac{2\pi}{3} + \theta^{+}) \\ \cos(wt + \frac{2\pi}{3} + \theta^{+}) \end{bmatrix} \qquad 4.2.1.a$$

$$v_{abc}^{-} = V^{-}\begin{bmatrix} \cos(-wt + \theta^{-}) \\ \cos(-wt + \frac{2\pi}{3} + \theta^{-}) \\ \cos(-wt - \frac{2\pi}{3} + \theta^{-}) \end{bmatrix} \qquad 4.2.1.b$$

$$v_{abc}^{0} = V^{0}\begin{bmatrix} \cos(wt + \theta^{0}) \\ \cos(wt + \theta^{0}) \\ \cos(wt + \theta^{0}) \end{bmatrix} \qquad 4.2.1.c$$

In Fig. 4.1 is shown the locus of the voltage v under unbalanced conditions. This voltage can be represented in general in three different ways.

- Three phase system abc
- Cartesian αβ representing a Stationary Reference Frame (SRF)
- Cartesian dq which is rotating with the synchronous speed and it represents the Synchronous Rotating Reference Frame (SRRF)

It can be seen that in this unbalanced case the rotation of vector v will generate in SRF $\widehat{v_\alpha} > \widehat{v_\beta}$ and in SRRF $v_d = \bar{v} + \tilde{v}(2w)$ if $w = w_{synch}$. This behavior will affect negatively the previous control systems with VSM implementations, hence a separation of the positive and negative sequences has to be done and taken into consideration. The main interest of power converter under unbalanced conditions lies in controlling the positive and negative sequence of the injected currents.

In VSC $v_a + v_b + v_c = 0$, then the zero sequence is not considered and the voltage becomes $v = v^+ + v^-$.

To show the voltage vector on the Cartesian αβ frame, a reduced version of the Clarke transformation matrix $T_{\alpha\beta}$ is used.

$$\begin{bmatrix} v_\alpha \\ v_\beta \end{bmatrix} = \begin{bmatrix} 1 & -1/2 & -1/2 \\ 0 & \sqrt{3}/2 & -\sqrt{3}/2 \end{bmatrix} \begin{bmatrix} v_a \\ v_b \\ v_c \end{bmatrix} \qquad 4.2.2$$

$$v_{\alpha\beta} = T_{\alpha\beta}\, v_{abc}$$

From (eq. 4.2.1) we can represent the positive and negative sequences of the voltage as follows.

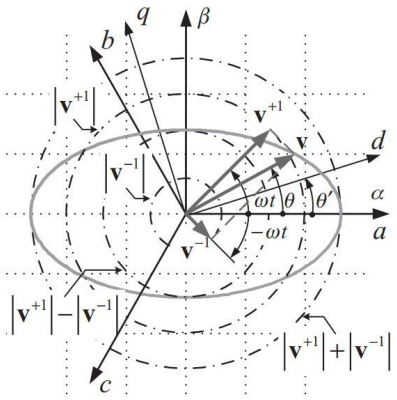

Fig. 4.1. Locus of voltage under unbalanced conditions.

$$\begin{bmatrix} v_a^+ \\ v_b^+ \\ v_c^+ \end{bmatrix} = \frac{1}{3}\begin{bmatrix} 1 & a^2 & a \\ a & 1 & a^2 \\ a^2 & a & 1 \end{bmatrix}\begin{bmatrix} v_a \\ v_b \\ v_c \end{bmatrix} \qquad 4.2.3$$

$$v_{abc}^+ = T^+ \, v_{abc}$$

$$\begin{bmatrix} v_a^- \\ v_b^- \\ v_c^- \end{bmatrix} = \frac{1}{3}\begin{bmatrix} 1 & a & a^2 \\ a^2 & 1 & a \\ a & a^2 & 1 \end{bmatrix}\begin{bmatrix} v_a \\ v_b \\ v_c \end{bmatrix} \qquad 4.2.4$$

$$v_{abc}^- = T^- \, v_{abc}$$

Where $a = e^{j\frac{2\pi}{3}}$ is a version of the Fortescue operator and represents a time-shifting equivalent to a 120˚ phase-shifting. Considering (eq. 4.2.3) , (eq. 4.2.4) and substituting v_{abc} using the inverse Clarke transform, we get (eq. 4.2.5). Moreover, by using the Clarke transformation again for the positive and negative sequence we will find new matrixes (eq. 4.2.7) for which we can find the positive and negative sequence from $v_{\alpha\beta}$.

$$v_{abc}^+ = T^+ \, v_{abc} = T^+ \, T_{\alpha\beta}^{-1} \, v_{\alpha\beta}$$
$$v_{abc}^- = T^- \, v_{abc} = T^- \, T_{\alpha\beta}^{-1} \, v_{\alpha\beta} \qquad 4.2.5$$

$$v_{\alpha\beta}^+ = T_{\alpha\beta} \, v_{abc}^+ = T_{\alpha\beta} \, T^+ \, T_{\alpha\beta}^{-1} \, v_{\alpha\beta}$$
$$v_{\alpha\beta}^- = T_{\alpha\beta} \, v_{abc}^- = T_{\alpha\beta} \, T^- \, T_{\alpha\beta}^{-1} \, v_{\alpha\beta} \qquad 4.2.6$$

$$T_{\alpha\beta} \, T^+ \, T_{\alpha\beta}^{-1} = T_{\alpha\beta}^+ = \frac{1}{2}\begin{bmatrix} 1 & -q \\ q & 1 \end{bmatrix}$$
$$T_{\alpha\beta} \, T^- \, T_{\alpha\beta}^{-1} = T_{\alpha\beta}^- = \frac{1}{2}\begin{bmatrix} 1 & q \\ -q & 1 \end{bmatrix} \qquad 4.2.7$$

Where $q = e^{-j\frac{\pi}{2}}$

$$v_{\alpha\beta}^+ = \frac{1}{2}\begin{bmatrix} 1 & -q \\ q & 1 \end{bmatrix} v_{\alpha\beta}$$
$$v_{\alpha\beta}^- = \frac{1}{2}\begin{bmatrix} 1 & q \\ -q & 1 \end{bmatrix} v_{\alpha\beta} \qquad 4.2.8$$

$$v_{\alpha}^{+} = \frac{1}{2}(v_{\alpha} - q\, v_{\beta}) \quad 4.2.9$$

$$v_{\beta}^{+} = \frac{1}{2}(q\, v_{\alpha} + v_{\beta}) \quad 4.2.10$$

$$v_{\alpha}^{-} = \frac{1}{2}(v_{\alpha} + q\, v_{\beta}) \quad 4.2.11$$

$$v_{\beta}^{-} = \frac{1}{2}(-q\, v_{\alpha} + v_{\beta}) \quad 4.2.12$$

As mentioned $q = e^{-j\frac{\pi}{2}}$ which means that there is a 90° lagging phase-shifting operator applied on the time domain to obtain an in-quadrature version of the input waveform. It can be created by delaying the signal with T/4, Integration, differentiation, or the most relevant using a low pass filter. Considering the last one, a second-order generalized integrator (SOGI) is going to be used as the quadrature signal generator (QSG), as shown in Fig. 4.2.

The SOGI-QSG behaves as a bandpass filter where the output is used as an in-phase signal introducing filtering and noise suppression in the system and low-pass filtered output is representing the phase-shifted signal.

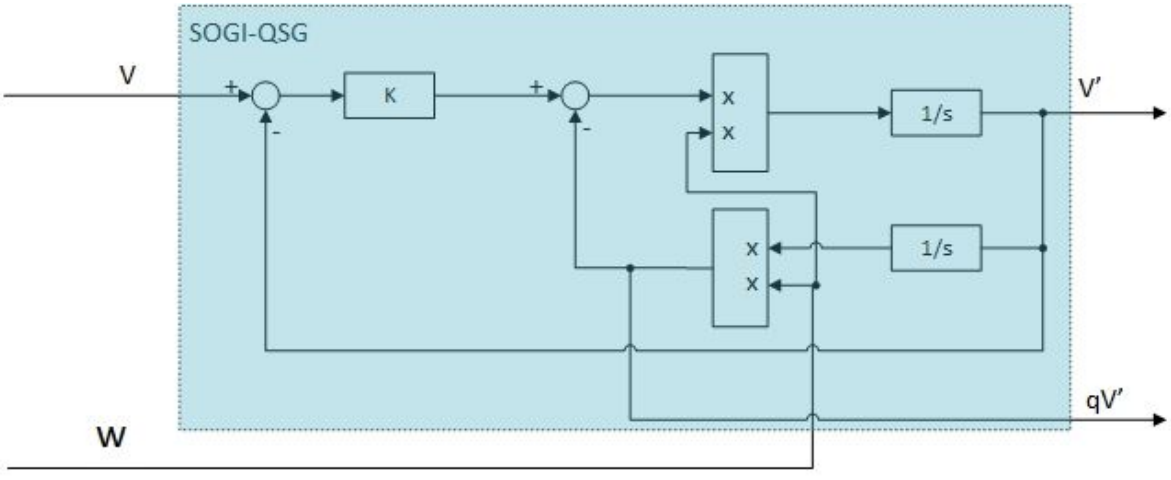

Fig. 4.2. SOGI-QSG structure.

$$\frac{v'(s)}{v(s)} = \frac{K * w * s}{s^2 + K * w * s + w^2} \quad 4.2.13$$

$$\frac{qv'(s)}{v(s)} = \frac{K * w^2}{s^2 + K * w * s + w^2} \quad 4.2.14$$

For these reasons a dual set of SOGI-QSGs Fig. 4.3 is used to obtain the signals and their quadrature components for both alpha and beta. This method is shown in [18] where is also considered $K = \sqrt{2}$ as the best suited coefficient considering a tradeoff of dynamic response and overshooting.

The positive and negative sequence of the current can be found using the same matrixes as the voltage (eq.4.2.7). As mentioned in the introduction, under unbalanced voltages there are unbalanced currents and therefore power oscillations. In the following paragraphs, these power oscillations are going to be explained.

Considering the powers expressed in αβ frame.

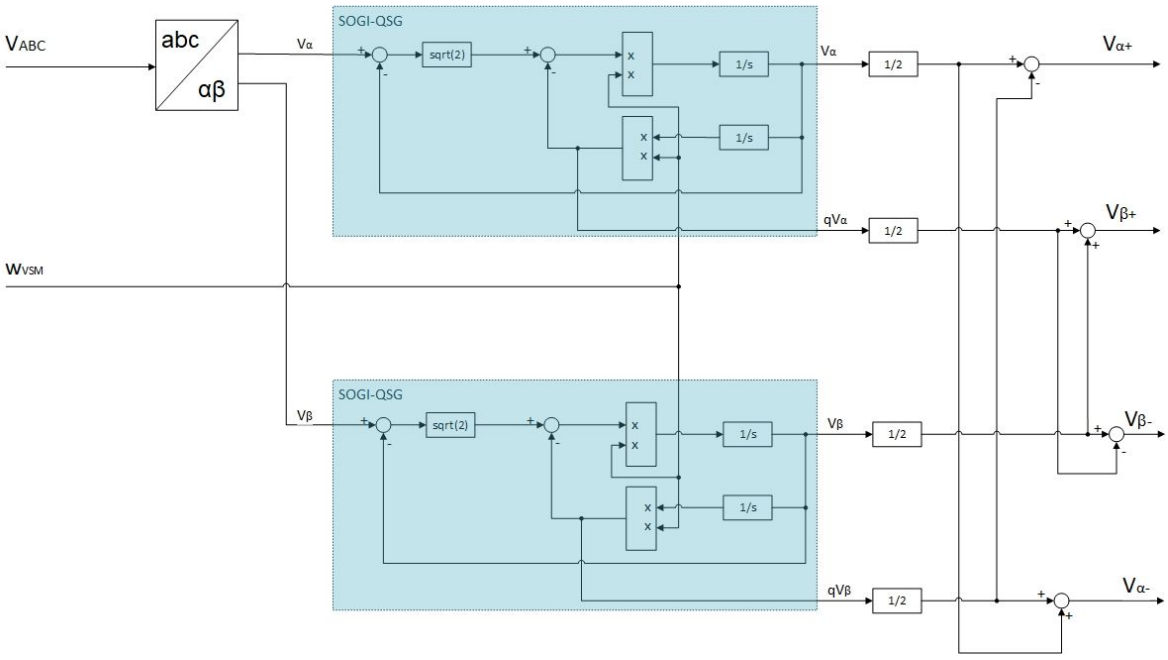

Fig. 4.3. Dual set of SOGI-QSGs used for sequence separation.

$$s = v * \bar{\imath} \quad 4.2.15$$

$$s = (v_\alpha + jv_\beta) * (i_\alpha - ji_\beta) \quad 4.2.16$$

$$p = v_\alpha * i_\alpha + v_\beta * i_\beta \quad 4.2.17$$

$$q = v_\beta * i_\alpha - v_\alpha * i_\beta \quad 4.2.18$$

Considering the case of unbalanced voltages and currents.

$$p = (v_\alpha^+ + v_\alpha^-) * (i_\alpha^+ + i_\alpha^-) + \left(v_\beta^+ + v_\beta^-\right) * \left(i_\beta^+ + i_\beta^-\right) \quad 4.2.19$$

$$= v_\alpha^+ i_\alpha^+ + v_\beta^+ i_\beta^+ + v_\alpha^- i_\alpha^- + v_\beta^- i_\beta^- + v_\alpha^+ i_\alpha^- + v_\alpha^- i_\alpha^+ + v_\beta^+ i_\beta^- + v_\beta^- i_\beta^+$$

$$q = \left(v_\beta^+ + v_\beta^-\right) * (i_\alpha^+ + i_\alpha^-) - (v_\alpha^+ + v_\alpha^-) * \left(i_\beta^+ + i_\beta^-\right) \quad 4.2.20$$

$$= v_\beta^+ i_\alpha^+ + v_\beta^- i_\alpha^- - v_\alpha^+ i_\beta^+ - v_\alpha^- i_\beta^- + v_\beta^+ i_\alpha^- + v_\beta^- i_\alpha^+ - v_\alpha^+ i_\beta^- - v_\alpha^- i_\beta^+$$

If

$$v_\alpha^+ = |v^+| \cos(wt + \theta^+) \quad 4.2.21$$

$$v_\alpha^- = |v^-| \cos(-wt + \theta^-)$$

$$v_\beta^+ = |v^+| \sin(wt + \theta^+)$$

$$v_\beta^- = |v^-| \sin(-wt + \theta^-)$$

$$i_\alpha^+ = |i^+| \cos(wt + \delta^+) \quad 4.2.22$$

$$i_\alpha^- = |i^-| \cos(-wt + \delta^-)$$

$$i_\beta^+ = |i^+| \sin(wt + \theta^+)$$

$$i_\beta^- = |i^-| \sin(-wt + \delta^-)$$

Then by substituting (eq. 4.2.19) and (eq. 4.2.20) the positive and negative sequences of the alpha-beta components of the current and voltage we get:

$$p = |v^+| * |i^+| * \cos(\theta^+ - \delta^+) + |v^-| * |i^-| * \cos(\theta^- - \delta^-) \quad 4.2.23$$

$$+(|v^+| * |i^-| * \cos(\theta^+ - \delta^-) + |v^-| * |i^+| * \cos(\theta^- - \delta^+))\cos(2wt)$$

$$+(|v^+| * |i^-| * \sin(\delta^- - \theta^+) + |v^-| * |i^+| * \sin(\theta^- - \delta^+))\sin(2wt)$$

$$q = |v^+| * |i^+| * \sin(\theta^+ - \delta^+) + |v^-| * |i^-| * \sin(\theta^- - \delta^-) \quad 4.2.24$$

$$+(|v^+| * |i^-| * \sin(\theta^+ - \delta^-) + |v^-| * |i^+| * \sin(\theta^- - \delta^+))\cos(2wt)$$

$$+(|v^+| * |i^-| * \cos(\delta^- - \theta^+) - |v^-| * |i^+| * \cos(\theta^- - \delta^+))\sin(2wt)$$

From these equations, it is visible that the power has two components, the average one and the oscillating one. The oscillating one is made by the sum of sinusoidal and cosinusoidal oscillations. It is worth mentioning that the oscillations come as a consequence of multiplying a component from the negative sequence to a component of the positive sequence and the result is an oscillating component whose frequency is twice the grid frequency.

4.3 Control Strategies for operating under unbalanced conditions

As mentioned in the introduction we can have different control strategies by controlling the unbalanced currents injections. The current injected into the grid should keep a certain relationship with the voltages at the PCC to deliver a given amount of active and reactive power.

The most extended solutions for controlling the current are based on SRRF which uses PI regulators operating in dq frame. However, if unbalanced currents are needed to be injected, the behavior of such controllers are not best suited since there is not a specific control loop for the negative sequence current components. If this loop was going to be considered, we would have 4 PI controllers for the current controller which increases the complexity of the control. On the other side, if PR current controllers implemented in the

SRF are used (as expressed in the previews chapter) then they can close the control loop for both positive and negative sequences of the current since both sequences have the same value of frequency.

In VSM implementation the unbalanced currents injected are generated with the usage of the virtual impedance for the positive sequence, in order to have the same VSM implementation as mentioned in chapter 2. For the negative sequence of the current, the reference changes depending on the control strategy. In the following paragraphs, the idea behind different control strategies for controlling the converter is going to be shown.

4.3.1. Control strategies for Balanced Current

To control the behavior of the converter we control the current in it, and in order to have balanced currents, we should control the negative sequence of the current to zero. This approach will result in the lowest possible current amplitudes for a specified average active power transfer during unbalanced conditions, but with the consequence of second harmonic oscillations in both the active and the reactive power flow.

$$i^* = i^{*+} + i^{*-} \tag{4.3.1}$$

$$i^{*-} = 0 \tag{4.3.2}$$

The positive sequence of the current will come from the Virtual Impedance, as expressed in Fig. 4.4:

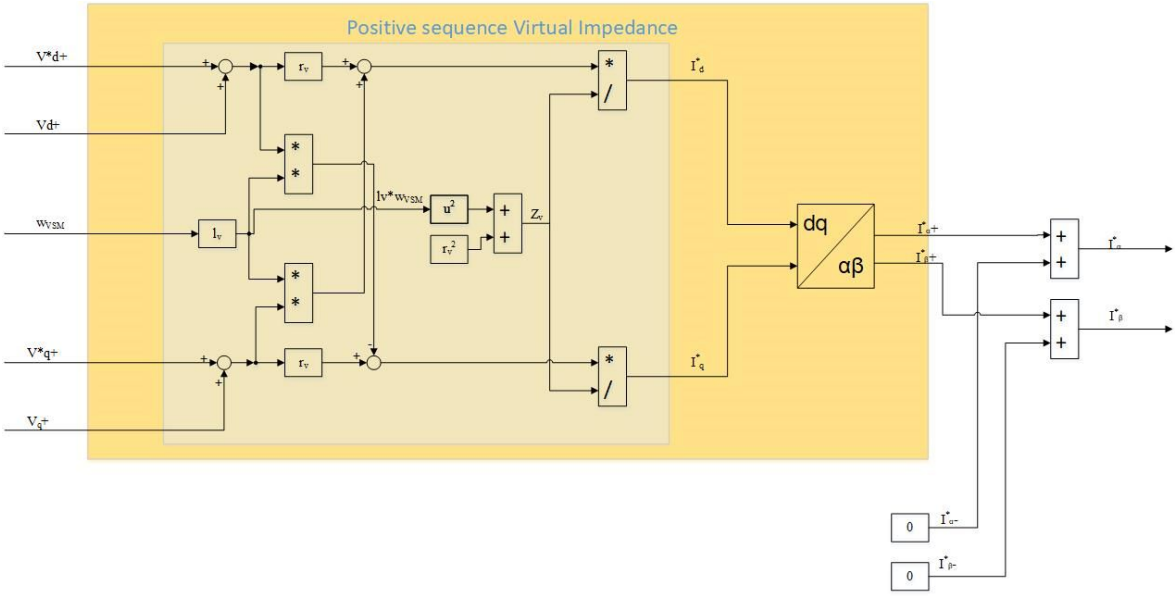

Fig. 4.4. Generated currents for controlling balanced three phase currents.

In Fig. 4.4 is considered a virtual impedance using a Quasi-Stationary electrical model implemented in the positive sequence dq frame. As previously explained, the current reference is changed in αβ frame and a PR current controller is used.

4.3.2. Control strategies for Balance Voltage

In this case, a virtual impedance for the negative sequence is considered as shown in Fig. 4.5. By doing so we can give current references in order to have the negative sequence of the internal voltage of VSM equal to zero (eq 4.3.6).

$$v^*_{dq} = v_{dq} + (r_v + jw_{VSM}l_v)i_{dq} \quad 4.3.3$$

$$v^*_{dq+} = v_{dq+} + (r_v + jw_{VSM}l_v)i^*_{dq+} \quad 4.3.4$$

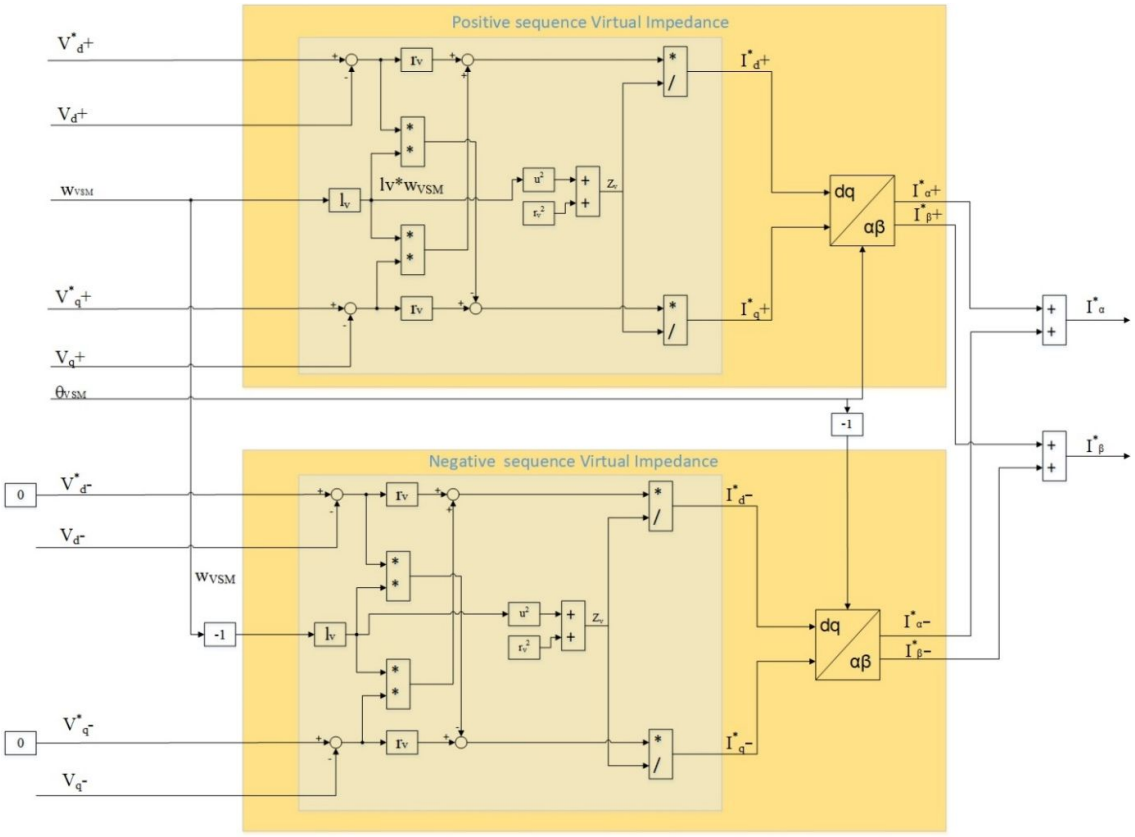

Fig. 4.5. Current generation with positive and negative virtual impedance.

$$v^*_{dq-} = v_{dq-} + (r_v + jw_{VSM}l_v)i^*_{dq-} \quad 4.3.5$$

$$0 = v_{dq-} + (r_v + jw_{VSM}l_v)i^*_{dq-} \quad 4.3.6$$

When connected with a strong grid, the negative sequence currents required to reach the balanced conditions are going to be very high and not reachable, thus, it is not able to influence the local voltage. On the other hand, for weak grids or in an islanded mode, having negative sequence currents to reach balanced voltages is more achievable.

Considering in islanded mode $v_{load} = v_o$ and $i_{load} = i_o$, it is possible to find the voltage and current sequence components through an unsymmetrical load.

$$\begin{bmatrix} v_{a,load} \\ v_{b,load} \\ v_{c,load} \end{bmatrix} = \begin{bmatrix} Z_a & 0 & 0 \\ 0 & Z_b & 0 \\ 0 & 0 & Z_c \end{bmatrix} \begin{bmatrix} i_a \\ i_b \\ i_c \end{bmatrix} \quad 4.3.7$$

$$\begin{bmatrix} v^0_{load} \\ v^+_{load} \\ v^-_{load} \end{bmatrix} = A^{-1} \begin{bmatrix} Z_a & 0 & 0 \\ 0 & Z_b & 0 \\ 0 & 0 & Z_c \end{bmatrix} A \begin{bmatrix} i^0 \\ i^+ \\ i^- \end{bmatrix} \quad 4.3.8$$

$$A = \begin{bmatrix} 1 & 1 & 1 \\ 1 & a^2 & a \\ 1 & a & a^2 \end{bmatrix}, \; A^{-1} = \frac{1}{3}\begin{bmatrix} 1 & 1 & 1 \\ 1 & a & a^2 \\ 1 & a^2 & a \end{bmatrix} \quad 4.3.9$$

$$v^0_{load} = \frac{1}{3} i^0 (Z_a + Z_b + Z_c) + \frac{1}{3} i^+ (Z_a + a^2 Z_b + a Z_c) + \frac{1}{3} i^- (Z_a + a Z_b + a^2 Z_c) \quad 4.3.10$$

$$v^+_{load} = \frac{1}{3} i^0 (Z_a + a Z_b + a^2 Z_c) + \frac{1}{3} i^+ (Z_a + Z_b + Z_c) + \frac{1}{3} i^- (Z_a + a^2 Z_b + a Z_c) \quad 4.3.11$$

$$v^-_{load} = \frac{1}{3} i^0 (Z_a + a^2 Z_b + a Z_c) + \frac{1}{3} i^+ (Z_a + a Z_b + a^2 Z_c) + \frac{1}{3} i^- (Z_a + Z_b + Z_c) \quad 4.3.12$$

Neglecting the zero-sequence current,

$$v^-_{load} = i^+ \left[\frac{1}{3} (Z_a + a Z_b + a^2 Z_c) \right] + i^- \left[\frac{1}{3} (Z_a + Z_b + Z_c) \right] \quad 4.3.13$$

From this equation it can be observed that the unbalances are created both from the negative and positive sequence of the current. To achieve balanced voltages a negative sequence current is required equal to the effect of the positive sequence current. Not knowing the unbalanced impedances of the load, a negative sequence virtual impedance is considered

in generating the negative sequence current. By not considering the filter the equation below is found.

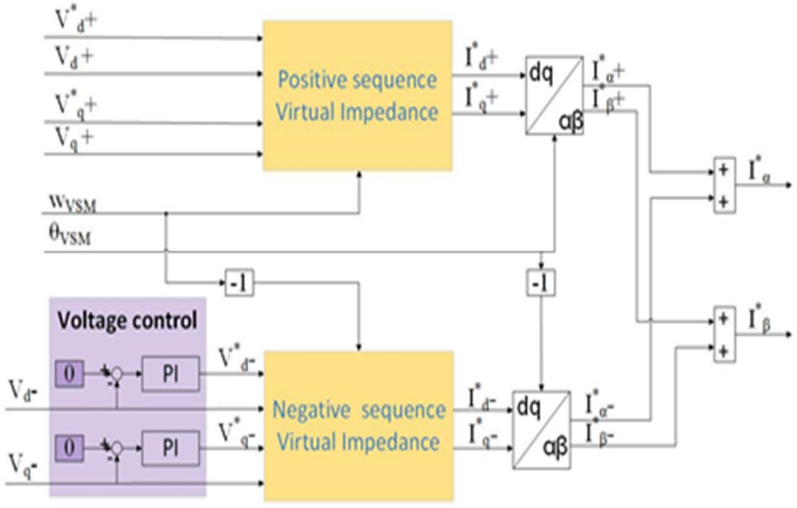

Fig. 4.6. Generated currents using negative sequence voltage control

$$v^{-*} = i^{-} z_{VSM} + v^{-}_{load} \qquad 4.3.14$$

The equation above looks like a control loop with just the proportional coefficient. By using the negative sequence of the voltage at the PCC as a process variable and the negative sequence of the internal voltage as a control variable we can inject the negative current needed to balance the voltage at the PCC. The virtual impedances use the same electrical model as expressed in equation (QS VI). In consequence, the currents will have the following equations

$$i_d^{-*} = \frac{(v_d^{-*} - v_d^{-}) r_v + (v_q^{-*} - v_q^{-})(-w_{VSM}) l_v}{r_v{}^2 + (w_{VSM} l_v)^2} \qquad 4.3.15$$

$$i_q^{-*} = \frac{(v_q^{-*} - v_q^{-}) r_v - (v_d^{-*} - v_d^{-})(-w_{VSM}) l_v}{r_v{}^2 + (w_{VSM} l_v)^2} \qquad 4.3.16$$

Consequently, if a PI controller is used to provide the reference for the internal negative sequence of the VSM voltage using for feedback the negative sequence voltage measured at the filter capacitor Fig. 4.6. Thus the negative sequence of the internal voltage of the VSM reaches such values that the PCC voltage becomes balanced.

In conclusion, under unbalanced conditions, unbalanced currents are injected to balance the voltage, which will depend upon the equivalent grid impedance. The negative sequence currents to be injected in the point of common coupling are obtained from the

negative sequence virtual impedance. The internal negative sequence of the VSM may be equal to zero, coping so the steady-state behavior of the synchronous machine, or it can be the output of a negative sequence voltage controller with the objective to balance the local voltages.

4.3.3. Control strategies for Constant Active or Reactive Power

As previously explained, both active and reactive powers have an average value and sinusoidal and cosinusoidal components oscillating with double the frequency.

$$p = p_0 + p_{c2}\cos(2wt) + p_{s2}\sin(2wt) \quad 4.3.17$$

$$q = q_0 + q_{c2}\cos(2wt) + q_{s2}\sin(2wt) \quad 4.3.18$$

Where p_0, q_0 is the average value of the instantaneous active and reactive power and $p_{c2}, p_{s2}, q_{c2}, q_{s2}$ represent the magnitude of the oscillating terms. If represented in dq the active and reactive power will have the following equation as expressed in [19]:

$$p_0 = v_d^+ i_d^+ + v_q^+ i_q^+ + v_d^- i_d^- + v_q^- i_q^- \quad 4.3.19$$

$$p_{c2} = v_d^- i_d^+ + v_q^- i_q^+ + v_d^+ i_d^- + v_q^+ i_q^- \quad 4.3.20$$

$$p_{s2} = v_q^- i_d^+ - v_d^- i_q^+ - v_q^+ i_d^- + v_d^+ i_q^- \quad 4.3.21$$

$$q_0 = v_d^+ i_d^+ - v_q^+ i_q^+ + v_d^- i_d^- - v_q^- i_q^- \quad 4.3.22$$

$$q_{c2} = v_q^- i_d^+ - v_d^- i_q^+ + v_q^+ i_d^- - v_d^+ i_q^- \quad 4.3.23$$

$$q_{s2} = v_d^- i_d^+ - v_q^- i_q^+ + v_d^+ i_d^- + v_q^+ i_q^- \quad 4.3.24$$

To have constant active power we need to provide $p_{c2} = p_{s2} = 0$ hence the injected negative sequence currents can be calculated from the matrix below.

$$\begin{bmatrix} i_d^- \\ i_q^- \end{bmatrix} = \frac{-1}{(v_d^+)^2 + (v_q^+)^2} \begin{bmatrix} v_d^+ v_d^- - v_q^+ v_q^- & v_q^+ v_d^- + v_d^+ v_q^- \\ v_q^+ v_d^- + v_d^+ v_q^- & v_q^+ v_q^- - v_d^+ v_d^- \end{bmatrix} \begin{bmatrix} i_d^+ \\ i_q^+ \end{bmatrix} \quad 4.3.25$$

Additionally, to obtain constant reactive power we need to provide $q_{c2} = q_{s2} = 0$ and consequently the injected negative sequence currents can be calculated from eq 4.3.26.

$$\begin{bmatrix} i_d^- \\ i_q^- \end{bmatrix} = \frac{1}{(v_d^+)^2 + (v_q^+)^2} \begin{bmatrix} v_d^+ v_d^- - v_q^+ v_q^- & v_q^+ v_d^- + v_d^+ v_q^- \\ v_q^+ v_d^- + v_d^+ v_q^- & v_q^+ v_q^- - v_d^+ v_d^- \end{bmatrix} \begin{bmatrix} i_d^+ \\ i_q^+ \end{bmatrix} \quad 4.3.26$$

It is interesting to notice that equation 4.3.25 and equation 4.3.26 have opposite signs with respect to each other. This provides convenience in implementing and unifying the algorithm.

4.3.4. Control strategies for suppressing dc side voltage fluctuations

Under unbalanced voltages, there will be double frequency oscillations on the active power, which are propagated on the dc side as well. The dc-link capacitor of the HVDC affected by these oscillations will give rise to voltage fluctuation on the dc side and consequently if the oscillations are above a certain threshold a stable operation of the converter won't be possible. To mitigate this problem, it is needed to suppress the double frequency oscillations of the active power p_{c2}, p_{s2} to zero by injecting proper negative sequence currents. The injected negative sequence currents can be calculated using equation 4.3.27 as expressed in 4.3.26 but in this case, the power oscillations to be considered are between the converter and the LC filter because the filter may introduce a phase shift on the fundamental frequency of the voltage.

$$\begin{bmatrix} i_d^{-*} \\ i_q^{-*} \end{bmatrix} \quad 4.3.27$$
$$= \frac{-1}{(v_{cv,d}^+)^2 + (v_{cv,q}^+)^2} \begin{bmatrix} v_{cv,d}^+ v_{cv,d}^- - v_{cv,q}^+ v_{cv,q}^- & v_{cv,q}^+ v_{cv,d}^- + v_{cv,d}^+ v_{cv,q}^- \\ v_{cv,q}^+ v_{cv,d}^- + v_{cv,d}^+ v_{cv,q}^- & v_{cv,q}^+ v_{cv,q}^- - v_{cv,d}^+ v_{cv,d}^- \end{bmatrix} \begin{bmatrix} i_{cv,d}^+ \\ i_{cv,q}^+ \end{bmatrix}$$

If the converter is considered in steady-state than $v_{cv} = v_{cv}^{ref}$. This consideration gives different advantages. Firstly, new measurements aren't needed and secondly, the harmonic presented by the converter will not affect the control.

4.4 Power and current limitations

Strategies to limit the converter currents must be implemented for safe operation of VSCs. This limitation takes into account the intended dynamic and steady-state performance of the converter. The current limitations can be implemented in several ways, either included as a simple limitation of the current controller references, or it can be considered as a part of the power control strategies used to calculate the current references. Current limitation strategies acting directly on the instantaneous phase currents will however lead to distorted currents and voltages as shown in [20], thus current limitation is often implemented by limiting the amplitude of the current reference in the synchronous reference frame.

The physical current limitation of a Voltage Source Converter will always be given by the current capability of the converter legs corresponding to each phase. It is useful to see this projection of the phase current limitation in the stationary αβ reference frame as shown in Fig. 4.7. As distinguishable from the figure, the phase current limitations form a hexagon in the stationary αβ reference frame, given by the intersections between the straight lines corresponding to the limitations of the different phases. The blue trajectories show the vector current limitation under different unbalanced conditions. The black circle corresponds to the trajectory of balanced three-phase currents with an amplitude equal to the phase current limitation. Can be noticed that the maximum of different current trajectories is higher than the phase current limitation and this is acceptable as long that is inside the hexagon. But this current limitation implemented in a synchronous reference frame or based on vector amplitude consideration in the stationary reference frame is more complicated and goes beyond the purpose of this thesis hence the maximum current to be considered from this point on is Imax corresponding to the black circle.

The current limitation can be obtained indirectly by limiting the injected power into the grid as shown in [21]. The power limit is calculated from the converter current limit and the grid voltage sequence components by using the instantaneous power theory.

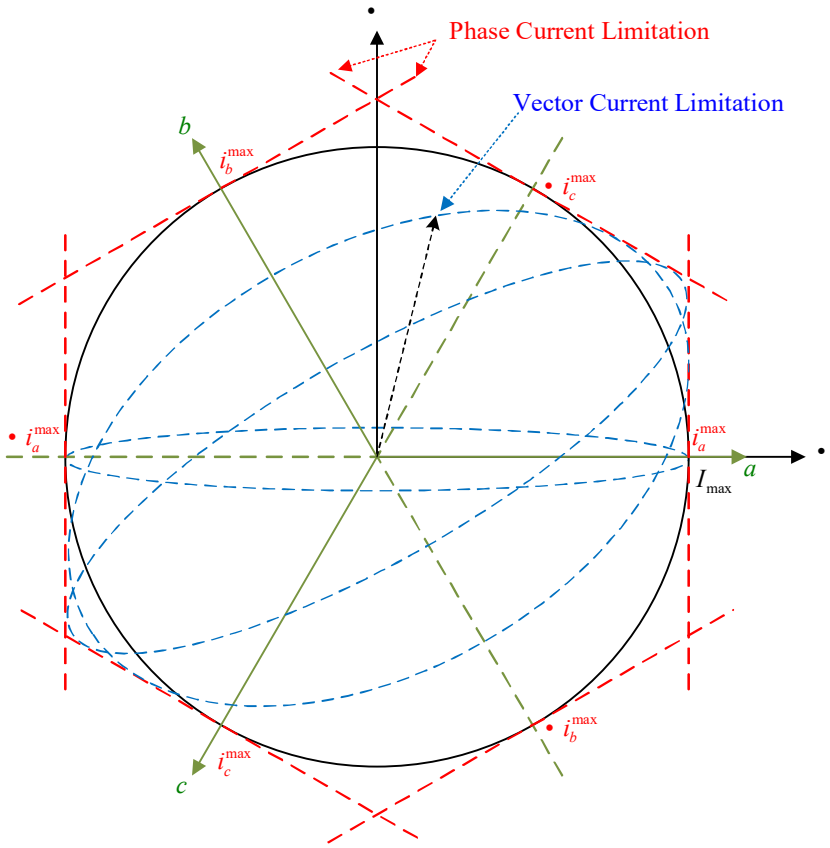

Fig. 4.7. Representation of the phase current limitation and vector current limitation in the SRF.

The maximum current is in the moment where the rotating positive sequence current vector is aligned with the negative sequence current vector which is rotating in the opposite direction. Therefore, the magnitude of the maximum current occurring at this moment is the sum of the positive and negative magnitudes of the sequences.

$$I_m = \sqrt{i_d^{+2} + i_q^{+2}} + \sqrt{i_d^{-2} + i_q^{-2}} \qquad 4.4.1$$

Under unbalanced conditions, the control has different purposes therefore the currents generated depend upon the strategy. To find the limiting power, the different strategies are considered separately.

4.4.1. When controlling for Constant Active Power:

the oscillating terms of the active power p_{c2}, p_{s2} are equal to zero. Hence the power equation is (4.4.2) and is possible to find the currents as shown in equation (3.5.3).

$$\begin{bmatrix} p_0 \\ q_0 \\ 0 \\ 0 \end{bmatrix} = \begin{bmatrix} v_d^+ & v_q^+ & v_d^- & v_q^- \\ v_q^+ & -v_d^+ & v_q^- & -v_d^- \\ v_q^- & -v_d^- & -v_q^+ & v_d^+ \\ v_d^- & v_q^- & v_d^+ & v_q^+ \end{bmatrix} \begin{bmatrix} i_d^+ \\ i_q^+ \\ i_d^- \\ i_q^- \end{bmatrix} \qquad 4.4.2$$

$$\begin{bmatrix} i_d^+ \\ i_q^+ \\ i_d^- \\ i_q^- \end{bmatrix} = \frac{p_0}{|v^+|^2 - |v^-|^2} \begin{bmatrix} v_d^+ \\ v_q^+ \\ -v_d^- \\ -v_q^- \end{bmatrix} + \frac{q_0}{|v^+|^2 + |v^-|^2} \begin{bmatrix} v_d^+ \\ -v_q^+ \\ v_d^- \\ -v_q^- \end{bmatrix} \qquad 4.4.3$$

By calculating I_m through the use of equation (4.4.1) and (4.4.3) the following is obtained:

$$I_m = \sqrt{\left(\frac{p_0}{|v^+|^2 - |v^-|^2}\right)^2 + \left(\frac{q_0}{|v^+|^2 + |v^-|^2}\right)^2} \left(|v^+| + |v^-|\right) \qquad 4.4.4$$

I_{max} is the permissible peak current of the converter which should be set below the overcurrent protection threshold to avoid the risk of overcurrent shutdown of the converter. The reference power limits will depend on I_{max} and the voltage sequence components as shown in equation (4.4.5). However, equation (4.4.5) cannot generate the active and reactive power limitations due to two unknown parameters (active power limit P_{lim} and reactive power limit Q_{lim}) in only one function.

$$\sqrt{\left(\frac{P_{lim}}{|v^+|^2 - |v^-|^2}\right)^2 + \left(\frac{Q_{lim}}{|v^+|^2 + |v^-|^2}\right)^2} = \frac{I_{max}}{\left(|v^+| + |v^-|\right)} \qquad 4.4.5$$

Under unbalanced conditions that may be caused by voltage sages, the VSM provides power support for the power grid. Depending on the grid there can be required higher reactive or active power demand. To provide frequency support the active power has the priority hence the reactive power will be expressed as a function of the active power.

$$Q_{lim} = kP_{lim} \qquad for \quad 0 \leq k \leq 1 \qquad 4.4.6$$

Then the power reference limitation for constant active power can be determined by solving equation (4.4.5) and (4.4.6).

$$\begin{cases} Q_{lim} = kP_{lim} \\ P_{lim} = \dfrac{I_{max}(\ |v^+| - |v^-|)\left(|v^+|^2 + |v^-|^2\right)}{\sqrt{k^2\left(|v^+|^2 - |v^-|^2\right)^2 + \left(|v^+|^2 + |v^-|^2\right)^2}} \end{cases} \quad 4.4.7$$

It can be proven that:

$$\frac{1.5(\ |v^+|^2 + |v^-|^2)}{\sqrt{k^2(\ |v^+|^2 - |v^-|^2)^2 + (\ |v^+|^2 + |v^-|^2)^2}} > 1 \qquad for \quad 0 \le k \le 1 \quad 4.4.8$$

Now equation (4.4.7) can be rewritten as:

$$\begin{cases} Q_{lim} = kP_{lim} \\ P_{lim} = \dfrac{I_{max}(\ |v^+| - |v^-|)}{1.5} \end{cases} \quad 4.4.9$$

Using equation (4.4.9) instead of (4.4.7) gives us two advantages. Firstly, there is a higher margin for overcurrent protection which is needed due to small disturbances or inaccuracies, and secondly, the equation obtained is easier to implement and it reduces the computational power needed in practical implementations.

4.4.2. When controlling for Constant Reactive Power:

the oscillating terms of the reactive power q_{c2}, q_{s2} are equal to zero. Consequently, equation (4.4.2) which was previously used for calculating the constant active power is changed to equation (4.4.10). From the last one the current components are calculated so that the maximum current I_m can be found.

$$\begin{bmatrix} p_0 \\ q_0 \\ 0 \\ 0 \end{bmatrix} = \begin{bmatrix} v_d^+ & v_q^+ & v_d^- & v_q^- \\ v_q^+ & -v_d^+ & v_q^- & -v_d^- \\ v_q^- & -v_d^- & v_q^+ & -v_d^+ \\ -v_d^- & -v_q^- & v_d^+ & v_q^+ \end{bmatrix} \begin{bmatrix} i_d^+ \\ i_q^+ \\ i_d^- \\ i_q^- \end{bmatrix} \quad 4.4.10$$

$$\begin{bmatrix} i_d^+ \\ i_q^+ \\ i_d^- \\ i_q^- \end{bmatrix} = \frac{p_0}{|v^+|^2 + |v^-|^2} \begin{bmatrix} v_d^+ \\ v_q^+ \\ -v_d^- \\ -v_q^- \end{bmatrix} + \frac{q_0}{|v^+|^2 - |v^-|^2} \begin{bmatrix} v_d^+ \\ -v_q^+ \\ v_d^- \\ -v_q^- \end{bmatrix} \quad 4.4.11$$

$$I_m = \sqrt{\left(\frac{p_0}{|v^+|^2 + |v^-|^2}\right)^2 + \left(\frac{q_0}{|v^+|^2 - |v^-|^2}\right)^2}\,(|v^+| + |v^-|) \qquad 4.4.12$$

$$\sqrt{\left(\frac{P_{lim}}{|v^+|^2 + |v^-|^2}\right)^2 + \left(\frac{Q_{lim}}{|v^+|^2 - |v^-|^2}\right)^2} = \frac{I_{max}}{(|v^+| + |v^-|)} \qquad 4.4.13$$

With equation (4.4.13) the new limits for constant reactive power control strategy are found, with I_{max}as the maximum permissible current for a safe operation of the converter. As previously mentioned equation (4.4.13) cannot be solved with two unknowns. Hence the reactive power is expressed as a function of the active power as shown in equation (4.4.6). Having now two equations the power limits are found.

$$\begin{cases} Q_{lim} = kP_{lim} \\ P_{lim} = \dfrac{I_{max}(\,|v^+| - |v^-|)\left(|v^+|^2 + |v^-|^2\right)}{\sqrt{k^2\left(|v^+|^2 + |v^-|^2\right)^2 + \left(|v^+|^2 - |v^-|^2\right)^2}} \end{cases} \qquad 4.4.14$$

Equation (4.4.14) is not suitable for practical implementation. By considering equation (4.4.14) and (4.4.15) is obtained equation (4.4.16) which is more suitable than (4.4.14) for practical application and has a higher margin from the overcurrent protection of the converter.

$$\frac{1.5(|v^+|^2 + |v^-|^2)}{\sqrt{k^2(|v^+|^2 + |v^-|^2)^2 + (|v^+|^2 - |v^-|^2)^2}} > 1 \qquad for \quad 0 \le k \le 1 \qquad 4.4.15$$

$$\begin{cases} Q_{lim} = kP_{lim} \\ P_{lim} = \dfrac{I_{max}(\,|v^+| - |v^-|)}{1.5} \end{cases} \qquad 4.4.16$$

4.4.3. When controlling Balanced Currents:

The negative sequence current becomes zero. Hence the power equation is (4.4.17) and is possible to find the currents as shown in equation (4.4.18).

$$\begin{bmatrix} p_0 \\ q_0 \end{bmatrix} = \begin{bmatrix} v_d^+ & v_q^+ & v_d^- & v_q^- \\ v_q^+ & -v_d^+ & v_q^- & -v_d^- \end{bmatrix} \begin{bmatrix} i_d^+ \\ i_q^+ \end{bmatrix} \quad 4.4.17$$

$$\begin{bmatrix} i_d^+ \\ i_q^+ \end{bmatrix} = \frac{p_0}{|v^+|^2} \begin{bmatrix} v_d^+ \\ v_q^+ \end{bmatrix} + \frac{q_0}{|v^+|^2} \begin{bmatrix} v_q^+ \\ -v_d^+ \end{bmatrix} \quad 4.4.18$$

It can be noticed that the negative sequence current components do not appear in the two equations above. Thus the maximum current I_m is a function of the positive sequence.

$$I_m = \sqrt{i_d^{+2} + i_q^{+2}} \quad 4.4.19$$

And I_m is equal to:

$$I_m = \frac{1}{|v^+|} \sqrt{(p_0)^2 + (q_0)^2} \quad 4.4.20$$

Knowing the positive sequence voltage and the allowable maximum current I_{max} for which a safe operation of the converter is ensured, it is possible to find the power reference limits:

$$\sqrt{(P_{lim})^2 + (Q_{lim})^2} = I_{max} |v^+| \quad 4.4.21$$

Expressing the reactive power as a function of the active power through equation (4.4.6), the power reference limits are obtained as:

$$\begin{cases} Q_{lim} = kP_{lim} \\ P_{lim} = \dfrac{I_{max}|v^+|}{\sqrt{k^2+1}} \end{cases} \quad 4.4.22$$

$$\frac{1.5}{\sqrt{k^2+1}} > 1 \qquad for \quad 0 \le k \le 1 \quad 4.4.23$$

$$\begin{cases} Q_{lim} = kP_{lim} \\ P_{lim} = \dfrac{I_{max}|v^+|}{1.5} \end{cases} \quad 4.4.24$$

Considering equation (4.4.23), new power reference limits are found as shown in equation (4.4.24). It is worth mentioning that I_{max} depends on the converter and the power limitation depends on the control strategy. In the case of constant active or reactive power,

the reference power limitation is a function of ($|v^+| - |v^-|$) and when balanced current are controlled the reference power limitation is a function of $|v^+|$. It can be noticed for the last one that the power limitation is going to be higher, therefore when balanced currents are used as a control strategy there will be maximum power transfer from the converter side to the grid side. This result can be intuitively understood as follows. When there are both positive and negative sequences of the current, the energy propagates from the converter to the grid using the positive sequence currents and from the grid to the converter using the negative sequence currents. In case there is just the positive sequence, all the 'available' current is used to propagate the energy from the converter to the grid, therefore resulting in the maximum power transfer.

4.4.4. When controlling with negative sequence virtual impedance or negative sequence voltage controller:

A simpler path with respect to the previous ones is used. The apparent power can be expressed as a function of the voltage and current amplitudes, equation (4.4.25). Hence the limit apparent power under unbalanced condition is a function of the maximum allowable current and the magnitude of the unbalanced voltage. The magnitude of the voltage under unbalanced conditions oscillates from $|v^+| + |v^-|$ to $|v^+| - |v^-|$. In *Fig. 4.8* is shown an unbalanced voltage condition with a resistive load and an inductive load, the magnitudes of the current and voltages for this conditions and the apparent power calculated by the equation (4.4.25). The limit apparent power for a resistive load where the angle between the voltage and current is 0˚ will depend on the maximum allowable current and maximum magnitude of the unbalanced voltage (this case can be seen at t=0.01). On the other hand, the limit apparent power for an inductive load where the angle between the voltage and current is 90˚ will depend on the maximum allowable current and minimum magnitude of the unbalanced voltage (this case can be seen at t=0.045). In this thesis is not going to be considered the load angle meaning that for the apparent power the worst case is considered and is calculated as shown in equation (4.4.26).

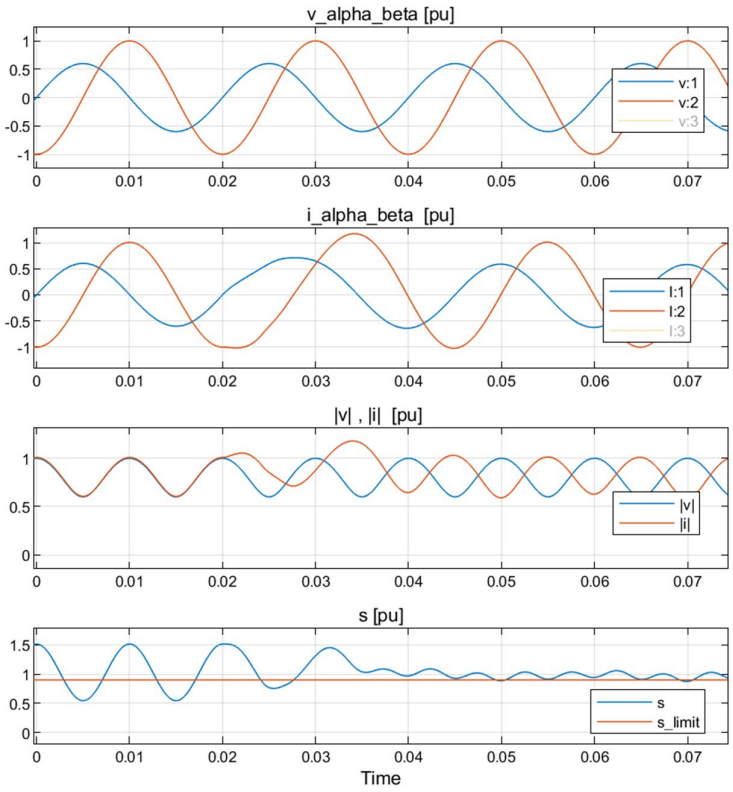

Fig. 4.8. Unbalanced voltage conditions and apparent power limitation.

The limited apparent power can be also expressed as in equation (4.4.27). Combining equation (4.4.26) with (4.4.27) is obtained equation (4.4.28).

$$s = \frac{3}{2}|v||i| \tag{4.4.25}$$

$$s_{Lim} = \frac{3}{2}(|v^+| - |v^-|)\, I_{max} \tag{4.4.26}$$

$$s_{Lim} = \sqrt{{P_{Lim}}^2 + {Q_{Lim}}^2} \tag{4.4.27}$$

$$\sqrt{(P_{lim})^2 + (Q_{lim})^2} = \frac{3}{2}(|v^+| - |v^-|)\, I_{max} \tag{4.4.28}$$

Expressing the reactive power as a function of the active power as shown in equation (4.4.6), the reference power limits are obtained as follows:

$$\begin{cases} Q_{lim} = kP_{lim} \\ P_{lim} = \frac{1.5(|v^+|-|v^-|)\, I_{max}}{\sqrt{k^2+1}} \end{cases} \quad for \quad 0 \le k \le 1 \qquad 4.4.29$$

By neglecting $\frac{1.5}{\sqrt{k^2+1}}$ the equation is simplified as:

$$\begin{cases} Q_{lim} = kP_{lim} \\ P_{lim} = (|v^+| - |v^-|)\, I_{max} \end{cases} \qquad 4.4.30$$

It is worth noticing that the active power reference limitation is limiting the virtual input power (p^{r*}) of the swing equation in the VSM and not the external reference set-point (see VSM inertia emulation in chapter 2). When the converter is in islanded mode the frequency droop may increase the power above the limit therefore the limitation has to take place after the frequency droop.

4.5 Simulation of VSC as VSM under unbalanced conditions

In this part of the chapter is presented the control and the response of a two-level VSC controlled as a VSM operating under unbalanced conditions. Simulations of different control strategies with different scenarios are done through the means of Matlab/Simulink/SimPowerSystem environment. The investigated strategies are: Balanced Three Phase Currents, Constant Active Power, Constant Reactive Power, Negative Sequence Virtual Impedance, Negative Sequence Voltage Control, Reduced dc side Power Fluctuations. These simulations are conducted not just in a wide range of grid conditions but also under islanded mode to evaluate the performance and applicability of all the presented control strategies. Further, inspection is done for current and power limitation and validation of the VSM inertial response behavior under unbalanced conditions

4.5.1. Configuration and control

The configuration taken into account is expressed in the figure where the VSC has as input the dc side voltage and provides ac voltage as an output. The voltage of the converter passes through an LC filter which reduces the harmonic content of the voltage waveforms and is feed into the grid.

The VSC is controlled through the control scheme shown in Fig. 4.10. Elements of this control scheme are:

- Simulated Synchronous Machine Model (see chapter 3)
    - Frequency Control
    - Inertia Model
    - Positive Sequence electrical model (Positive Sequence Virtual Impedance)
    - Voltage Control
- Phase Lock-Loop (see section 3.3.2)
- Proportional-Resonant Current Controller (see section 3.6.2)
- Active Damping (see section 3.7)
- Pulse Width Modulation (PWM)
- Negative Sequence Current Generator Fig. 4.9(see section 4.3)
- Measurement processing and sequence separation (see section 4.2)

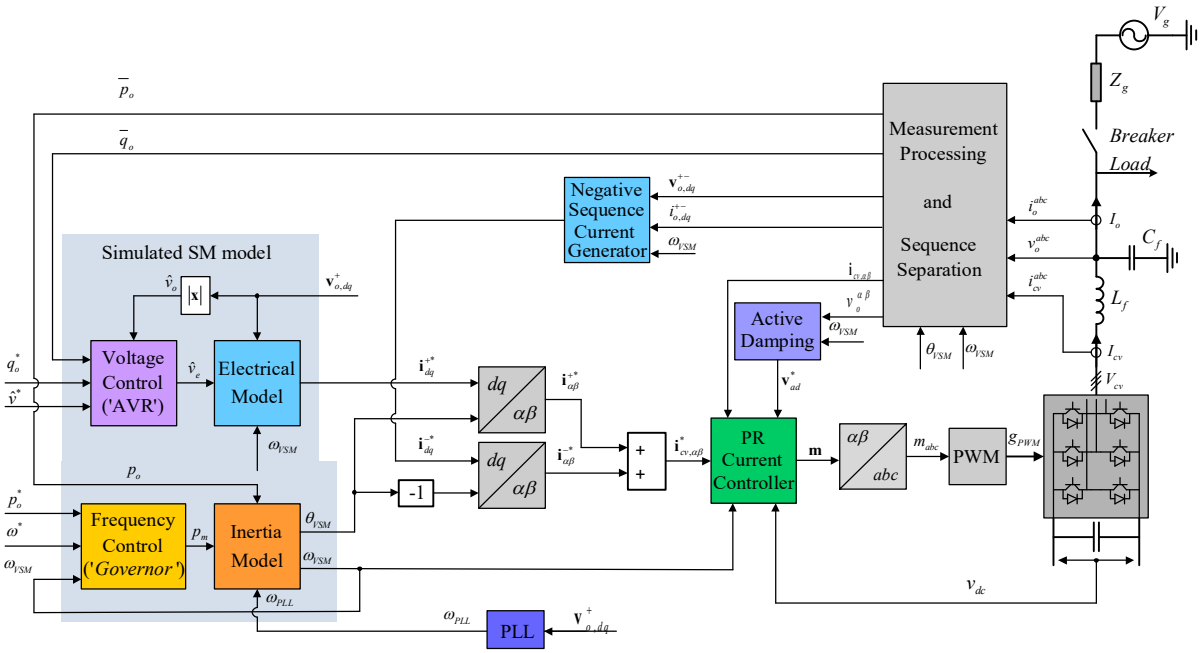

Fig. 4.10. Overview of the CCVSM-based control strategy for unbalanced grid-connected and islanded operation.

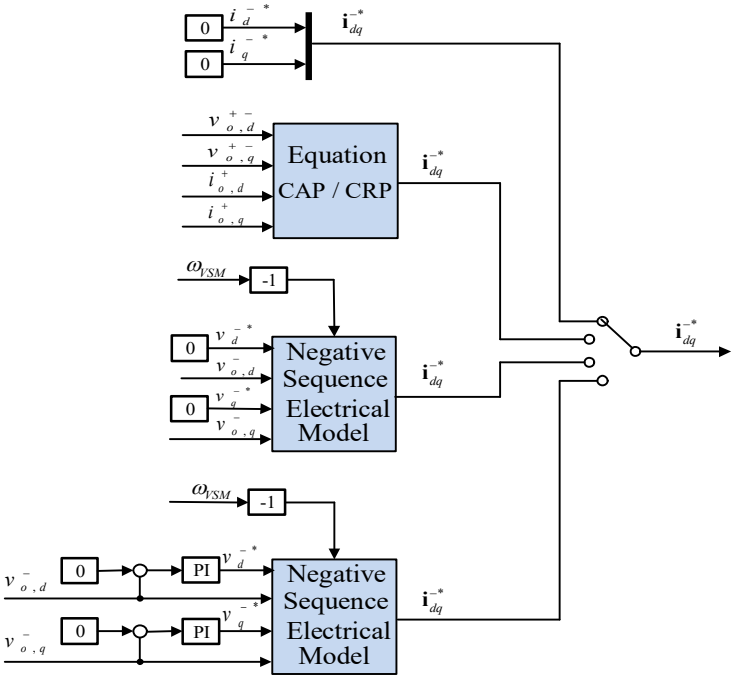

Fig. 4.9. Flexible selection of control objectives for negative sequence current references.

The parameters used for the configuration and the control are shown in Table II

Table II: Parameters of the Investigated System Configuration

Parameter	Value	Parameter	Value
AC Voltage $V_{ll,g,n}$	400 V	Rated current	72 A
Rated angular frequency ω_n	2π·50 Hz	Primary filter inductance l_f , r_{lf}	0.08pu, 0.008pu
DC voltage V_{dcn}	686 V	Filter capacitance c_f	0.079 pu
Active damping k_{SOGI}, k_{AD}	√2, 0.5 pu	Grid-side filter inductance l_g, r_g	0.2pu, 0.01pu
Current controller gains, kpc,kic	1.2 0.8	DSOGI-QSGs for sequence separation k_{SOGI}	√2
VSM Positive Seq. Impedance, r_v^+, l_v^+	0.01 pu 0.2 pu	PLL PI controller, $k_{p,PLL}$, $k_{i,PLL}$	2, 70
VSM Negative Seq.Impedance, r_v^-, l_v^-	0.01 pu, 0.2 pu	Negative sequence voltage control, $k_{p,NS}$, $k_{i,NS}$	0.1, 5
Virtual inertia Ta	10 s	VSM damping k_d	200 pu
Frequency droop k_ω	20 pu	Reactive power droop k_q	0 pu

4.5.2. Transient response under unbalanced conditions

The performances of the proposed control strategies for controlling the unbalanced conditions are investigated in a transient response to a 25% unbalanced voltage sag and 100% unbalanced voltage sag thus considering a mild and a severe fault. For the first one together with the transient responses are verified also the inertial responses for power and frequency.

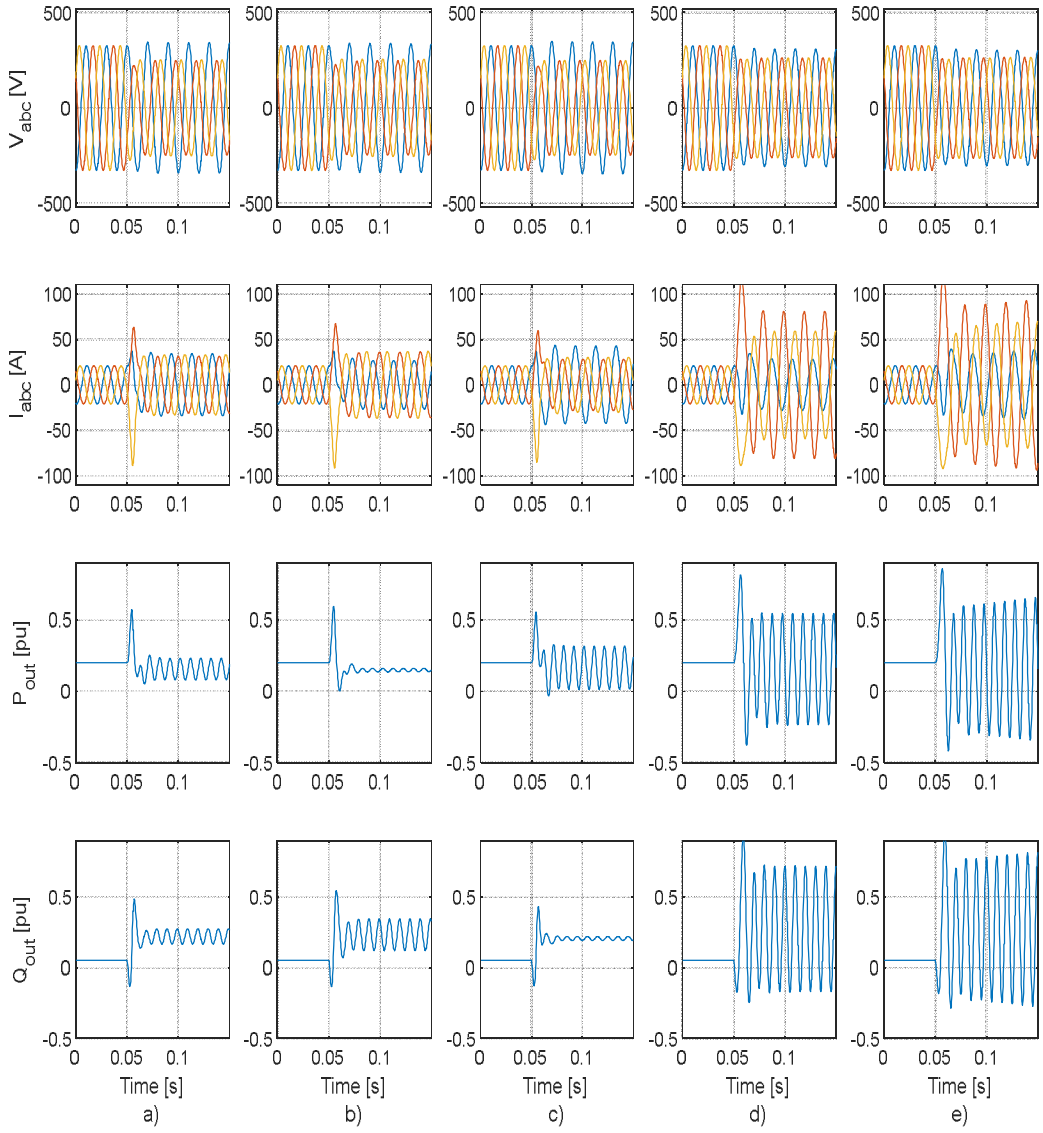

Fig. 4.11. Simulation results in grid-connected mode showing the transient response to an unbalanced voltage sag occurring at t=0.05 a) Balanced positive sequence currents b) Constant active power c) Constant reactive power, d) Negative sequence virtual impedance e) Negative sequence voltage controller.

As the first test, the CCVSM (Current Controlled Virtual Synchronous Machine) is exposed to an unbalanced in the grid voltage. The unbalanced created is 0.8 p.u. for the positive sequence and 0.2 p.u. for the negative sequence of the voltage, resulting in a grid voltage with 25% unbalanced ($|v^-|/|v^+| = 0.2/0.8 = 0.25$). In Fig. *4.11*) are shown the active and reactive power and the three phase currents and voltages measured at the point of

common connection (PCC). To make a better comparison between the control strategies some quantitative parameters are going to be considered.

When controlling balanced currents Fig. *4.11*.a) after the unbalanced voltage sags transient, the control keeps under 3% of the current unbalanced ($|i^-|/|i^+|$). As for the voltage unbalance, it is kept at 23%. There is a small reduction coming from the control since the reactive power increases and consequently, the positive sequence voltage magnitude is increased. But there is no noticeable change since the control objectives are not the voltage unbalance. It has to be mentioned that in order to limit the reactive power flow during voltage sags, $\hat{v}_e$ is also limited to be within ± 0.05 p.u. of the actual measured positive sequence voltage, such that $0.95|\mathbf{v}_o^+| < \hat{v}_e < 1.05|\mathbf{v}_o^+|$. As expected the active and reactive power will have an average power and double frequency oscillations. Respectively the power oscillations are 0.13 p.u. and 0.12 p.u.

When controlling constant active power Fig. *4.11*.b) the negative sequence currents injected into the grid reduces the oscillations of the active power. It can be noticed that the negative sequence currents increase in value with respect to the previews control and now has 20% of current unbalance. Meanwhile, the voltage unbalanced factor is at 22%. The active power oscillation is not perfectly constant since to generate the current are used the measurements at the PCC as for feedback for controlling the current, the output current of the converter is used. A small current passes through the capacitor of the LC filter so the current before and after the filter is not the same. Even though the generated current to keep constant active power is not exactly equal to the controlled current, the active power oscillations have a value of 0.01p.u.

When utilizing constant reactive power Fig. *4.11*.c) as a control strategy the negative sequence current generator produces the currents. These current components reduce the cosinusoidal and sinusoidal terms of the reactive power (measured at the PCC) to zero. Under this strategy and for the simulated case the voltage unbalanced factor is 24% and the current unbalanced factor is 26%.

When controlling the negative sequence currents through the use of the negative sequence impedance the response under an unbalanced condition is shown in Fig. *4.11*.d). For this strategy the voltage unbalanced factor is 12% and the current unbalanced factor is 75%. It is noticeable that very high unbalances in the current had to be created to reduce the

voltage unbalance. This result depends strictly on the grid equivalent impedance. For a strong grid and a low grid equivalent impedance, the needed currents to reduce the unbalanced are very high and the reverse also holds true.

When using the negative sequence voltage control strategy the results are shown in Fig. *4.11*.e). By introducing the closed loop control for eliminating the voltage unbalanced achieving an unbalanced factor of 0%, the unbalanced of the three phase currents is further

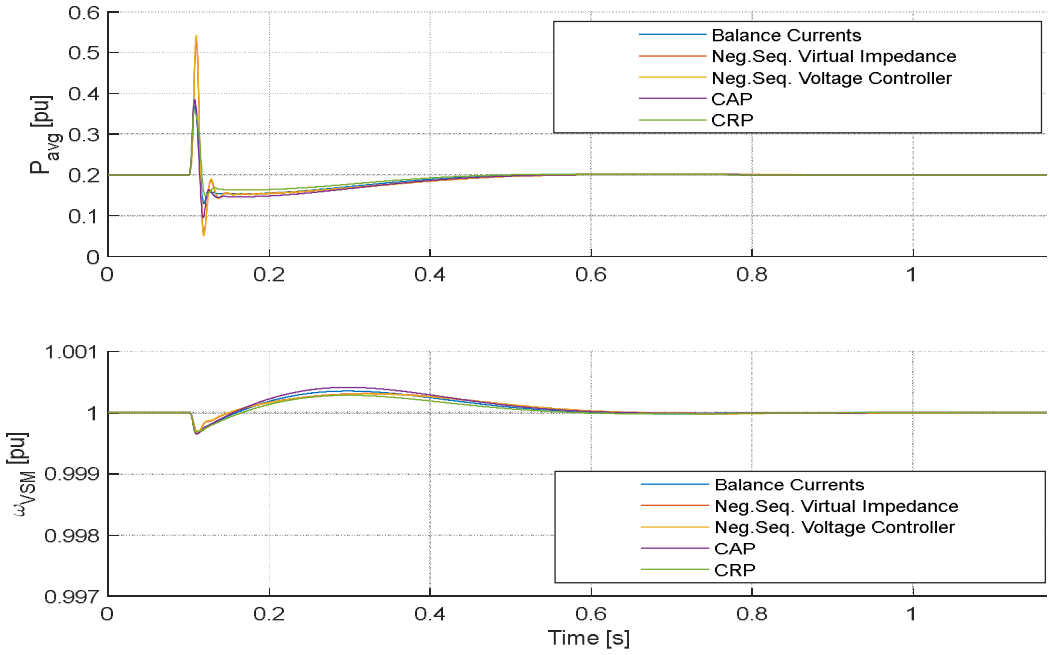

Fig. 4.12. Comparison of inertial response to an unbalanced voltage sag

increased. Relatively slow response of the balancing controller can also be seen from the figure resulting in achieving a voltage unbalanced factor of 0%, meaning three phase balanced voltages. It can be also noticed that in this last two controls the active and reactive power have higher oscillations due to the high increase in the unbalanced currents.

It is important to show that during this unbalanced voltage sag is kept the inertial response of the VSM Fig. 4.12. Between the different simulated cases, there are small differences in the initial transient of the average active power flow due to the negative sequence currents. The small differences in the average active power flow influence also the

VSM speed. After a transient determined by the inertia model, the power is controlled back to the reference value, and ω_{VSM} returns to the grid frequency.

To provide support to the grid during a severe fault is fundamental for all the generating units in the transmission system. In Fig. 4.13 is shown the transient when a severe fault occurs. The fault is generated by the grid where the grid voltage is 0.5 of positive sequence and 0.5 of negative sequence, thus resulting in a simulation done with 100% of voltage unbalance. It can be noticed that the voltage in all the control strategies does not change visibly, since the grid is strong and has a low equivalent grid impedance. It can also be noticed the difference in the current between the first three controls and the last two. The first three control strategies control the power flow, since the power limitation limits the

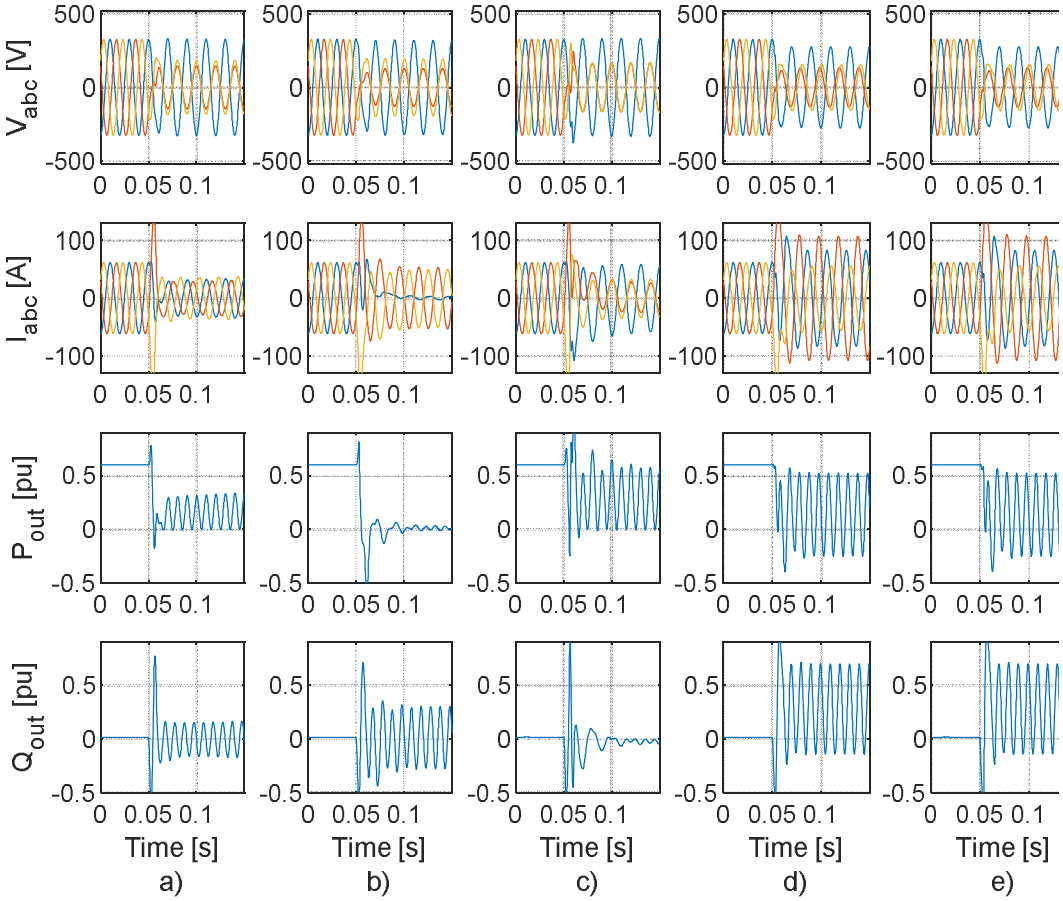

Fig. 4.13. Simulation results in grid-connected mode showing the transient response to an unbalanced voltage sag occurring at t=0.05 with 100% of voltage unbalanced factor a) Balanced positive sequence currents b) Constant active power c) Constant reactive power, d) Negative sequence virtual impedance e) Negative sequence voltage controller.

power transfer the current does not reach the maximum allowable current. On the other hand, when the current comes from the Negative Sequence Virtual Impedance the current reference is limited to the maximum allowable current.

4.5.3. Current and power limitation

For the same case as shown in the previews section is possible to identify the power delivered during a severe unbalanced condition. In *Fig. 4.14* is shown the transient when changing the control strategy from Constant Active Power (CAP) to Balanced Positive Sequence Currents (BPSC). When CAP is used the reference power is limit to zero and it can be seen that the output power is zero. Meanwhile, BPSC has a higher power that is injected into the grid and is able to keep balanced currents. It can be seen that the voltage unbalanced does not change and is noticeable that the power transfer during BPSC is higher and the currents are balanced which makes this strategy the preferred one when severe faults affect the grid.

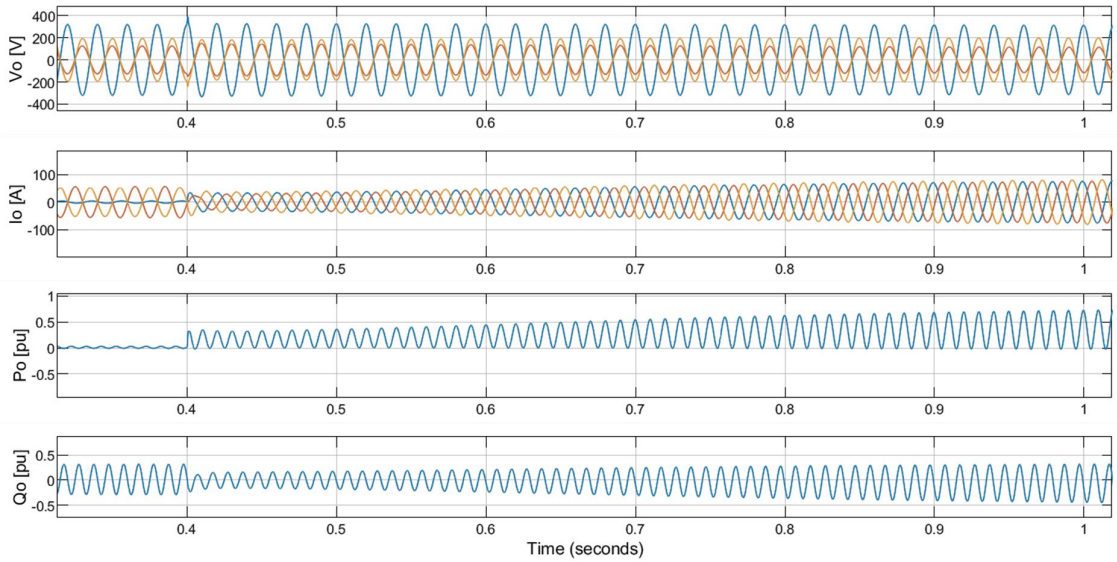

Fig. 4.14. Simulation results in grid-connected mode with 100% of voltage unbalanced factor showing the transient when passing from CAP to BPSC control strategy

4.5.4. Reducing the dc side power fluctuations

As identified previously, it is possible to suppress the dc side voltage fluctuations by reducing the oscillations on the dc side power. This last one is achieved in a VSC by reducing the oscillations in the active power on the ac side. Considering a case with 25% of

unbalanced voltage factor, it is possible to show how the system behaves for such control. At time t=0s an unbalanced in the grid side occurs which can be seen in the voltage measurement from *Fig.4.15*. The dc side power after a transient with a settling time of 25ms, achieves a constant value thus reducing the dc side voltage oscillations. It can be also seen that for the same control strategy the active power oscillations in the output of the converter are reduced as well.

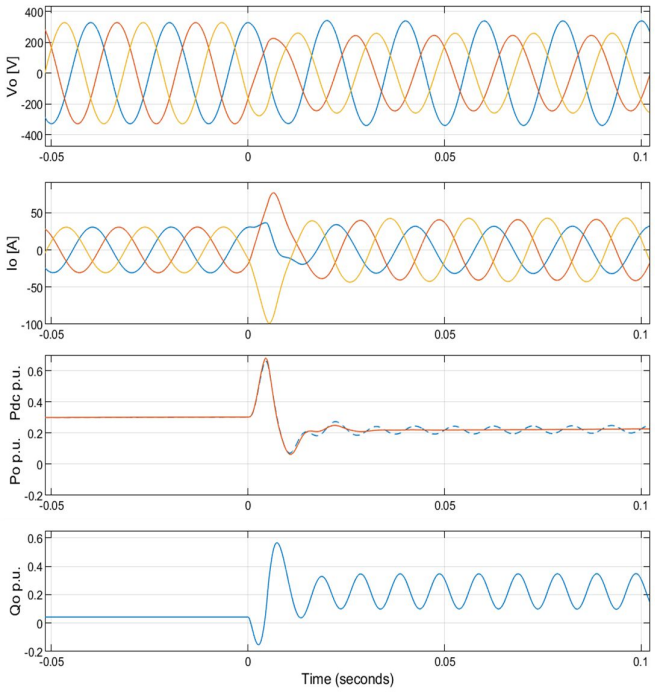

Fig.4.15. Control strategy results for keeping constant DC power oscillations P_{DC} (——) P_o (- - -)

4.5.5. Transient response when islanding under unbalanced conditions

In this section, the control strategies performance is investigated for islanded operation. The test is important since we are considering a VSM-based control for which the capability to operate as grid forming (consequently islanded operation) is a key feature. Therefore, driving the converter disconnected from the grid under unbalanced conditions is

of paramount importance. Simulation results are shown both for the transient when islanding operation occurs and the inertial response that the VSM provides.

In this case, the converter is subject to an unbalanced local load with a total power demand of 0.5 pu at rated voltage. The unbalanced is created by adding another load between phase a and b with half the impedance of the initial delta-connected load. The studied control strategies are exposed to an islanding transient by switching the breaker indicated in Fig. 4.10 from closed to open position. The response of the islanding transient is presented in Fig. 4.16. for all the simulated control strategies. As clearly shown by the results in Fig. 4.16 a), b) and c), the cases where the negative sequence current references are directly specified to shape the power flow characteristics are not suitable for islanded operation. Indeed, all these three strategies are generating over-voltages in the phase with the lowest load. The case with balanced three phase currents is even increasing the amplitude of the local negative sequence voltage to 0.4 pu, while the case with constant active power is maintaining a negative sequence voltage in the range of 0.2 pu. The case with CRP is even resulting in an uncontrolled increase in the negative sequence voltage, and a significant increase in the total average load power due to the increased voltage, but without being able to eliminate the reactive power oscillations. Thus, even if operation with BPSC, CAP, and CRP can be suitable for operation in strong grids, these control functions should be immediately disabled when transitioning into an islanded mode.

The response to the islanding transient for the case with virtual impedance defining the negative sequence currents is shown in Fig. 4.16 d). In this case, the transient response to the islanding is smooth and fast, with the resulting negative sequence currents contributing to the balancing of the load voltage. The resulting amplitude of the negative sequence voltage is then reduced to 0.04 pu. However, since the negative sequence currents are resulting from the virtual impedance, they cannot fully compensate for the unbalanced caused by the load.

Finally, Fig. 4.16 e) shows the results with the closed loop control for eliminating the voltage unbalance. As expected, this strategy can maintain balanced three phase voltages independently of the unbalance in the load resistance. Indeed, the negative sequence currents resulting from this control strategy in steady-state operation correspond to the currents that would result from feeding the load with a balanced three phase voltage source. It is also noted that both these strategies provide unbalanced currents to the local unbalanced load also

before the islanding. Thus, the grid is (partially) relieved from supplying unbalanced currents to the unbalanced local load.

A comparison of the response in average active power and virtual speed of the VSM after islanding with the unbalanced load is presented in Fig. 4.17. As shown in the figure, the cases with balanced currents or constant active power are not able to maintain the desired average voltage of the load, which is resulting in reduced power provided to the resistive load. Thus, the frequency droop control is also resulting in a higher steady-state frequency than when the load voltage is maintained close to the rated value. The case with constant reactive power is instead resulting in a significant increase of the load power and a corresponding reduction in the steady-state frequency. This further confirms how this control strategy is unsuitable for operation in islanded mode.

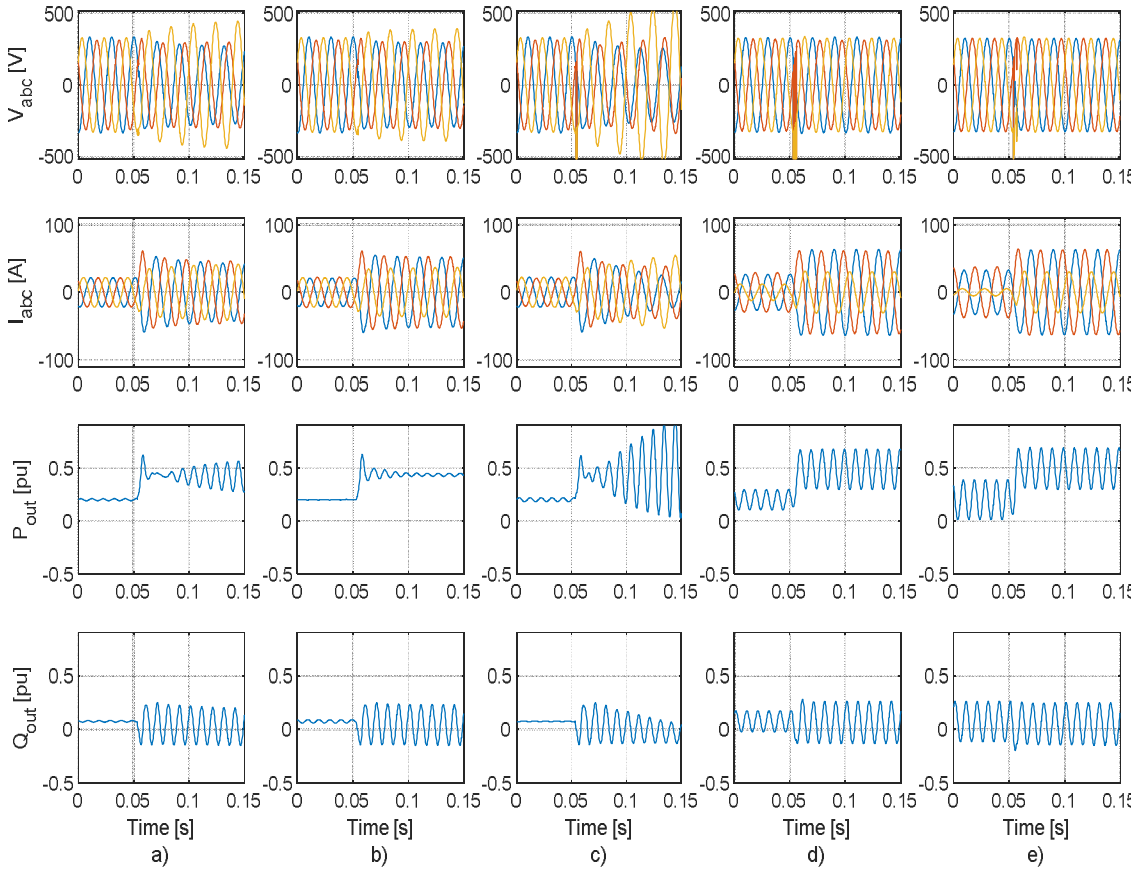

Fig. 4.16. Simulation results show the transient to sudden islanding occurring at t=0.05 when connected to an unbalanced local load a) Balanced positive sequence currents b) Constant active power c) Constant reactive power, d) Negative sequence virtual impedance e) Negative sequence voltage controller.

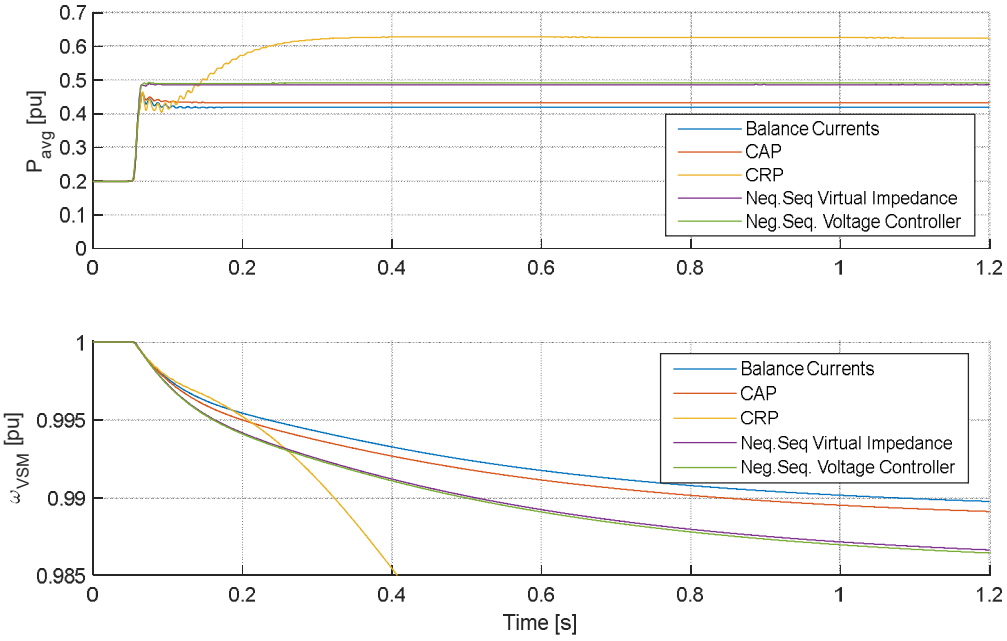

Fig. 4.17. Comparison of response to the transition from grid-connected operation to islanded mode with an unbalanced load

The case with negative sequence voltage control results in the expected load power of 0.5 pu and a corresponding droop effect in the frequency. The results for the case with only a negative sequence virtual impedance are also very close to the case with closed loop balancing of the voltage.

4.5.6. Inertial responses upon different perturbations

In this section are presented the capabilities of the VSM to provide virtual inertia under unbalanced conditions. Simulations are done both in grid connected and islanded operation. In grid connected operation the simulated perturbations are in the converter power reference and perturbation in the grid side frequency. On the other hand, in islanded operation is simulated a perturbation in the local load.

The CCVSM is exposed to a step in the active power reference of 0.3 pu and a step in the grid frequency of −0.002 pu, as shown in Fig. 4.18 a) and b), respectively. As a point of reference, these figures also include a case with balanced grid voltages. The results show some minor differences in the average power during the transients, which results in corresponding differences in the VSM speed. However, these differences are very small, demonstrating that the influence from the negative sequence current control on the inertial dynamics of the VSM swing equation is limited when operating in grid-connected mode.

The results in Fig. 4.19, show the response to a change of the local load under unbalanced islanded operation. In this figure, the cases with constant active or reactive power are not included since the operation with these control strategies is unacceptable. A case with the initial balanced load is also included as a point of reference. The figure shows how the case with balanced three phase currents results in a total average load close to the case with balanced loads since no additional current is provided to the phases with increased load. The load power and the steady-state frequency of the case with negative sequence virtual impedance is almost identical to the case with closed loop control of the voltage. Indeed, these

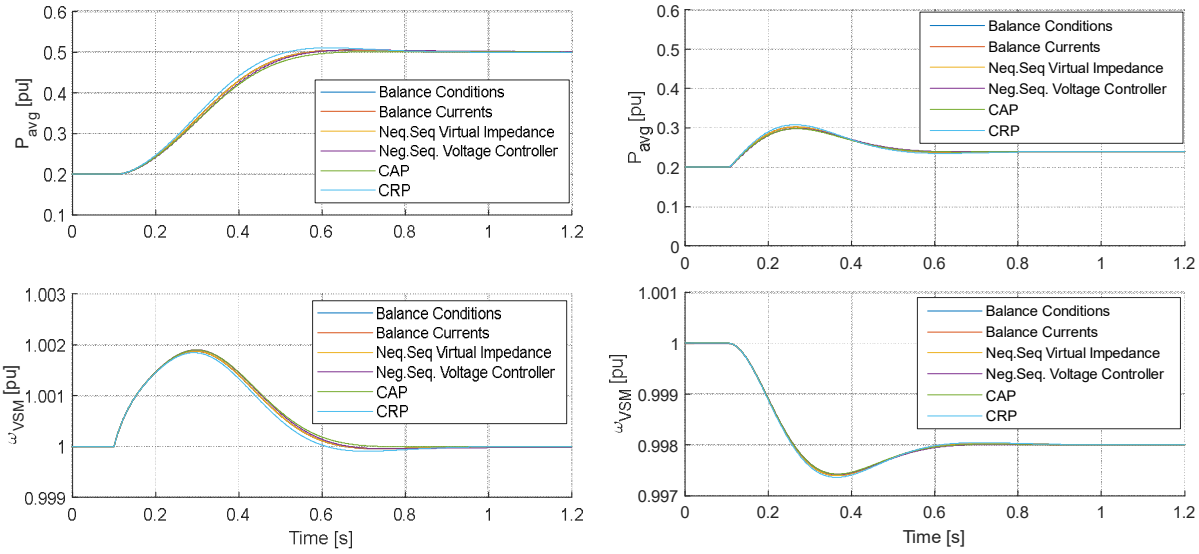

Fig. 4.18. Comparison of responses under unbalanced voltage conditions to a step: a) increase of 0.3 pu in the power reference at t= 0.1 s b) decrease of 0.1 Hz (=0.002 pu) in the grid frequency at t = 0.1 s

two strategies are the only cases providing reasonable performance for operation in islanded mode with unbalanced loads.

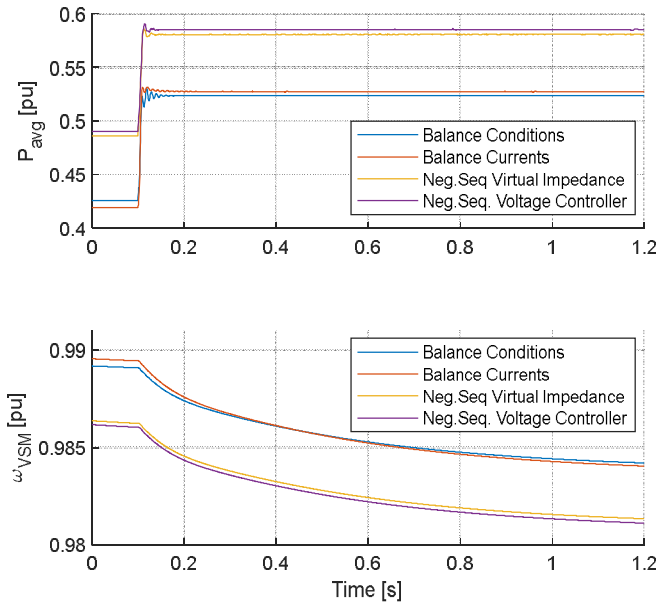

Fig. 4.19. Response to a step increase of the load by 0.1 pu at t=0.1 s under unbalanced conditions

4.6 Conclusion

In this chapter have been evaluated the options for operating a current controlled Virtual Synchronous Machine (CCVSM) under unbalanced conditions and are shown the performance in both grid-connected and islanded modes. Six different strategies for controlling the negative sequence currents are identified, balanced three phase currents, constant active power, constant reactive power, reducing the dc side oscillations, negative sequence virtual impedance, and closed loop control on the negative sequence voltage. Their performance is assessed by time-domain simulations. The simulation results clearly show how the control strategies based on the calculation of the negative sequence current references for shaping the power flow characteristics are only suitable for grid-connected

operation. Thus, if any of these strategies are preferred for grid-connected operation, they should be immediately disabled in case of transitioning to islanded mode. Operation with a negative sequence virtual impedance results in a similar steady-state response to unbalances as would result from a synchronous machine and can ensure stable operation in both grid-connected and islanded operation. However, this approach will not fulfill any specific objectives of shaping the power flow characteristics or balancing of the voltage. Closed loop control of the negative sequence components for balancing the local voltages is suitable for islanded operation with unbalanced local loads. Although this approach also can be utilized for grid-connected operation in weak grids with high equivalent impedance, the controllers will saturate if the system is operated in a strong grid. Thus, there is no universal control strategy that will be suitable for all types of unbalanced operation. Instead, a flexible mechanism can be useful for choosing between different objectives, depending on the operating conditions. Further analysis should consider how to adapt the operation of the VSM to any grid-connected or islanded conditions by automatically selecting the proper objective for control of the negative sequence currents.

5 OPERATION AND CONTROL OF MODULAR MULTILEVEL CONVERTERS

5.1 Introduction

The modular multilevel converter (MMC) has become the most attractive multilevel converter for high voltage and high power applications such as VSC-HVDC transmission. The features that set apart MMC from the other multilevel converters are[22]

1) Modularity and scalability that allows to meet any voltage level.
2) High efficiency (1% of the transmitted power) which for high power application is of significant importance.
3) Superior harmonic performance and consequently reduced passive filters.

Having these advantages, MMC is becoming an important part of the grid. Therefore, it should be able to transfer power and at the same time provide support for the grid. The technical challenges of operation and control of MMCs over the last few years are addressed both by manufacturers and academia. Some of the challenges are related to the decrease of the equivalent inertia of the grid thus using the MMC as a Virtual Synchronous Machine [43][44][45]. Other challenges are related to insure a proper operation of the MMC under unbalanced conditions [37][46][47].

This chapter is adressing the use of the MMC as a Virtual Synchronous Machine, by assuring proper control under unbalanced conditions. The chapter starts by considering the MMC topologies, the modulations and balancing techniques for a normal operation of the MMC. After the used mathematical model and the internal energy controls are explaind. Furthermore the necessary adaptations are made for the converter to be controlled as a VSM and assure operation under unbalanced conditions. Lastly, simulations are done considering the converter in unbalanced conditions both in grid connected and islanded mode. The simulations are made using MatLab/Simulink

5.2 **Operation**

5.2.1. Topology

I n *Fig. 5.2* is shown a schematic of a three-phase MMC. There are two arms per leg (upper "u" and lower "l") and one leg per phase. Each arm has N series-connected submodules (SMs), and an arm inductor L which suppresses the high-frequency components in the arm current. The SMs in each arm are controlled to provide an ac phase voltage. Each SM can be realized by a, a) half-bridge circuit or copper-cell, b) full-bridge circuit or bridge-cell, c) clamp-double circuit, d) three-level flying capacitor (FC) converter circuit, e) three-level neutral-point-clamped (NPC) converter circuit, or five-level cross-connected circuits as represented in *Fig. 5.1*. In *Table III* are provided comparisons between these circuits in terms of voltage levels, dc side short-circuitd handling, and power losses.

Among all this different circuit configurations, the half-bridge SM has been mostly adopted for the MMC [23].

Table III: Parameters of the Investigated System Configuration

SM circuit	***Voltage levels***	***dc-fault handling***	***Losses***
Half-bridge	*0, v_C*	*No*	*Low*
Full-Bridge	*0, v_C*	*Yes*	*High*
Clamp-double	*0, v_{C1}, v_{C2},(v_{C1}+ v_{C2})*	*Yes*	*Moderate*
Three-level NPC	*0, v_{C2}, (v_{C1}+ v_{C2})*	*No*	*Moderate*
Three-level FC	*0, v_{C1} v_{C2}, (v_{C1}- v_{C2})*	*No*	*Low*
Five-Level Cross-connected	*0, v_{C1} v_{C2}, (v_{C1}+ v_{C2})*	*Yes*	*Moderate*

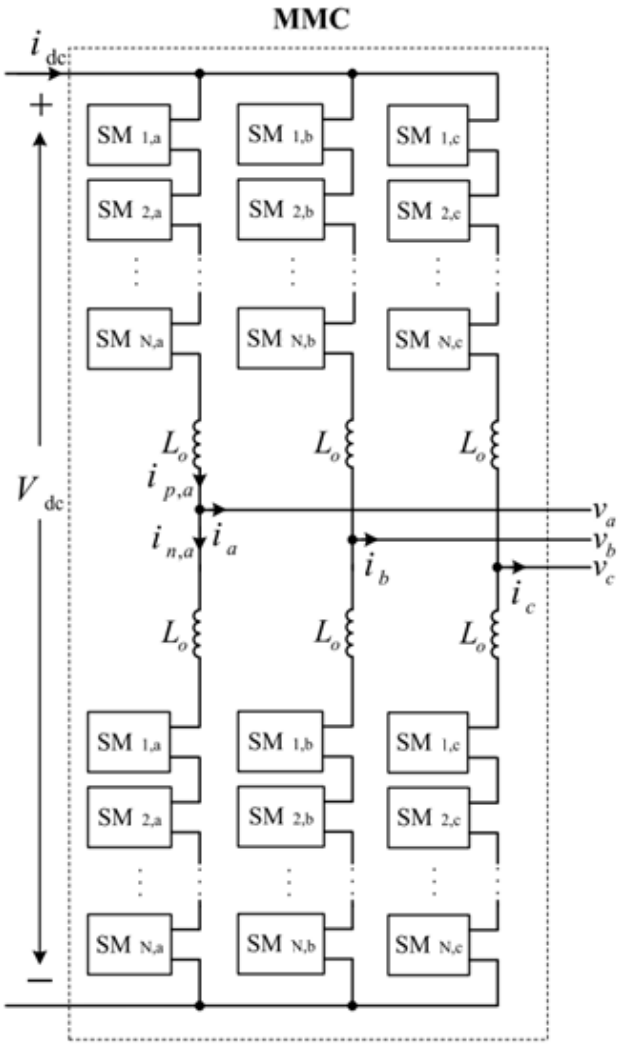

Fig. 5.2. Schematic of MMC

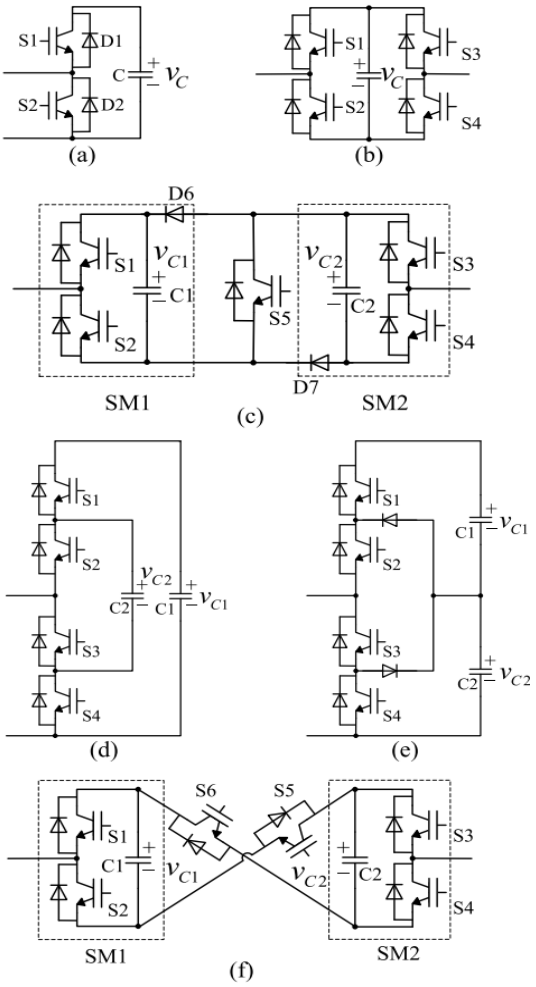

Fig. 5.1. SM topologies, a)half-bridge, b)full-bridge, c)clamp-double, d)three-level FC, e)three-level NPC, f)five-level cross-connected

5.2.2. Modulation

Different pulse-width modulation (PWM) techniques have been developed to turn on and off the switches of the MMC. The ac side voltage and the internal dynamic of the MMC will depend on the carrier waveforms and the reference waveforms [24].

Firstly, there are carrier-disposition PWM (CD-PWM) techniques and Subharmonic techniques. CD-PWMs require N (number of SMs per arm) identical triangular carrier waveforms displaced symmetrically with respect to the zero axis. These carriers are compared with the phase voltage reference waveform thus providing the desired switched output. Voltage transitions corresponding to a carrier are associated with the insertion or bypass of a specific SM. Depending on the phase shift among the carriers these techniques can be classified into phase disposition (PD), phase opposite disposition (POD), and alternated phase opposition disposition (APOD). No stability control is needed for these techniques if used with one reference signal therefore, these techniques become easy to be implemented. The drawback is that these techniques include unequal distribution of voltage ripple across the capacitors impacting on the total harmonic distortion in the ac side voltage, and large magnitude of the circulating

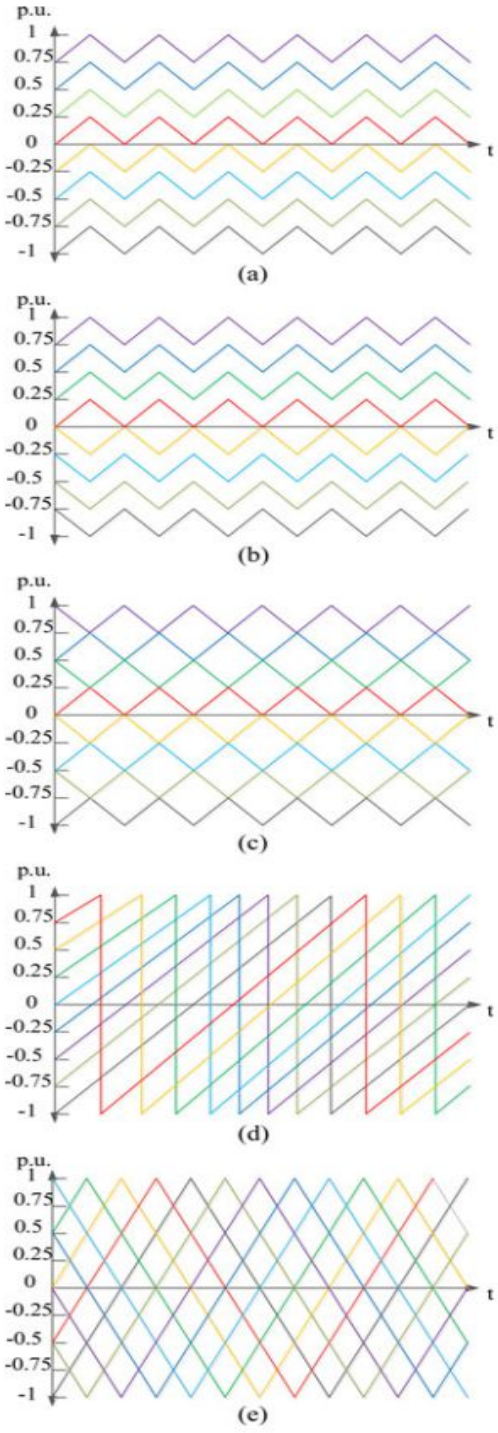

Fig. 5.3. Carries for MMC, a)PD, b)POD, c)APOD, d)Saw-tooth, e)phase-shifted carriers [48]

currents (for circulating currents see section 5.3.1). As for the subharmonic techniques, there are 2N identical carriers per phase-leg, either saw-tooth or triangular waveforms with a phase shift of 360˚/2N as shown in *Fig. 5.3*. Considering the same number of switching for PD-PWM and subharmonic techniques, the PD-PWM techniques produce better line-to-line voltages.

Secondly, there are several modulation techniques based on the number of references, there can be one, two, or multiple references. When using two reference waveforms the modulation techniques may be with direct or indirect modulation. Direct modulation controls the upper and lower arm voltages, by two complementary sinusoidal references waveforms as given in (eq 5.2.1) and (eq. 5.2.2) where $n^*_{u,k}$ and $n^*_{l,k}$ (for k =a, b, c are the reference waveforms for the number of inserted SMs respectively in the upper and lower arms (are also known as insertion indices), and $\mathbf{v}^*_{cv,k}$ represents the reference ac side voltages. A major disadvantage of this modulation technique is the presence of oscillating circulating currents, which increase the converter power losses and current rating values of the components.

$$n^*_{u,k} = N\frac{\frac{v_{dc}}{2} - v^*_{cv,k}}{v_{dc}} \tag{5.2.1}$$

$$n^*_{l,k} = N\frac{\frac{v_{dc}}{2} + v^*_{cv,k}}{v_{dc}} \tag{5.2.2}$$

Indirect modulation gives the upper and lower arm voltages in order to control the energy balance within the converter and provide the reference ac side voltages. The reference insertion indices can be calculated as shown in equation(5.2.3) and equation (5.2.4). Where $v_{c,k}$ is used to drive the circulating current, $e_{cv,k}$ is used to drive the ac current and $v^{\Sigma}_{cap,u,k}$ and $v^{\Sigma}_{cap,l,k}$ are the sum voltage of the capacitors on each arm.

$$n^*_{u,k} = N\frac{\frac{v_{dc}}{2} - e_{cv,k} - v_{c,k}}{v^{\Sigma}_{cap,u,k}} \tag{5.2.3}$$

$$n_{l,k}^{*} = N\frac{\frac{v_{dc}}{2} + e_{cv,k} - v_{c,k}}{v_{cap,l,k}^{\Sigma}} \quad 5.2.4$$

These techniques can be in a closed loop or open loop depending if the capacitor voltages are measured and there is a closed loop in the energy control or if the voltages of the capacitors are estimated and $v_{c,k}$ is estimated to reduce the harmonics of the circulating current.

5.2.3. Balancing

The MMC requires an active capacitor-voltage balancing strategy to balance and maintain the SM capacitor voltage at Vdc/N. There are different strategies with open-loop or closed loop control for each SM capacitor voltage [25][26]. In [27] is developed a predictive strategy to control the MMC, this strategy consists in a predefined cost function in which are balanced the SM capacitor voltages. The most adopted balancing strategy is shown in [28] [29] [30]and is based on a sorting method. In this strategy, the SM capacitor voltages of each arm are measured and sorted. If the current passing through the arm is positive, out of N, SM capacitors per arm the one with the lower voltage are inserted. Consequently the positive current will charge and increase the voltage of the capacitors. On the other hand, in case the arm current is negative, the SMs with the higher voltages are inserted. Therefore, the capacitor voltages corresponding to these SMs will decrease. The number of inserted submodules will depend on the insertion indices. The disadvantage of this method is that it produces unnecessary switching transitions among SMs. Even if the insertion index for the arm remains the same for two consecutive control periods, the inserted or bypassed SMs may change. Therefore, resulting in increased switching frequency and consequently increased power losses. For high power systems, the losses are very high. Hence to reduce the switching frequency of the MMC closed or open loop methods in conjunction with sorting method or harmonic elimination are considered [31][32].

5.3 Control

5.3.1. Mathematical model

In the circuit diagram shown in *Fig. 5.4* are presented the arm inductors L_0 and also an arm resistance R_0 which models the power losses within the arm of the MMC. The upper and lower arm currents for each phase are $i_{u,k}$ and $i_{l,k}$ for k being phase a, b, and c. The most adopted mathematical model of the MMC is shown in [28] [33].

The arm current will be influenced by the converter output current and the current that passes through the leg. The converter output current is $i_{cv,k}$ and the contribution to this current under stable operation is considered equal from the upper arm and the lower arm. The current that passes through the leg is the circulating current $i_{cir,k}$. Thus the upper and lower arm current can be expressed as:

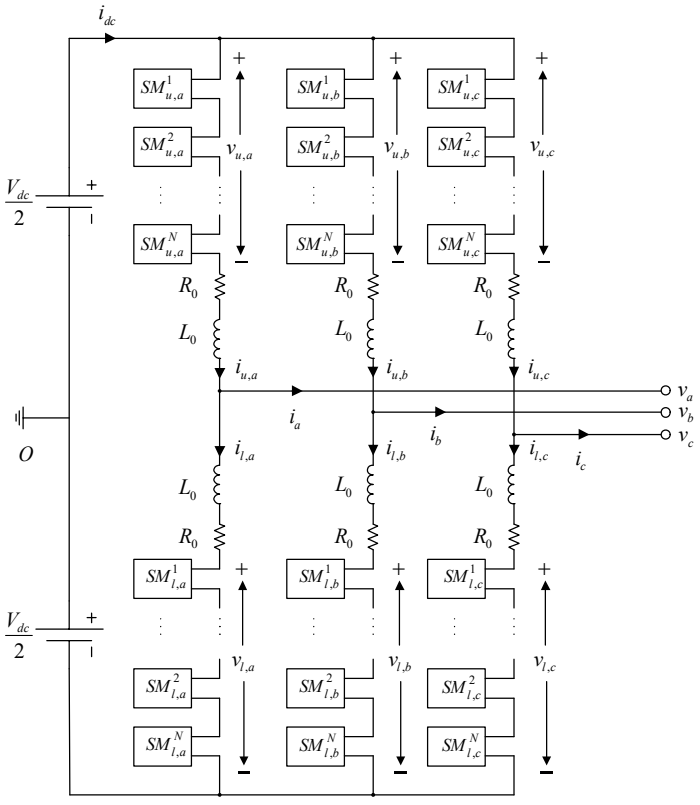

Fig. 5.4. Circuit diagram of the MMC

$$i_{u,k} = i_{cir,k} + \frac{i_{cv,k}}{2} \quad 5.3.1$$

$$i_{l,k} = i_{cir,k} - \frac{i_{cv,k}}{2} \quad 5.3.2$$

Consequently $i_{cv,k}$ and $i_{cir,k}$ can be expressed as:

$$i_{cv,k} = i_{u,k} - i_{l,k} \quad 5.3.3$$

$$i_{cir,k} = \frac{i_{u,k} + i_{l,k}}{2} \quad 5.3.4$$

By using Kirchhoff's voltage law are obtained the equations below.

$$\frac{V_{dc}}{2} - v_{u,k} = L_0 \frac{di_{u,k}}{dt} + R_0 i_{u,k} + v_{cv,k} \quad 5.3.5$$

$$\frac{V_{dc}}{2} - v_{l,k} = L_0 \frac{di_{l,k}}{dt} + R_0 i_{l,k} - v_{cv,k} \quad 5.3.6$$

Where V_{dc} is the dc side voltage, $v_{cv,k}$ is the output voltage of the converter for phase k (k = a, b, c) and $v_{u,k}$ is the sum voltage of the inserted SM capacitors. By subtracting equation (5.3.6) from equation (5.3.5) we get equation (5.3.7). Furthermore, by substituting in equation (5.3.7) equation (5.3.1) and (5.3.2), is found equations (5.3.8).

$$v_{l,k} - v_{u,k} = L_0 \left(\frac{di_{u,k}}{dt} - \frac{di_{l,k}}{dt}\right) + R_0 (i_{u,k} - i_{l,k}) + 2v_{cv,k} \quad 5.3.7$$

$$v_{cv,k} = \frac{v_{l,k} - v_{u,k}}{2} - \frac{L_0}{2}\frac{di_{cv,k}}{dt} - \frac{R_0}{2} i_{cv,k} \quad 5.3.8$$

$$e_{cv,k} = \frac{v_{l,k} - v_{u,k}}{2} \quad 5.3.9$$

Where:

$$e_{cv,k} = v_{cv,k} + \frac{L_0}{2}\frac{di_{cv,k}}{dt} + \frac{R_0}{2} i_{cv,k} \quad 5.3.10$$

On the other hand by adding equation (5.3.6) with equation (5.3.5) is obtained equation (5.3.11). In addition by utilizing equation (5.3.4) in equation (5.3.11) is possible to get equation (5.3.12).

$$V_{dc} - (v_{u,k} + v_{l,k}) = L_0 \left(\frac{di_{u,k}}{dt} + \frac{di_{l,k}}{dt}\right) + R_0 (i_{u,k} + i_{l,k}) \quad 5.3.11$$

$$\frac{V_{dc}}{2} - \frac{(v_{u,k} + v_{l,k})}{2} = L_0 \frac{di_{cir,k}}{dt} + R_0 i_{cir,k} \quad 5.3.12$$

$$\frac{V_{dc}}{2} - \frac{(v_{u,k} + v_{l,k})}{2} = v_{c,k} \quad 5.3.13$$

Where:

$$v_{c,k} = L_0 \frac{di_{cir,k}}{dt} + R_0 i_{cir,k} \quad 5.3.14$$

From equations (5.3.8) and (5.3.12), can be concluded that the alternating voltage $v_{cv,k}$ depends only on the alternating current $i_{cv,k}$ and the difference between the arm voltages. Furthermore, the circulating current depends on the dc-link voltage and the sum of the arm voltages. Thus subtracting the same voltage contribution from both arms will not affect the ac side quantities but will impact the circulating current instead[34].

Assuming that the balancing techniques work properly the total voltage v_{cap}^{Σ} stored in each arm is shared equally among the submodules of the arm.

$$v_{cap,u,k} = \frac{1}{N} v_{cap,u,k}^{\Sigma} \quad 5.3.15$$

$$v_{cap,l,k} = \frac{1}{N} v_{cap,l,k}^{\Sigma} \quad 5.3.16$$

Consequently, the energy stored in each arm is equally shared between the SMs and is expressed as in the equations below.

$$W_{C,u,k}^{\Sigma} = N\left[\frac{C}{2}(v_{cap,u,k})^2\right] = N\left[\frac{C}{2}(\frac{1}{N}\ v_{cap,u,k}^{\Sigma})^2\right] = \frac{\mathrm{C}}{2N}\ (v_{cap,u,k}^{\Sigma})^2 \quad 5.3.17$$

$$W_{C,l,k}^{\Sigma} = N\left[\frac{C}{2}(v_{cap,l,k})^2\right] = N\left[\frac{C}{2}(\frac{1}{N}\ v_{cap,l,k}^{\Sigma})^2\right] = \frac{\mathrm{C}}{2N}\ (v_{cap,l,k}^{\Sigma})^2 \quad 5.3.18$$

Where $W_{C,u,k}^{\Sigma}$ and $W_{C,l,k}^{\Sigma}$ represent the total energy stored into the capacitors in the upper and lower arm of a phase k, and C is the capacitance of each submodule. The equations provided in this section give a generalized dynamic model of the MMC, which can be used for control purposes.

5.3.2. Circulating current

To keep the capacitor voltages at the right levels, different energy balances are needed. They are needed also to provide a stable operation to the MMC. The balancing can be at the total capacitor energy in the leg and at the difference (unbalance) energy between the upper and lower arms. In the following is going to be shown how the circulating current affects the energy balancing and consequently the capacitor voltages.

$$W_{C,k}^{\Sigma} = W_{C,u,k}^{\Sigma} + W_{C,l,k}^{\Sigma} \quad 5.3.19$$

$$W_{C,k}^{\Delta} = W_{C,u,k}^{\Sigma} - W_{C,u,k}^{\Sigma} \quad 5.3.20$$

From equations (5.3.9) and (5.3.13) can be found equation (5.3.21) and (5.3.22) which are the same equations used for indirect modulation.

$$v_{u,k} = \frac{v_{dc}}{2} - e_{cv,k} - v_{c,k} \quad 5.3.21$$

$$v_{l,k} = \frac{v_{dc}}{2} + e_{cv,k} - v_{c,k} \quad 5.3.22$$

It is possible to say that:

$$\frac{dW_{C,u,k}^{\Sigma}}{dt} = p_{u,k} = i_{u,k}\, v_{u,k} = (i_{cir,k} + \frac{i_{cv,k}}{2})(\frac{v_{dc}}{2} - e_{cv,k} - v_{c,k}) \quad 5.3.23$$

$$\frac{dW_{C,l,k}^{\Sigma}}{dt} = p_{l,k} = i_{l,k}\, v_{l,k} = (i_{cir,k} - \frac{i_{cv,k}}{2})(\frac{v_{dc}}{2} + e_{cv,k} - v_{c,k}) \quad 5.3.24$$

By differentiating equations (5.3.19) and (5.3.20) and substituting in them equations (5.3.23) and (5.3.23) the following is obtained.

$$\frac{dW_{C,k}^{\Sigma}}{dt} = i_{cir,k}\left(v_{dc} - 2v_{c,k}\right) - i_{cv,k}\, e_{cv,k} \quad 5.3.25$$

$$\frac{dW_{C,k}^{\Delta}}{dt} = i_{cv,k}\left(\frac{v_{dc}}{2} - v_{c,k}\right) - 2i_{cir,k}\, e_{cv,k} \quad 5.3.26$$

The equation (5.3.25) and equation (5.3.26) show that the circulating current $i_{cir,k}$ plays a crucial role in controlling the total capacitor energies in the converter arms. The circulating current has different components. The dc component of the circulating current multiplies with the dc-link voltage $v_{dc}$to balance the power transferred to the ac side plus the losses that are made in the arm. Furthermore, the dc component of the circulating current does not affect the energy balance between the upper and the lower arm as long as there are no dc components in $e_{cv,k}$. Therefore, the dc component of the circulating current can be used to control the sum energy level or the sum voltage level sored in the capacitors in each converter leg. Because the power transferred to the ac side in a leg is a power term which oscillates with twice the fundamental frequency.

On the other hand, the fundamental harmonic component of the circulating current which has the same frequency as the output phase voltage impacts the distribution of the capacitor energies between the upper and lower arms in a converter leg. It has to be mentioned that the term $i_{cir,k}\, e_{cv,k}$ and $i_{cv,k}\, v_{c,k}$ will create a dc term witch will influence $\frac{dW_{C,k}^{\Delta}}{dt}$. However, this component is smaller than the one discussed earlier if there are high output voltage amplitudes and a reasonably small arm inductance [34].

5.3.2.1. Energy control

To control the stored energy in the MMC and ensure energy balance between the upper and lower arm both $W_{C,k}^{\Sigma}$, $W_{C,k}^{\Delta}$ have to be controlled. There are different controls proposed in [34][36][45]. In this thesis is considered a practical and intuitive control. As mentioned previously, the sum energy has mainly a dc component and a double frequency component. This double frequency energy component can create an oscillating circulating current or oscillating arm voltages. For the proposed control in this thesis, the double frequency of the oscillating current is controlled to zero. But this may create higher voltage oscillations. To solve this potential problem in [39]-[42]different strategies are proposed to reduce the voltage oscillations. The energy difference has mainly a fundamental component. The control task is to keep the average capacitor voltages in the rated values and reduce the unbalanced between the upper and lower arm of the leg-phase. To do so a simplification of equations (5.3.25), (5.3.26) are used as expressed below.

$$\frac{d\bar{W}_{C,k}^{\Sigma}}{dt} = i_{cir,k}\, v_{dc} - \frac{1}{3} p_{ac} \tag{5.3.27}$$

$$\frac{d\bar{W}_{C,k}^{\Delta}}{dt} = -2 i_{cir,k}\, e_{cv,k} \tag{5.3.28}$$

Where $\bar{W}_{C,k}^{\Sigma}$ is the average sum energy accumulated in the leg of the converter and $\bar{W}_{C,k}^{\Delta}$ is the difference in average energy between the upper and lower leg. The sum energy is proportional to the sum of the total capacitor voltage squared, and the difference energy is proportional to the difference of the total capacitor voltage squared, respectively shown in equation (5.3.29) and equation (5.3.30).

$$\frac{d\bar{W}_{C,k}^{\Sigma}}{dt} \equiv \frac{d[(\bar{v}_{cap,u,k}^{\Sigma})^2 + (\bar{v}_{cap,l,k}^{\Sigma})^2]}{dt} \tag{5.3.29}$$

$$\frac{d\bar{W}_{C,k}^{\Delta}}{dt} \equiv \frac{d[(\bar{v}_{cap,u,k}^{\Sigma})^2 - (\bar{v}_{cap,l,k}^{\Sigma})^2]}{dt} \tag{5.3.30}$$

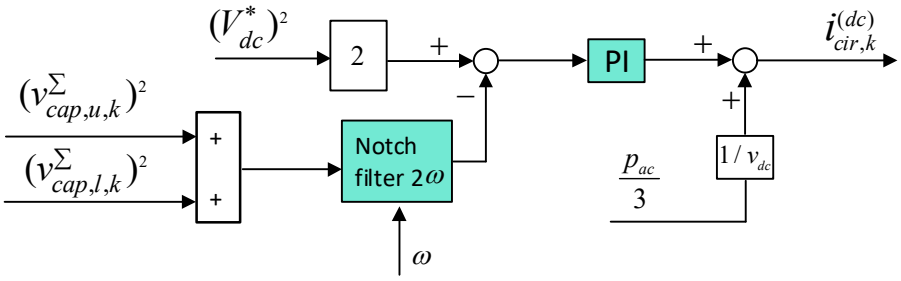

Fig. 5.5.Generating dc component of the circulating

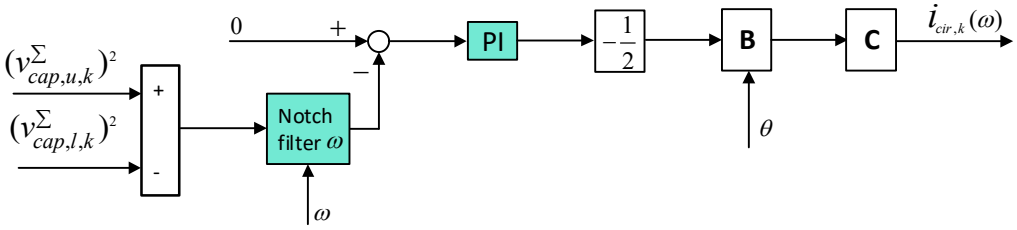

Fig. 5.6.Generating the first harmonic component of the circulating current

Considering the equations (5.3.27)-(5.3.30) the is achieved the control as shown in *Fig. 5.5* and *Fig. 5.6*. When generating the first harmonic of the circulating current reference, the magnitude of $e_{cv,k}$ is not considered, since in balanced conditions the converter is providing a magnitude of 1 p.u. and if it changes the integral part of each phase will charge accordingly. For a better performance under unbalanced conditions the control structure is changed and explained in the next section. In *Fig. 5.6* are also two matrixes, the matrix **B** generates the first harmonic of the circulating currents with the same phase angle as the converter phase voltage. And the matrix **C** is used to cancel the sum of the different ac components in order to mitigate this first harmonic component into the dc current [38].

$$\boldsymbol{B} = \begin{bmatrix} cos(\theta) & 0 & 0 \\ 0 & cos(\theta - \frac{2\pi}{3}) & 0 \\ 0 & 0 & cos(\theta + \frac{2\pi}{3}) \end{bmatrix} \quad 5.3.31$$

$$\boldsymbol{C} = \begin{bmatrix} 1 & -\frac{1}{2} & -\frac{1}{2} \\ -\frac{1}{2} & 1 & -\frac{1}{2} \\ -\frac{1}{2} & -\frac{1}{2} & 1 \end{bmatrix} \quad 5.3.32$$

5.3.2.2. Adapting the energy control for VSM under unbalanced conditions

The first point of improvement of the internal control for the MMC used as a VSM is the frequency adaptability for the notchfilter or also known as a band-stop filter. The first approach is not to implement a notchfilter but to do an averaging over one period since for the control, just the average value is needed. This solution is easy to be implemented in the discrete-time domain, removes the presence of any high harmonic from the signal, and averages the noise of the signal. But, if the period changes from the tuned one errors are introduced in the control. A proper solution is to implement a SOGI structure which tunes to a specific harmonic, and after this harmonic can be removed from the signal. The SOGI has also the capability of changing the tuning frequency depending on the speed of the VSM. Therefore, allow proper operation when the grid frequency changes or when the converter is operating in islanded mode.

The second point of improvement is for operation under unbalanced conditions. As seen from equation (5.3.28), to have just the first harmonic oscillations in the difference energy control, $i_{cir,k}$ should be in phase with the leg-phase voltage and its amplitude is inverse to the phase voltage. Under balanced conditions, the 3 phase voltages are shifted by 120˚ and their amplitude in normal operation are within 5% of the nominal voltage. But under unbalanced conditions, the voltage magnitudes have a higher variation while the voltage phases are not shifted anymore by 120˚, but it will depend on the unbalance. In [37] is considered the nominal phase voltage and a PLL is used for each phase to find the phase angle. In this thesis is considered an approach using the SOGI-QSG structure so that for each phase can be found the quadrature signal. By having the signal and its quadrature is possible to find the magnitude which can be used for the control. Furthermore, if the phase signal is divided by the magnitude the cosinusoidal term is obtained. Therefore, the structure becomes

like the one shown in *Fig. 5.7*. The new element introduced with respect to the previous control scheme is the SOGI-QSG which is used to calculate the magnitude and angle of the voltage in each phase.

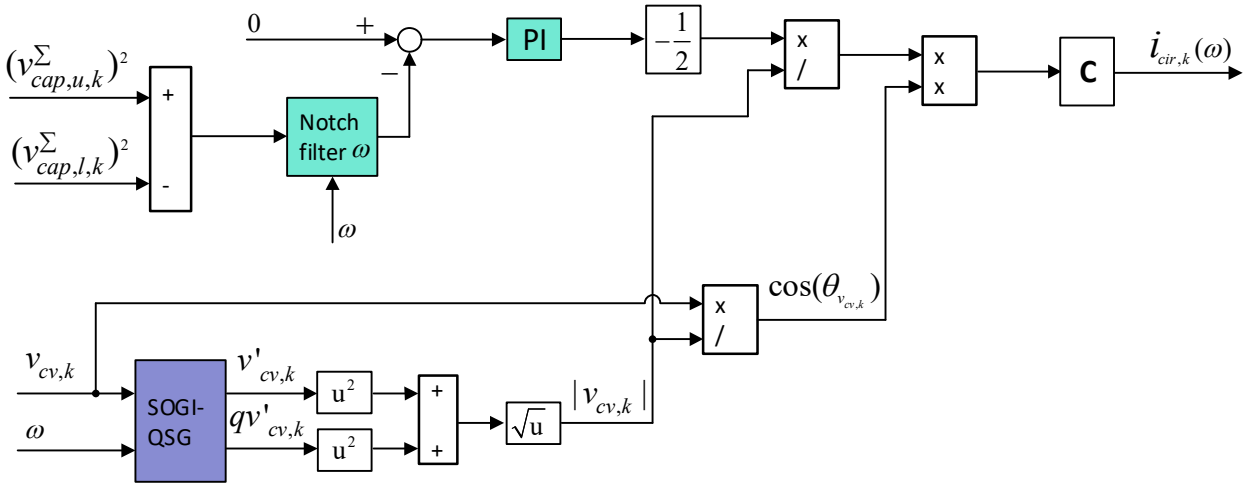

Fig. 5.7.Generating the first harmonic component of the circulating current under unbalanced conditions

5.3.2.3. Circulating current controller

For controlling the circulating current usually is used a PI controller. In this thesis a PIR controller is considered, *Fig. 5.8* with two resonant terms one for the fundamental component used for controlling the energy balancing in the leg (difference energy), and the other for reducing the second harmonic component that is created in the leg when transferring power from the dc side the ac phase.

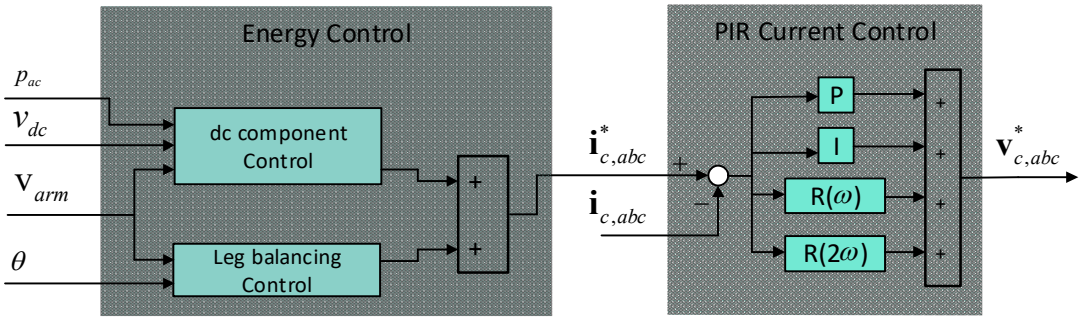

Fig. 5.8.Energy control and circulating current control

5.4 Simulations for MMC as VSM under unbalanced conditions

In this part of the chapter are presented the controls and responses of an MMC controlled as a Virtual Synchronous Machine. The simulated scenarios show the behavior of the internal dynamic of the MMC controlled under balanced conditions and also under unbalanced voltage conditions for grid connected and islanded mode. The simulation environment used is SimPowerSystem/ Simulink/ Matlab.

5.4.1. Configuration and control

The configuration taken into account is shown in *Fig. 5.9* where the MMC has a constant dc voltage in the dc side and provides the ac voltage as output. The output of the converter is connected to an inductive filter which reduces the high curret harmonics. The converter can work in grid connected, and if the breaker is opend, in islanded mode.

To control the MMC is used the control scheme shown in *Fig. 5.10*. The elements form which this control is formed are:

- Virtual Synchronous Machine Model (see chapter 3)
- Phase Lock-Loop (see section 3.3.2)
- Proportional-Resonant Current Controller (see section 3.6.2)

Fig. 5.9. System configuration with MMC

- Active Damping (see section 3.7)
- Pulse Width Modulation (PWM)
- Negative Sequence Current Generator (Fig. 4.9, see section 4.3)
- Measurement processing and sequence separation (see section 4.2)
- Balancing (see section 5.2.3)
- Modulation (see section 5.2.2)
- PIR Current Controller (see section 5.3.2.3)
- Energy Control (see section 5.3.2.1)

The switching signals for the SMs are obtained by the balancing block which ensures equal capacitor charging among the SMs in the arm. To provide the insertion indices utilized by the balancing, a PD modulation is used. The modulation reference for the upper and lower arm comes from an indirect modulation. For the indirect modulation are needed the converter voltage that drives the ac current and the circulating voltage that drives the circulating current. Thus, these currents are driven by current controllers implemented respectively in the alpha-beta frame and in the abc frame. The current reference for the circulating current comes from the MMC energy control. The current reference for the ac current derives from two SRRF currents where one is rotating in the positive direction and the other one is in the

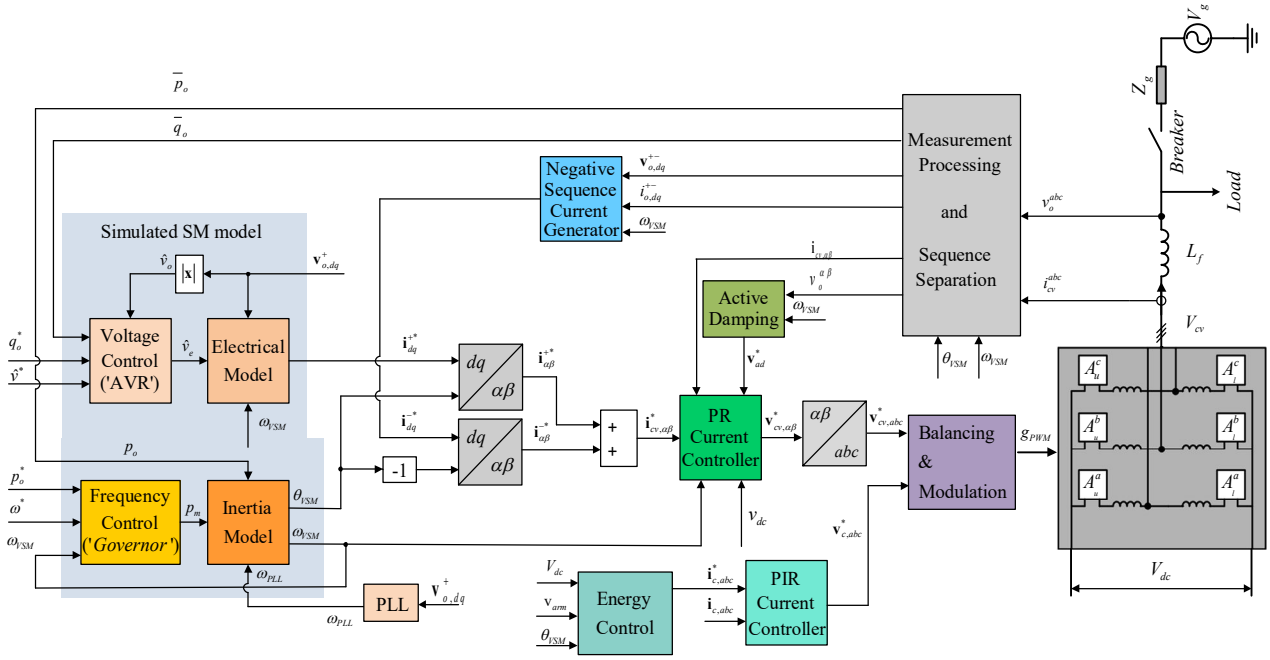

Fig. 5.10. The control structure for MMC controlled as VSM under unbalanced conditions

negative direction. The positive sequence current is issued from the positive sequence virtual impedance as part of the Synchronous Machine model and the negative sequence current results from the Negative Sequence Current Generator. This last one generates negative sequence currents that brings forth different strategies for controlling the unbalances at the point of common connection. These strategies are Balanced Three Phase Currents, Constant Active Power, Constant Reactive Power, Negative Sequence Virtual Impedance, Negative Sequence Voltage Control.

Furthermore can be noticed that this control scheme is similar to the one used for the two-level VSC shown in *Fig. 4.10*. The main difference between these two controls is the presence of the elements that control the dynamic behavior of the MMC such as the modulation technique for a higher number of switches, balancing technique for SMs capacitor voltages, energy control, and circulating current control.

The Configuration and control parameters are shown in Table IV

Table IV: Parameters of the MMC System Configuration and Control

Parameter	Value	Parameter	Value
AC Voltage $V_{ll,g,n}$	9 KV	Rated current, I_n	245 A
Rated angular frequency ω_n	$2\pi \cdot 50$ Hz	SMs per arm, N	50
DC voltage $V_{dc,n}$	30 KV	Primary filter inductance l_f , r_{lf}	0.08pu, 0.008pu
Active damping k_{SOGI}, k_{AD}	√2, 0.5 pu	Filter capacitance c_f	0.079 pu
AC Current controller gains, $k_{p,c}$, $k_{i,c}$	0.8 0.8	Grid-side filter inductance l_g, r_g	0.2pu, 0.01pu
Circulating current controller gains $k_{p,cir}$, $k_{i,cir}$ $k_{i,wcir}$ $k_{i,2wcir}$	1.3, 16.2 0.029, 0.014	DSOGI-QSGs for sequence separation k_{SOGI}	√2
Circulating current dc component control, $k_{p,dc}$, $k_{i,dc}$	0.59 13	PLL PI controller, $k_{p,PLL}$, $k_{i,PLL}$	2, 70
Leg balancing control $k_{p,leg}$, $k_{i,leg}$	1.36 13.6	Negative sequence voltage control, $k_{p,NS}$, $k_{i,NS}$	0.1, 1.5
VSM Positive Seq. Impedance, r_v^+, l_v^+	0.01 pu 0.2 pu	VSM damping k_d	200 pu
VSM Negative Seq.Impedance, r_v^-, l_v^-	0.01 pu, 0.2 pu	Reactive power droop k_q	0 pu
Virtual inertia Ta	10 s	Frequency droop k_ω	20 pu

5.4.2. The internal dynamic of the MMC controlled as VSM

In this section is investigated the internal dynamic of the MMC when the converter is controlled as a Virtual Synchronous Machine. The inertial response of a power perturbation or frequency perturbation will influence the energy control of the MMC.

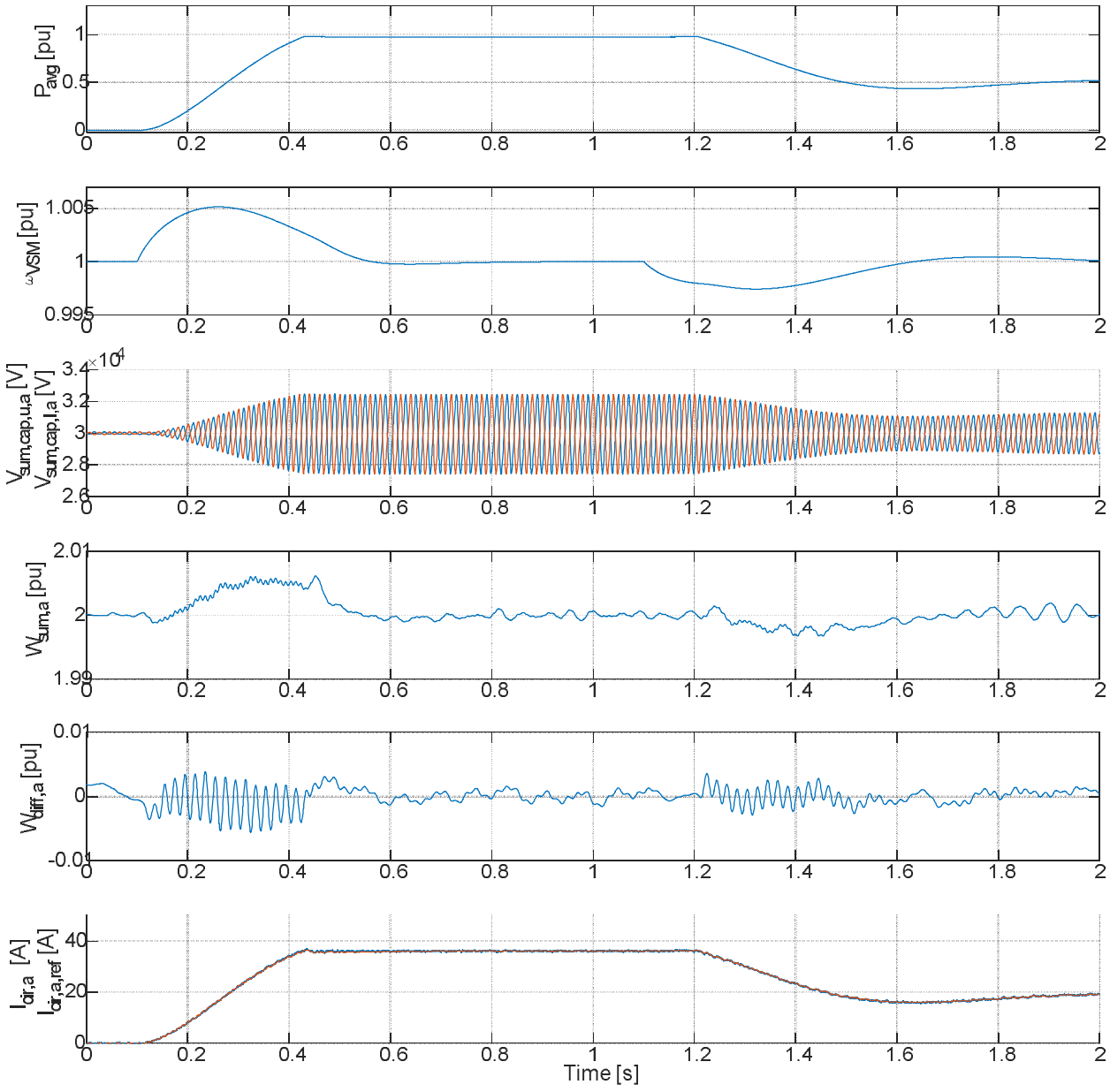

Fig. 5.11. MMC dynamic in a step perturbation from the VSM active power set-point

In *Fig. 5.11* are shown the transients form a perturbation of 1 p.u. at t=0.1 and a perturbation of -0.5 p.u. at t=1.2 both in the active power set-point. From top to bottom the graphs show the active power in the point of common connection, the speed of the VSM, upper and lower arm of phase a sum capacitor voltages ($v_{cap,u,a}^{\Sigma}$, $v_{cap,l,a}^{\Sigma}$), the average sum energy for phase a ($\bar{W}_{C,a}^{\Sigma}$), the average difference energy for phase a ($\bar{W}_{C,a}^{\Delta}$), and on the last one is the reference circulating current and the circulating current for phase a.

It can be seen that the circulating current has mainly a dc component and it resembles the ac power. In controlling a zero second harmonic in the circulating current, the second harmonic power oscillations in the single-phase-leg are influencing just the capacitor voltages. Thus, it can be seen that the arm sum capacitor voltages increase the oscillation magnitude with increased power transfer. The control aimes at removing the harmonic from the circulating current and consequently from the arm due to the loses that they produce, but should be taken into account that the sum arm voltages remain within their limit.

For the energies can be distinguished some first and second order harmonics during the transients. The oscillations are related to the inertial response of the VSM. More specifically on the way how the averaging of the energy is done. As previously mentioned the sum energy has mainly a dc component and a second harmonic component and the difference energy has mainly the first harmonic. With the energy controls the aim is to keep the average sum energy to a nominal dc component and the average difference energy to a zero dc component. To keep just dc values of the signal a low pass filter with a low cut-off frequency may be used, even though is not a very good idea because the dynamic of the converter will slow down. What is preferred is to use a notch filter tuned at the fundamental grid frequency and twice the fundamental frequency. The notch filter allows the signal to pass and filters out the tuned frequency. For the control structure to work just the dc component of the energy is needed hence a easy solution is to do a local averaging. Since the implementation is in discrete time, this simulation uses a local averaging with a sliding window. This last one for a fixed period sums the samples and divides them by the number of samples taken in one period getting as a consequence an average value. The downfall of this type of approach are the changes in the frequency. Consequently, the period is not fixed and this average will have oscillations. This effect is very visible in the average difference energy graph shown in *Fig. 5.11*. During the transient, the speed of the VSM changes the

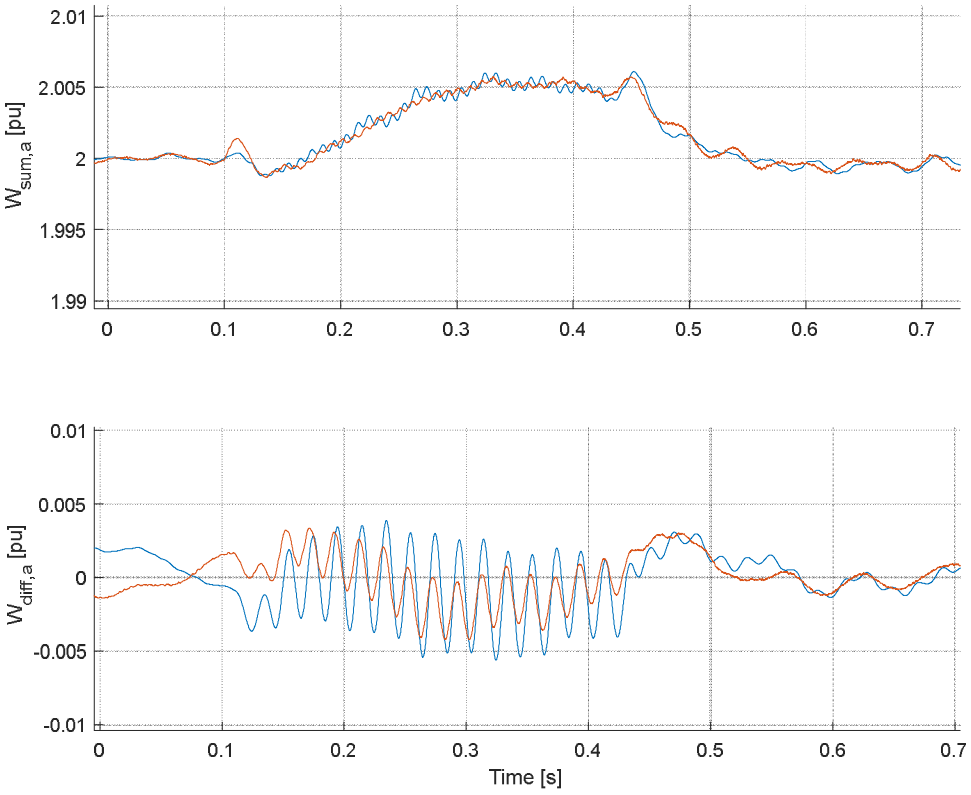

Fig. 5.12. Active power perturbation effect in the energy control, averaging using SOGI (——), averaging with Sliding window(——)

period changes from the nominal one and as a result the oscillations occur and influence the energy control. The oscillations continue until the speed of the VSM returns to the nominal value.

To reduce the average energy ripples a frequency adaptive notch filter is considered using SOGIs structures so that the fundamental and second harmonic component can be removed and still be frequency adaptive. In *Fig. 5.12* is shown a comparison of the energy controls when using SOGI and Sliding window to find the average. The blue curves are a zoom-in of the first perturbation shown in *Fig. 5.11*, and the red ones show how the energy control behave if for the averaging are used the SOGI structures. It can be noticed that the second harmonics on the average sum energy are eliminated and the first harmonics in the average difference energy are reduced.

This change in the control structure becomes more important if there is a frequency perturbation. In that case, the frequency will not return to the nominal value thus there is going to be a constant ripple in the average energy. In *Fig. 5.13* is shown how the energy controls behave if there is a change in the grid frequency with 0.3% of the nominal value. There are simulated 2 cases in each graph the first one uses SOGIs for the energy averaging (the blue curve), and the second case uses a sliding window for the averaging. In the top left-hand side of the figure, it can be seen that the average sum energy control has a better-damped transient. And on the right-hand side, it can be seen that the control with the SOGIs

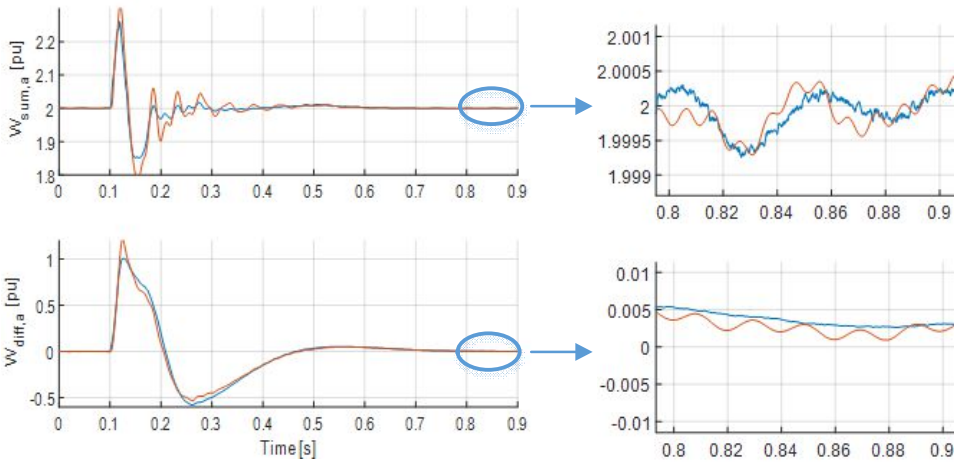

Fig. 5.13. Frequency power perturbation effect in the energy control, averaging using SOGI (——), averaging with Sliding window(——)

removes the second harmonic oscillations from the sum energy control and the first harmonic from the difference energy control.

A small disadvantage of using SOGI over the sliding window is the noise presence, as can be seen in the top right-hand side of *Fig. 5.13*. This happens because the sliding window does the sum over one period and the noise in average will cancel and the SOGIs remove just the harmonics. This is not a big drawback since the SNR (Signal to Noise Ration) is high and also the PI will attenuate the noise.

5.4.3. The internal dynamic of the MMC controlled as VSM under grid unbalanced conditions

In this section, is tested the MMC control for 25% voltage unbalanced ($|V^-|/|V^+|$ = 0.2/0.8=0.25) happening at t=0.05. The control strategies tested are a) balanced three phase currents, b) constant active power, c) constant reactive power, d) negative sequence virtual impedance, e) negative sequence voltage control. For these control strategies are shown the three phase currents and voltages and the active and reactive power at the point of common connection. If compared with the results from the two-level VSC can be noticed that the control strategies for grid connected unbalanced conditions work better. This comes as a consequence of having just an inductor as a filter and not the LC filter. Hence the current generated by the converter for the unbalances is the same as the one going at the grid.

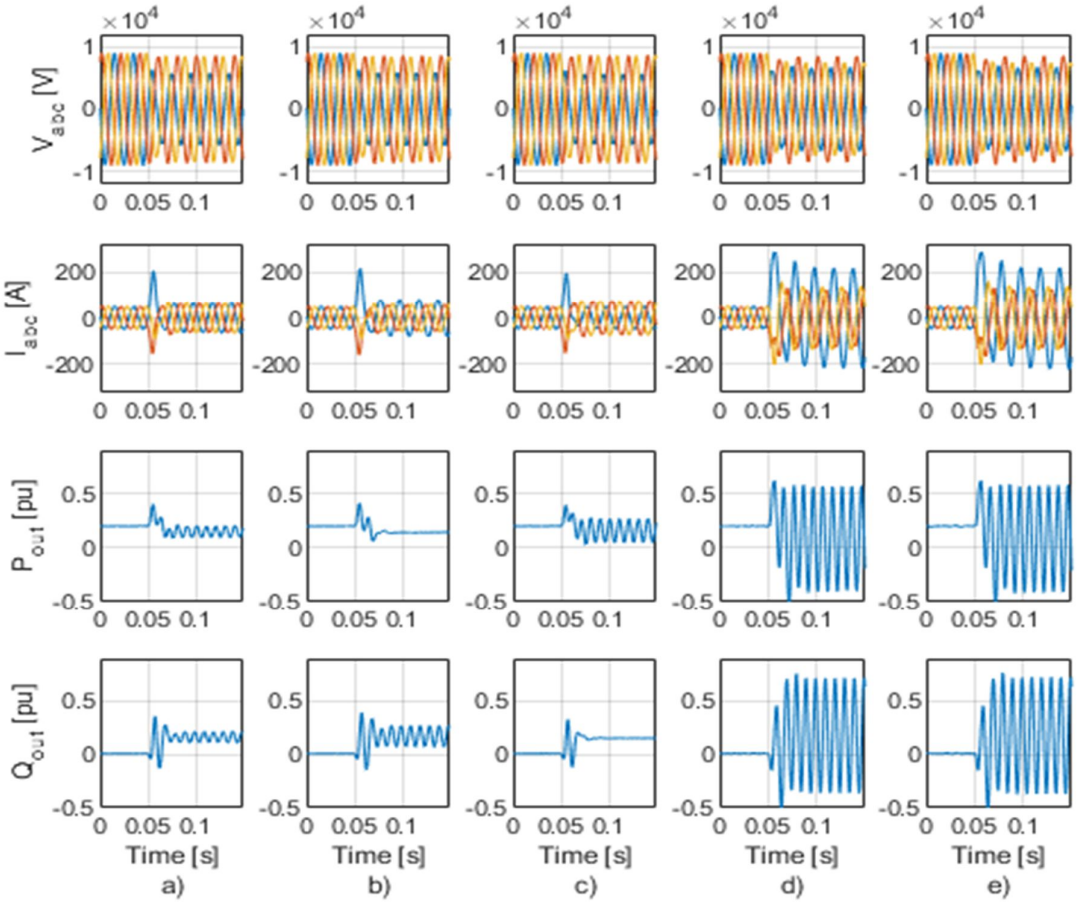

Fig. 5.14. Simulation results of MMC in grid-connected mode showing the transient response to an unbalanced voltage sag occurring at t=0.05 a) Balanced positive sequence currents b) Constant active power c) Constant reactive power, d) Negative sequence virtual impedance e) Negative sequence voltage controller.

Meantime the current for the two-level converter passes partly through the capacitor of the LC filter.

In figure *Fig. 5.15* are shown the sum of the SMs capacitor voltages for the upper and lower arm of phase a and also the circulating current of phase a. It can be noticed that the voltage oscillation is higher for the last two control strategies which are related with reducing the negative sequence voltage. For this strategies, the negative sequence current increases and for phase a, the current are higher with respect to the previous control cases. Thus meaning that the power transfer for this phase is higher. By controlling the second harmonic of the circulating current to zero, in the phase-leg the power transfer is higher which means higher oscillating voltages as explained in the previous section.

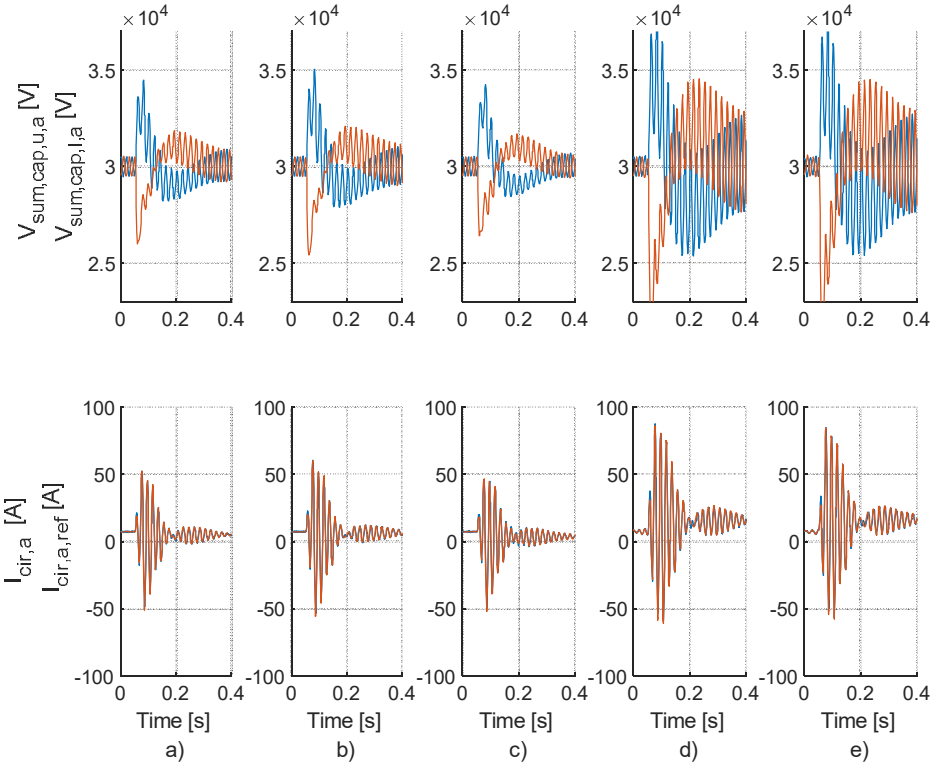

Fig. 5.15. Simulation results of MMC in grid-connected mode showing the transient response of the arm voltages and circulating current for an unbalanced voltage sag occurring at t=0.05 a) Balanced positive sequence currents b) Constant active power c) Constant reactive power, d) Negative sequence virtual impedance, e) Negative sequence voltage controller.

In *Fig. 5.16* are compared to the inertial responses of the different control strategies. It can be noticed that the converter is able to provide inertia support. The power absorbed by the fault when negative sequence virtual impedance or negative sequence voltage controller are used is higher. This comes as a consequence of the higher negative sequence current that these two strategies produce in order to reduce the negative sequence voltage at the point of common connection.

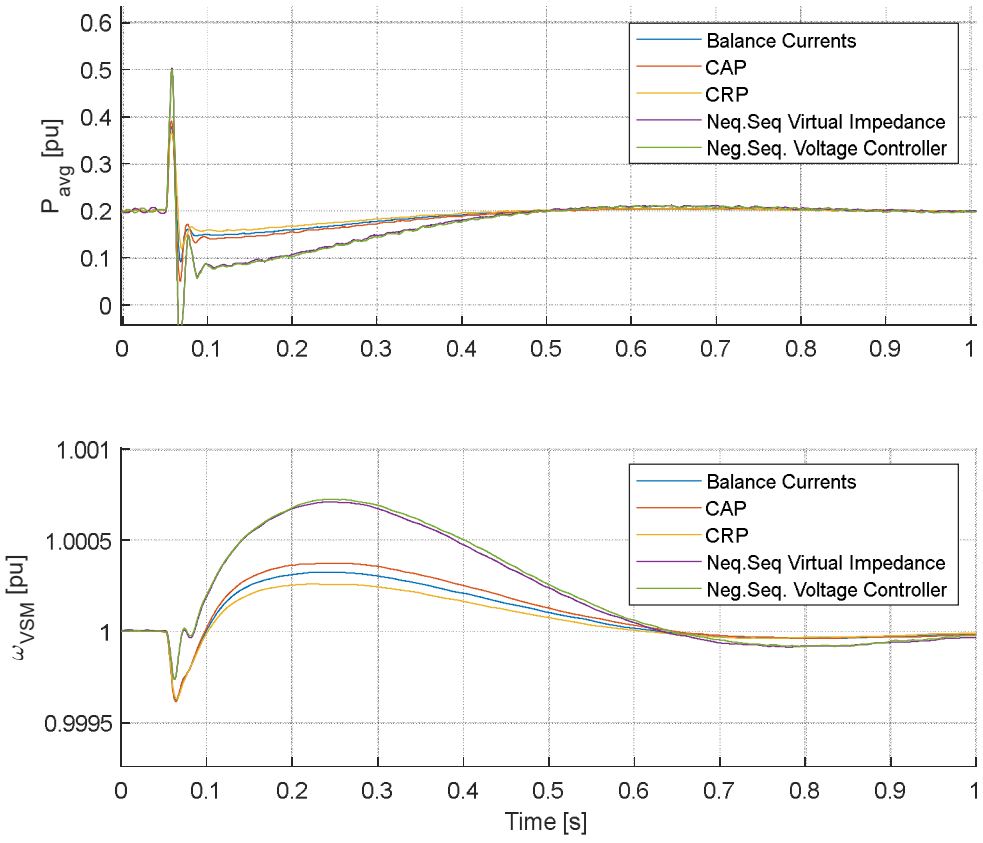

Fig. 5.16.Inertia response for the MMC under unbalanced conditions .

5.4.4. Transient response of the MMC when islanding under an unbalanced local load

In this section, the MMC control performance is investigated for islanded operation. This test is important since the islanded operation is a key feature of the VSM. For this simulation, the MMC converter is subject to an unbalanced three phase load. The unbalanced load is created by adding another load between phases a and b. The added load has half the impedance of the initial delta-connected load. The simulated scenario is a converter connected with the grid and an unbalanced local load where at t=0.05 the breaker indicated in *Fig. 5.9* goes from closed position to open position. The response of the islanding transient is shown in *Fig. 5.17*. In islanded mode the first three strategies that control the power (balanced three phase currents, constant active power, constant reactive power) are not acceptable since they produce overvoltages, meanwhile the last two strategies that reduce

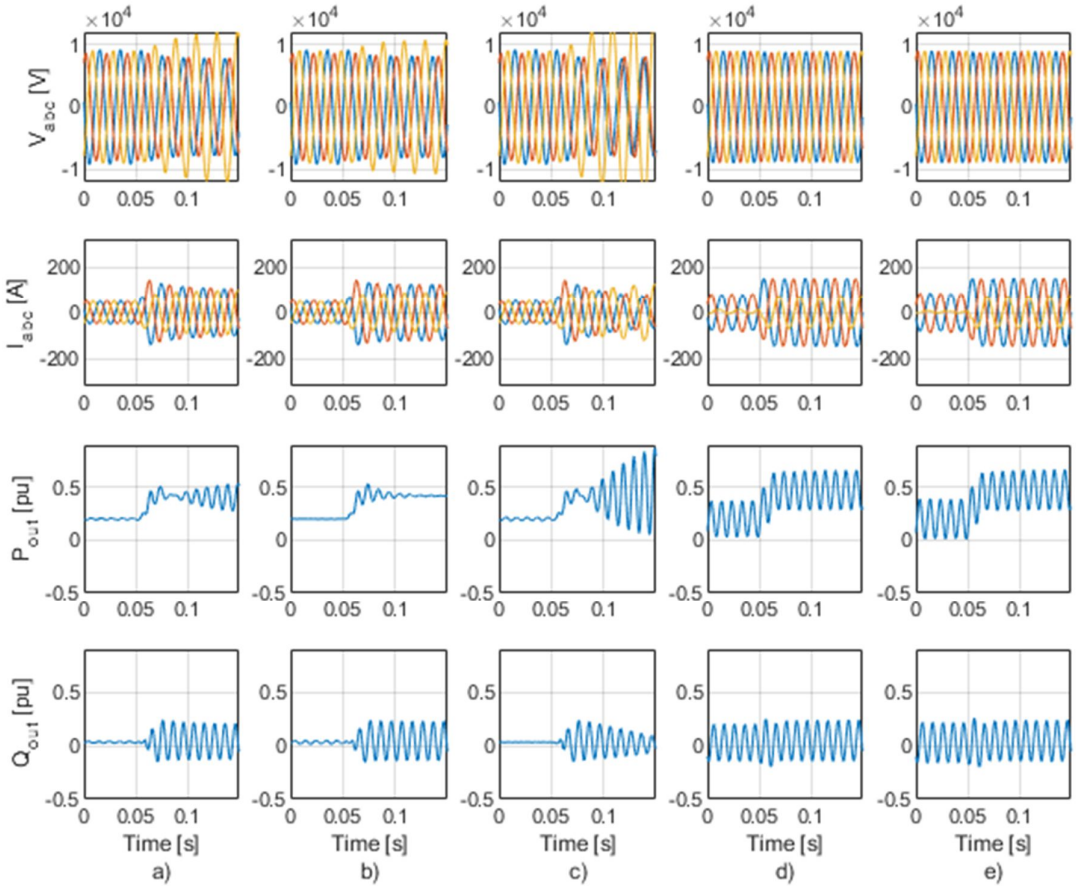

Fig. 5.17. Islanding operation of a MMC connected with an unbalanced local load a) Balanced positive sequence currents b) Constant active power c) Constant reactive power, d) Negative sequence virtual impedance e) Negative sequence voltage controller.

the negative sequence voltage behave properly. These results validate further the conclusions drawn from the third chapter. Moreover, the same can be said for the inertial response shown in *Fig. 5.18* where the behavior in islanded mode is the same as obtained from the two-level VSC.

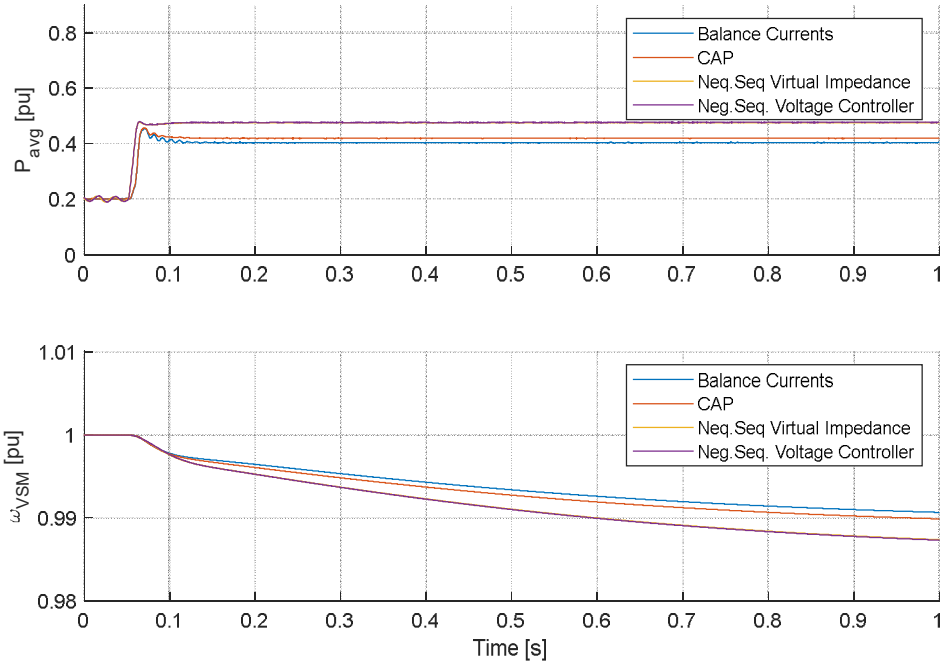

Fig. 5.18.Inertia response for the MMC under unbalanced conditions.

From the two figures above is understood that the MMC if seen from the point of common connection can operate under unbalanced conditions in islanded operations as a Virtual Synchronous Machine. The control strategies for unbalanced conditions under islanded operation should aim to reduce the voltage unbalance.

The transient responses and the inertial responses are similar when using negative sequence virtual impedance or negative sequence voltage controller. The same happens for the internal dynamic of the MMC as well. Therefore, in *Fig. 5.19* is shown the internal dynamic of the MMC when using negative sequence virtual impedance as an example for both the control strategies. In this figure are shown the sum capacitor voltage of the SMs of the upper and lower arms for phase a, the average sum energy, the average difference energy, and the circulating current for phase a,b,c.

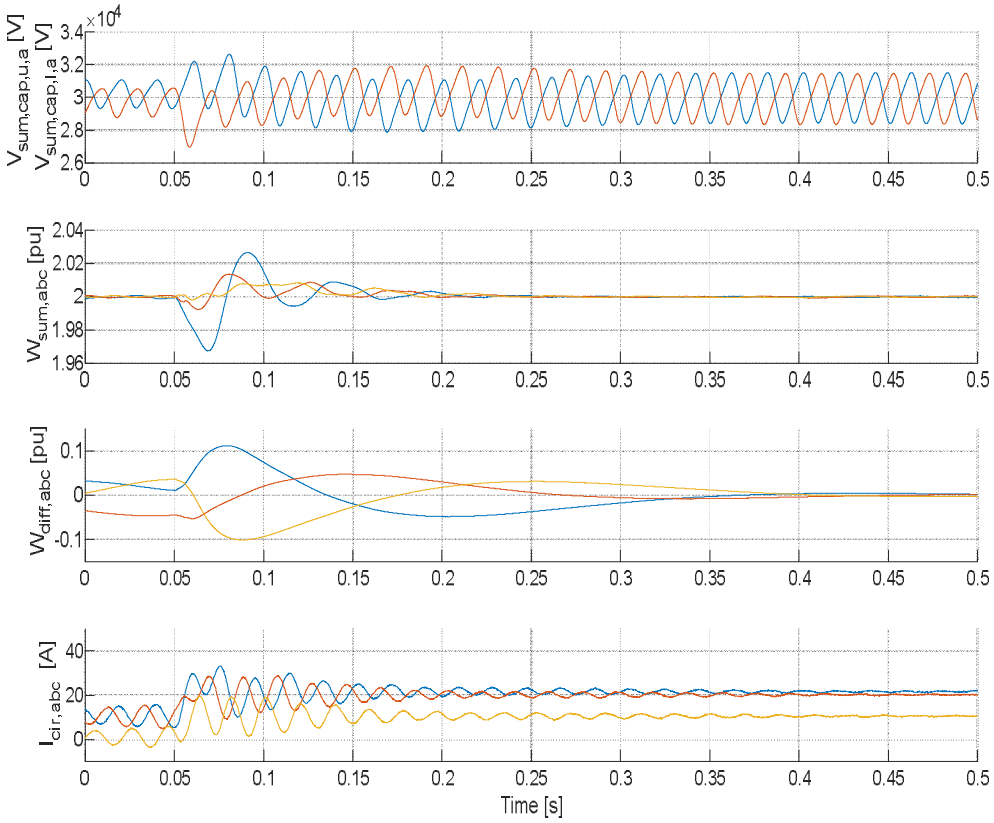

Fig. 5.19. MMC dynamic when islanding with an unbalanced local load

Firstly, can be noticed that the transient is faster for the sum energy with respect to the difference energy, which comes as a result of the regulator tunings. Secondly, when the energy difference is balanced the fundamental component in the circulating current is reduced. And, the power transfer from each phase for these control strategies is different hence the dc component of the circulating current has different values. Thirdly, in the average sum and difference energies, there are no first and second harmonic ripples even though in islanded operation the frequency deviation from the nominal value is higher. This comes as a result of the used SOGIs to remove these harmonics.

5.5 Conclusions

In this chapter is considered how to operate and control the MMC as a VSM under unbalanced conditions. The operation of the MMC starts with the sub-modules. Depending on the application the sub-modules of the MMC may have different topologies but the half-bridge is the most used at the moment. The arm of the MMC has several SMs. How these SMs are inserted or bypassed depend on the modulation techniques and the balancing technique. The modulation tells how many SMs per arm are inserted to do so the preferred technique is the PD-PWM with two references (one for the upper and the other for the lower arm). And the balancing techniques tell which SMs from the arm are inserted/bypassed. Depending on what is the control objective the two references for the modulation can be for direct and indirect modulation. To have a stable operation under unbalanced conditions is needed to control the capacitor voltages thus indirect modulation with energy control is used.

The energy control considers the energy accumulated in the arms and the legs of the converter. There is the sum energy control which considers the average total energy accumulated in the legs. And there is the difference energy control which controls that the energy is shared equally between the upper and lower arms of the leg. It is shown that for a good internal dynamic there should be adaptability in the frequency when controlling the average energy. This was achieved by using SOGI structures as notch filters to remove the first and second harmonic ripples in the average sum and difference energy. Furthermore, the difference energy control is improved so that the converter can operate better under unbalanced conditions. This improvement is done by finding the magnitude and angle of each phase during the unbalanced conditions and using this information to properly generate the current reference for the difference energy control. Moreover, simulations are done considering in balanced conditions the internal dynamic when the MMC is used as a Virtual Synchronous Machine. And other simulations are done for controlling the MMC under unbalanced conditions both in grid-connected and islanded operation.

6 CONCLUSIONS

Conclusions and contributions

The purpose of this thesis is to find a control system for power electronic converters that provides inertia support, grid forming capabilities and assure reliable operation under unbalance conditions. For this thesis HVDC converters are chosen since the importance HVDC applications is increasing and its technologies can be good candidates for providing the virtual inertia and grid forming capabilities in the power system.

In the first chapter are expressed the possible HVDC technologies from which two converters are considered to achieve the stated purpose for the HVDC application. The first is a two-level Voltage Source Converter and the second is a Modular Multilevel Converter.

A control able to provide the inertia support for the grid is the Virtual Synchronous Machine. The components of this control structure are shown and explained in chapter 2. The control structure chosen for this thesis is a Current Controlled VSM with a Proportional-Resonant current controller implemented in the alpha-beta Stationary Reference Frame.

In the third chapter are investigated the unbalanced conditions and through the use of a dual set of Second Order Generalized Integrator with Quadrature Signal Generator was possible to obtain the positive and negative components of the grid current and voltages. Six different strategies for controlling the negative sequence currents are identified, from which Balanced Three Phase Currents, Constant Active Power, Constant Reactive Power are well known in the literature. And Reduction of DC Side Oscillations, Negative Sequence Virtual Impedance, and Closed Loop Control on the Negative Sequence Voltage are a contribution

of this thesis. Additionally, in this chapter is considered a worst-case scenario for the current limits and the power transfer is actively limited to ensure a safe operation of the converter under unbalanced conditions.

The strategies to control the unbalanced conditions are simulated in grid connected and islanded mode for both the two-level Voltage Source Converter in chapter 3 and the MMC in chapter 4. The results clearly show how the control strategies based on the calculation of the negative sequence current references for shaping the power flow characteristics are only suitable for grid-connected operation. Operation with a negative sequence virtual impedance can ensure stable operation in both grid-connected and islanded operation. However, this approach will not fulfill any specific objectives of shaping the power flow characteristics or balancing the voltage. Closed loop control of the negative sequence components for balancing the local voltages is suitable for islanded operation with unbalanced local loads. Although this approach also can be utilized for grid-connected operation in weak grids with high equivalent impedance, the controllers will saturate if the system is operated in a strong grid. Therefore, there is no universal control strategy that will be suitable for all types of unbalanced operation. The converters and their control structures studied in this thesis can assure virtual inertia under unbalanced conditions.

Moreover, the MMC control structure is similar to the two-level Voltage Source Converter control structure for controlling the ac currents in the point of common connection, but it has additional components for controlling the internal energy of the MMC. There is a sum energy control and a difference energy control investigated in chapter 4. These two controls try to keep the total average energy in the leg to a reference and share this energy equally between the upper and lower arms of a given phase. It is found that for a good internal dynamic there should be adaptability in the frequency when controlling the average sum/difference energy. This is achieved by using SOGI structures and their frequency adaptivity capabilities as notch filters. By doing so is possible to remove the first and second harmonic ripples in the average sum and difference energy. Moreover, the difference energy control is improved so that the converter can operate better under unbalanced conditions. This improvement is done by finding the magnitude and angle of each phase during the unbalanced conditions and using this information to properly generate the current reference for the difference energy control.

7 REFERENCES

[1] ENTSO-E AISBL, “HVDC Links in System Operations”, 2 December 2019

[2] N. Flourentzou, V.G. Agelidis, and G.D. Demetriades, ‘VSC-Based HVDC Power Transmission Systems: An Overview,’ IEEE Trans. Power Electron., vol. 24, no. 3, 2009, pp. 592–602

[3] E. Pierri, O. Binder, N. G. Hemdan and M. Kurrat, Challenges and opportunities for a European HVDC grid, vol. 70, Elsevier Ltd, 2017, pp. 427-456

[4] O. E. Oni, I. E. Davidson and K. N. Mbangula, "A Review of LCC-HVDC and VSC HVDC Technologies and Applications", IEEE, 2016

[5] O. G. I. Okwe Gerald Ibe, “Concepts of Reactive Power Control and Voltage Stability Methods in Power System Network,” IOSR Journal of Computer Engineering, vol. 11, no. 2, 2013, pp. 15-25.

[6] Chao, C., Adam, G.P., Finney, S., et al.: ‘H-bridge modular multi-level converter: control strategy for improved DC fault ride-through capability without converter blocking’, IET Power Electron., 2015, 8, pp. 1996–2008

[7] B. Rafferty, J., Lie, X., Morrow, J.: ‘Analysis of voltage source converter-based high-voltage direct current under DC line-to-earth fault’, IET Power Electron., 2015, 8, pp. 428–438

[8] Li, T., Zhao, C.: ‘Recovering the modular multilevel converter from a cleared or isolated fault’, IET Gener. Transm. Distrib., 2015, 9, pp. 550–559

[9] Oluwafemi E. Oni, Innocent E. Davidso, Kamati N.I. Mbangula ‘A Review of LCC-HVDC and VSC-HVDC Technologies and Applications’ 978-1-5090-2320-2016 IEEE

[10] F. Wang, L. Bertling and T. Le, “An Overview Introduction of VSC-HVDC: State-of-art and Potential Applications in Electric Power Systems”, 2011

[11] M. Jafar and M. Molinas, “A series injection strategy for reactive power compensation of line commutated HVDC for offshore wind power,” in Industrial Electronics, International Symposium on Industrial Electronics, Trondheim, Norway, 2010

[12] S. D’Arco, J.A. Suul, Virtual Synchronous Machines – classification of implementations and analysis of equivalence to droop controllers for microgrids, in: Proc. of IEEE PowerTech Grenoble 2013, Grenoble, France, 16–20 June 2013

[13] V. Kaura, V. Blasko, Operation of a phase locked loop system under distorted utility conditions, IEEE Trans. Ind. Appl. 33 January/February 1997, 58– 63

[14] A. Rodriguez-Cabero, J. Roldan-Perez and M. Prodanovic, “Virtual Impedance Design Considerations for Virtual Synchronous Machines in Weak Grids,” IEEE Journal of Emerging and Selected Topics in Power Electronics, 23 5 2019, pp. 1-1

[15] J. A. Suul and S. D’Arco, “Comparative Analysis of Small-Signal Dynamics in Virtual Synchronous Machines and Frequency Derivative-Based Inertia Emulation” IEEE, 2018, pp. 344-351

[16] O. Mo, S. D'Arco, J. A. Suul, "Evaluation of Virtual Synchronous Machines with Dynamic or Quasi-stationary Machine Models," in IEEE Trans. Ind. Electron., Vol. 64, No. 7, Jul. 2017, pp. 5952-5962

[17] D. N. Zmood, D. G. Holmes, G. H. Bode “Frequency-Domain Analysis of Three-Phase Linear Current Regulators”, IEEE TRANSACTIONS ON INDUSTRY APPLICATIONS, VOL. 37, NO. 2, MARCH/APRIL 2001 pg 601-609

[18] P. Rodriguez, A. Luna, R. S. Munoz-Aguilar, I. Etxeberria-Otabui, R. Teodorescu, F. Blaabjerg, “A Stationary Reference Frame Grid Synchronization System for Three-Phase Grid-Connected Power Converters Under Adverse Grid Conditions.” IEEE TRANSACTIONS ON POWER ELECTRONICS, VOL. 27, NO. 1, JANUARY 2012 pg.99-112

[19] Teodorescu Liserre Rodriguez “Grid Converters for Photovoltaic and Wind Power Systems, p.237-287

[20] M. Brucoli, T. C. Green, “Fault Response of Inverter Dominated Microgrids.” in International Journal of Distributed Energy Resources, Vol. 3, No. 2, April/June 2007, pp. 157-175

[21] T. Zheng, L. Chen, Y. Guo, S.Mei, “Flexible unbalanced control with peak current limitation for virtual synchronous generator under voltage sags” in Journal of Modern Power Systems and Clean Energy, Vol. 6, No. 1, January 2018, pp. 61-72

[22] M. Ardelean, P. Minnebo and European Commission. Joint Research Centre. Institute for Energy and Transport., HVDC submarine power cables in the world: state-of-the art knowledge., Publications Office, 2015

[23] Suman Dednath, Jiangchao Qin, Behrooz Bahrani, Maryam Saeedifard, Peter Barbosa, “Operation, Control, and Applications of the Modular Multilevel Converter: A Review”, IEEE TRANSACTIONS ON POWER ELECTRONICS, VOL. 30, NO. 1, JANUARY 2015

[24] G. Konstantinou and V. Agelidis, “Performance evaluation of half-bridge cascaded multilevel converters operated with multicarrier sinusoidal)PWM techniques,” in Proc. IEEE Conf. Ind. Electron. Appl., 2009,pp. 3399–3404.

[25] F. Deng and Z. Chen, “A control method for voltage balancing in modular multilevel converters,” IEEE Trans. Power Electron., vol. 29, no. 1, pp. 66–76, Jan. 2014.

[26] M. Hagiwara and H. Akagi, “Control and experiment of pulse width modulated modular multilevel converters,” IEEE Trans. Power Electron.,vol. 24, no. 7, pp. 1737–1746, Jul. 2009.

[27] J. Qin and M. Saeedifard, “Predictive control of a modular multilevel converter for a back-to-back HVDC system,” IEEE Trans. Power Del., vol. 27, no. 3, pp. 1538–1547, Jul. 2012.)

[28] M. Saeedifard and R. Iravani, “Dynamic performance of a modular multilevel back-to-back HVDC system,” IEEE Trans. Power Del., vol. 25, no. 4, pp. 2903–2912, Oct. 2010.

[29] J. Huber and A. Korn, “Optimized pulse pattern modulation for modular multilevel converter high-speed drive,” in Proc. Int. Power Electron. Motion Control Conf., 2012, pp. LS1a-1.4-1–LS1a-1.4-7

[30] S. Rohner, S. Bernet, M. Hiller, and R. Sommer, “Modulation, losses, and semiconductor requirements of modular multilevel converters,” IEEE Trans. Ind. Electron., vol. 57, no. 8, pp. 2633–2642, Aug. 2010

[31] J. Qin and M. Saeedifard, “Reduced switching-frequency voltagebalancing strategies for modular multilevel HVDC converters,” IEEE Trans. Power Del., vol. 28, no. 4, pp. 2403–2410, Oct. 2013.

[32] K. Ilves, A. Antonopoulos, S. Norrga, and H.-P. Nee, “A new modulation method for the modular multilevel converter allowing fundamental switching frequency,” IEEE Trans. Power Electron., vol. 27, no. 8, pp. 3482–3494, Aug. 2012.

[33] L. Harnefors, A. Antonopoulos, S. Norrga, L. Angquist, and H. Nee, “Dynamic analysis of modular multilevel converters,” IEEE Trans. Ind. Electron., vol. 60, no. 7, Jul. 2013, pp. 2526–2537.

[34] A. Antonopoulos, L. Ängquist, H.-P. Nee, "On Dynamics and Voltage Control of the Modular Multilevel Converter," in Proceedings of the 13th European Conference on Power Electronics and Applications, EPE'09, Barcelona, Spain, 8- 10 September 2009

[35] L. Angquist, A. Antonopoulos, D. Siemaszko, K. Ilves, M. Vasiladiotis,and H.-P. Nee, “Open-loop control of modular multilevel converters using estimation of stored energy,” IEEE Trans. Ind. Appl., vol. 47, no. 6, Nov./Dec. 2011, pp. 2516–2524.

[36] M. Hagiwara and H. Akagi, “Control and experiment of pulsewidthmodulated modular multilevel converters,” IEEE Trans. Power Electron., vol. 24, no. 7, Jul. 2009, pp. 1737–1746

[37] Zh. Ou, G. Wang, L. Zhang, “Modular Multilevel Converter Control Strategy Based on Arm Current Control Under Unbalanced Grid Condition”, IEEE TRANSACTIONS ON POWER ELECTRONICS, VOL. 33, NO. 5, pp. 3826-3836, MAY 2018

[38] K. Shinoda, J. Freytes, A. Benchaib, J. Dai, H. Saad, and X. Guillaud, “Energy Difference Controllers for MMC without DC Current Perturbations,” in 2nd International Conference on HVDC (HVDC2016 - CIGRE), 2016

[39] S. P. Engel and R. W. D. Doncker, “Control of the modular multi-level converter for minimized cell capacitance,” in Proc. Eur. Conf. Power Electron. Appl., Aug./Sep. 2011, pp. 1–10

[40] M. Winkelnkemper, A. Korn, and P. Steimer, “A modular direct converter for transformerless rail interties,” in Proc. IEEE Int. Symp. Ind. Electron., 2010, pp. 562–567

[41] R. Picas, J. Pou, S. Ceballos, V. G. Agelidis, and M. Saeedifard, “Minimization of the capacitor voltage fluctuations of a modular multilevel converter by circulating current control,” in Proc. Conf. IEEE Ind. Electron. Soc., 2012, pp. 4985–4991.

[42] R. Picas, J. Pou, S. Ceballos, J. Zaragoza, G. Konstantinou, and V. Agelidis, “Optimal injection of harmonics in circulating currents of modular multilevel converters for capacitor voltage ripple minimization,” in Proc. IEEE Energy Convers. Congr. Expo. Asia Downunder,2013, pp. 318–324

[43] R. wang, L. Chen, T. Zheng, Sh. Mei, “ VSG-based Adaptive Droop Control for Frequency and Active Power Regulation in the MTDC System”, CSEE JOURNAL OF POWER AND ENERGY SYSTEMS, VOL. 3, NO. 3, SEPTEMBER 2017, pp. 260-268.

[44] G.B. Diaz, J.A. Suul, S. D’Arco, “Small-Signal State-Space Modeling of Modular Multilevel Converters for System Stability Analysis” 978-1-4673-7151-3/15/$31.00 ©2015 IEE, pp. 5822-5829

[45] S. D’Arco, G.Guidi, J.A. Suul, “Operation of a Modular Multilevel Converter Controlled as a Virtual Synchronous Machine”, The 2018 International Power Electronics Conference, IEEJ, 2018

[46] J Zhang, C Zhao “Control Strategy of MMC-HVDC under Unbalanced Grid Voltage Conditions” Journal of Power Electronics, Vol. 15, No. 6, 2015, pp. 1499-1507.

[47] A.E. Leon, S.J. Amodeo, “Energy Balancing Improvement of Modular Multilevel Converters Under Unbalanced Grid Conditions”, IEEE TRANSACTIONS ON POWER ELECTRONICS, VOL. 32, NO. 8, AUGUST 2017, pp. 6628-6637

[48] G. Konstantinou and V. Agelidis, “Performance evaluation of half-bridgecascaded multilevel converters operated with multicarrier sinusoidal)PWM techniques,” in Proc. IEEE Conf. Ind. Electron. Appl., 2009,pp. 3399–3404.

[49] J. Liang, O. Gomis-Bellmunt, J. Ekanayake, N. Jenkins, W. An, “A multi-terminal HVDC transmission system for offshore wind farms with induction generators”, International Journal of Electrical Power & Energy Systems, Vol 43, No. 1, December 2012, Pg 54-62

[50] E. Avdiaj, J. Are Suul, S. D'Arco and L. Piegari, "A Current Controlled Virtual Synchronous Machine Adapted for Operation under Unbalanced Conditions," 9th International Conference on Renewable Energy Research and Application (ICRERA), Glasgow, United Kingdom, 2020, pp. 263-270

APPENDIX

Publication

This paper is presented in the 9th International Conference on Renewable Energy Research and Application (ICRERA), Glasgow, United Kingdom

A Current Controlled Virtual Synchronous Machine Adapted for Operation under Unbalanced Conditions

[*]Eros Avdiaj, [†,#]Jon Are Suul, [†]Salvatore D'Arco,[*]Luigi Piegari
[*]Department of Electronics, Information and Bioengineering, Politecnico di Milano. Milano, Italy
[†]SINTEF Energy Research, Trondheim, Norway
[#]Department of Engineering Cybernetics, Norwegian University of Science and Technology, Trondheim, Norway
e-mail: eros.avdiaj@mail.polimi.it , Jon.A.Suul@sintef.no, salvatore.darco@sintef.no, luigi.piegari@polimi.it

***Abstract*—This paper presents a comprehensive evaluation of control strategies for operation of a Virtual Synchronous Machine (VSM) under unbalanced conditions in both grid-connected and islanded mode. The basis for the evaluation is a Current Controlled VSM where a quasi-stationary virtual impedance emulates a simplified positive sequence electrical model of a synchronous machine. It is shown how three general strategies can be selected for controlling the negative sequence currents: i) calculation of the negative sequence current references according to the desired active and reactive power flow characteristics, ii) applying a negative sequence virtual impedance resulting in unbalanced currents as in the steady-state response of a synchronous machine, or iii) operation with a negative sequence voltage controller for eliminating unbalances in the locally measured voltages. For the first approach, three**

This work was supported by the project "HVDC Inertia Provision" (HVDC Pro), financed by the ENERGIX program of the Research Council of Norway (RCN) with project number 268053/E2, and the industry partners; Statnett, Statoil, RTE and ELIA.

objectives for shaping the power flow characteristics can be selected: i) balanced three-phase currents, ii) constant instantaneous active power flow, or iii) constant instantaneous reactive power flow. Comprehensive simulation results are presented to evaluate the performance and applicability under grid connected and islanded operation. The results demonstrate how utilization of the negative sequence currents to control the power flow characteristics is only applicable for grid connected operation, while the other two approaches can be utilized in both islanded and grid-connected modes. However, closed loop control for balancing the local voltages depends on a high equivalent grid impedance and is not suitable for operation in strong grid conditions.

Keywords— Grid connected VSCs, Islanded Power Systems, Unbalanced Grids, Virtual Synchronous Machines

- Introduction

The control of power electronic converters as Virtual Synchronous Machines (VSMs) has been extensively studied during the last decade [1]-[3]. Indeed, many control schemes for emulating the behaviour of Synchronous Machines (SMs) with power converters have been proposed, including concepts labelled as Virtual Synchronous Generators (VSGs) Synchronverters, or Synchronous Power Controllers (SPCs)[3]-[7]. A first motivation for pursuing such control strategies has been to provide virtual inertia in modern power systems with declining equivalent rotating inertia due to the increased share of generation with power electronic interfaces. Furthermore, control strategies relying on a similar power-balance-based synchronization mechanism as SMs enable operating in grid-connected as well as in islanded mode. Thus, a second motivation for pursuing VSM-based control strategies is to ensure grid forming capability, which is attractive for applications where both grid-connected and stand-alone operation are required.

In the literature, three general control approaches have been applied for actuating the reference voltage amplitude and the phase angle resulting from the inertia model of a VSM [3]: i) In the simplest strategies, these reference values are directly applied to the modulation stage of the converter [3]-[6]. This approach can be referred to as VSMs with Directly Applied Voltage (DAV); ii) alternatively, a closed loop voltage control cascaded with an inner current control loop can be implemented [3], [8]. This control structure can be referred

to as a Voltage Controlled (VC) VSM. For both these types of control, a virtual impedance can be utilized to emulate the stator impedance of an SM. iii) The third common approach for VSM-based control is to utilize a virtual impedance, or a virtual admittance, to translate the voltage reference from the SM model into current references for a conventional current control loop [3], [7], [9]. This approach can be generally referred to as a Current Controlled (CC) VSM.

The majority of the VSM-based control implementations proposed in literature are not directly applicable under unbalanced conditions. Indeed, further enhancements are needed for controlling the response to the negative sequence component of the voltages. Recent publications have addressed this issue by proposing different ways of controlling the negative sequence currents during operation in unbalanced grids [10]-[15]. Although configurations including direct or closed loop voltage control have been applied for unbalanced conditions in [10], [11], the requirements for limiting the currents under unbalanced grid faults generally favours current controlled implementations. Thus, it is shown in [12]-[16] how CCVSM-based strategies can be combined with different objectives for calculating negative sequence current references. Specifically, it is shown how the negative sequence currents can be calculated by imposing either I) balanced three phase currents, II) elimination of active power oscillations or III) elimination of reactive power oscillations. However, these studies consider only the operation under unbalanced conditions in grid-connected mode when the negative sequence currents can be controlled without significantly influencing the voltage. On the other hand, [17] discusses a VSM-based control for an islanded system where a CCVSM-based strategy controlling the positive sequence currents is combined with a negative sequence voltage controller for eliminating unbalances in the local voltage. Similarly, the VCVSM based control in [11] includes an option for directly generating balanced voltages when operating in islanded mode. However, none of these publications have comprehensively studied the alternative control options under unbalanced conditions for both grid-connected and islanded operation.

This paper presents a thorough evaluation of operating strategies for a CCVSM under unbalanced conditions in both grid-connected and islanded modes. It is first shown how three general strategies can be utilized for controlling the negative sequence currents: 1) calculation of the negative sequence current references according to the desired active and reactive power flow characteristics, 2) introduction of a negative sequence virtual

impedance, and 3) operation with a negative sequence voltage controller. For all cases, only the dc-components of the power flow are used as feedback signals for the active and reactive power control, ensuring that the outer control loops are not influenced by double frequency power oscillations. A comprehensive set of simulation results illustrates the performance of the presented options for controlling the negative sequence currents under unbalanced conditions in grid-connected and islanded modes, as well as for the transition from grid-connected to islanded operation. The results demonstrate how the strategies for controlling the power flow characteristics are only suitable for grid-connected operation Furthermore, the results indicate how operation with negative sequence voltage control is only applicable in islanded operation or in conditions with a relatively high equivalent grid impedance. The results offer an overview of the general control objectives that can be applied for VSM-based control under unbalanced conditions and can serve as a basis for defining suitable strategies for transitioning between grid-connected and islanded operation.

- VSM-based control Under Unbalanced Conditions

The system configuration shown in Fig. 1 is utilized to evaluate the different options for operation during unbalanced conditions. In this structure, a Voltage Source Converter (VSC) operated as a CCVSM is connected to a local power system through an LC filter. The configuration includes a local passive load connected close to the converter and can be separated from the main grid by a breaker. In the figure, upper case symbols indicate physical variables or parameters, while lower case symbols indicate per unit quantities used in the control system. The main measurements utilized by the VSM-base control are the three phase values of the converter currents i_{cv}, the filter output voltages v_o, and the output current i_o.

- *Overview of CCVMS control structure*

The general structure of the CCVSM implementation shown in Fig. 1 is adapted from the control system presented in [9]. However, Proportional-Resonant (PR) controllers are utilized for the inner loop current regulation to simplify the implementation while ensuring the capability to control positive and negative sequence currents. These controllers operate directly on the converter currents $\mathbf{i}_{cv}$ in the stationary $\alpha\beta$ reference frame. Furthermore, active damping of LC filter oscillations is introduced by using a band-pass filter based on a Second Order Generalized Integrator (SOGI) configured as a Quadrature Signal Generator

(QSG) [18]. The structure of the active damping can be considered as a stationary frame equivalent to the *dq*-frame active damping used in [9] Thus, the frequency characteristics of the damping can be adjusted by tuning the internal gain of the SOGI-QSG.

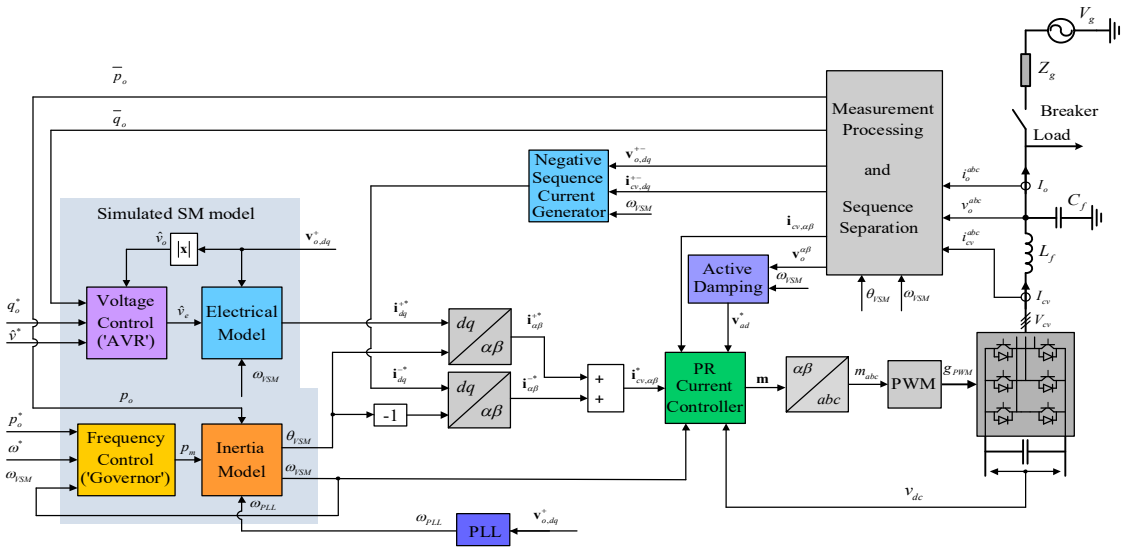

Fig. 1 Overview of the CCVSM-based control strategy for unbalanced grid-connected and islanded operation

- *Sequence separation and power calculation for VSM operation under unbalanced conditions*

Access to the positive and negative sequence components of the voltages and currents is needed to control the converter operation under unbalanced conditions. This is achieved by a dual set of SOGI-QSGs (i.e. a DSOGI-QSG) according to [18]. Using the voltage as an example, a block diagram showing how the DSOGI-QSGs structure generates the in-phase and in-quadrature components required for Positive and Negative Sequence Calculation (PNSC) is shown in Fig. 2. The only difference from the implementation in [18] is that frequency adaptivity of the DSOGI-QSG is ensured by using the VSM speed instead of a frequency estimation based on the voltage measurements.

By estimating the positive and negative sequence components of the measured voltages and currents, the average values or dc-components of the active and reactive power flow can be directly calculated as:

$$\bar{p}_o = v^+_{o,\alpha} \cdot i^+_{o,\alpha} + v^+_{o,\beta} \cdot i^+_{o,\beta} + v^-_{o,\alpha} \cdot i^-_{o,\alpha} + v^-_{o,\beta} \cdot i^-_{o,\beta}$$
$$\bar{q}_o = -v^+_{o,\alpha} \cdot i^+_{o,\beta} + v^+_{o,\beta} \cdot i^+_{o,\alpha} - v^-_{o,\alpha} \cdot i^-_{o,\beta} + v^-_{o,\beta} \cdot i^-_{o,\alpha} \quad (1)$$

The resulting values of average active and reactive powers are used directly as the feedback signals indicated in Fig. 1.

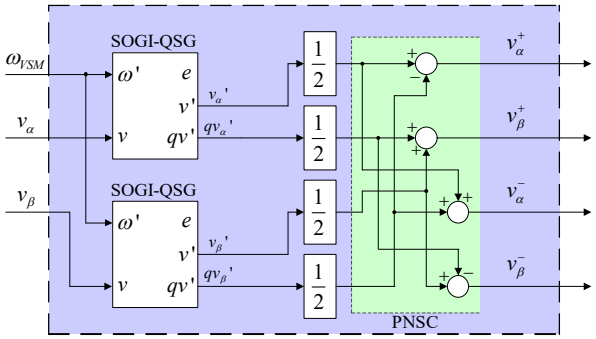

Fig. 2 Sequence separation of voltage measurements by DSOGI-QSG with frequency adaptivity provided by the VSM speed

- *Virtual Swing equation and electrical model of CCVSM*

The structure of the virtual swing equation used for inertia emulation and power-balance-based synchronization in the CCVSM is the same as presented in [8], [20]. A block diagram of the implemented Inertia Model, given by a virtual swing equation, and the frequency droop (i.e. 'governor' function in Fig. 1) acting on the input power to the swing equation, is shown in Fig. 3. Thus, the VSM swing equation can be expressed as:

$$T_a \frac{d\omega_{VSM}}{dt} = p^* + k_\omega \left(\omega^*_{VSM} - \omega_{VSM}\right) - \bar{p}_o + k_d \left(\omega_{VSM} - \omega_{PLL}\right) \quad (2)$$

Here, p_o^* is the external power reference set-point and $\bar{p}_o$ is the average power flowing from the VSC into the grid as given by (1). Furthermore, k_ω is the droop gain acting on the difference between the frequency reference, ω^*_{VSM}, and the emulated speed ω_{VSM}, while k_d is the damping coefficient. The inertial damping is implemented by multiplying k_d with the difference between ω_{VSM} and a frequency estimate ω_{PLL} provided by a Phase Locked Loop (PLL). It should be noted that the PLL is operating on the positive sequence voltage component and is only used for estimating the frequency since the grid synchronization is provided by the virtual swing equation. Indeed, the emulated speed is defined by the integral of the power balance, and the phase angle of the positive sequence rotating reference frame

is given by the integral of the VSM speed. The only difference between (2) and the dynamic equation for the VSM speed in [8], [20] is that $\bar{p}_o$ from (1) is used instead of the instantaneous three phase power flow. Thus, any double frequency power oscillations resulting from unbalanced conditions will not influence the inertial dynamics of the VSM.

The Quasi-Stationary Electrical Model (QSEM) from [9] is used for emulating an SM stator impedance for the positive sequence control. Thus, the positive sequence current reference vector is calculated as:

$$\mathbf{i}_o^+ = \frac{\hat{v}_e - \mathbf{v}_o^+}{r_v^+ + j\omega_{VSM} l_v^+} \qquad (3)$$

In this equation, $\hat{v}_e$ is the internal positive sequence voltage amplitude of the VSM, and r_v^+, l_v^+ are the corresponding per unit virtual resistance and inductance. The positive sequence voltage component $\mathbf{v}_o^+$ is obtained from the DSOGI-QSG as shown in Fig. 2. Due to the filtering effect of the DSOGI-QSG, there is no need for additional filtering of the voltages as discussed in [18].

Finally, the amplitude of the internal positive sequence VSM voltage in (3) is calculated by a reactive power droop,

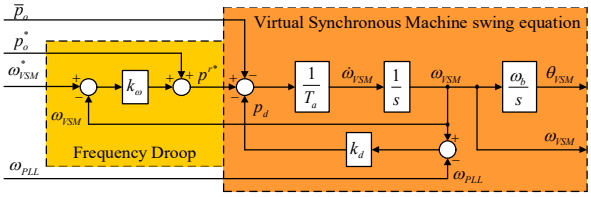

Fig. 3 Flexible selection of control objectives for the negative sequence current references

$$\hat{v}_e = \hat{v}_e^* + k_q\left(q^* - \bar{q}_o\right), \qquad (4)$$

where $\hat{v}_e^*$ is the internal reference for the positive sequence voltage amplitude. Furthermore, q^* is the reactive power reference, $\bar{q}_o$ is the average measured reactive power and k_q is the reactive power droop gain. In order to limit the reactive power flow during voltage sags, $\hat{v}_e$ is also limited to be within ± 0.05 pu of the actual measured positive sequence voltage, such that $0.95|\mathbf{v}_o^+| < \hat{v}_e < 1.05|\mathbf{v}_o^+|$.

- *Control of the negative sequence currents*

The power flow characteristics of the VSM and the impact on the local voltages during unbalanced conditions will be determined by the control of the negative sequence currents. In general, three different approaches can be pursued for controlling the negative sequence current: I) calculation of the negative sequence current references for shaping the active and reactive power flow characteristics, II) applying a negative sequence virtual impedance resulting in unbalanced currents equivalently to the steady-state response of a synchronous machine, or III) operation with a negative sequence voltage controller for eliminating unbalances in the locally measured voltages. These three approaches are explained in the following.

Calculation of negative sequence current references for shaping the power flow characteristics.

As discussed in [13], [14], the negative sequence current references can be calculated according to the desired power flow characteristics. This control approach is equivalent to corresponding conventional PLL-based strategies for active and reactive power flow control under unbalanced conditions [19]. Thus, three different objectives can be defined for controlling the negative sequence currents as I) obtaining balanced three-phase currents, II) eliminating oscillations in the active power flow, or III) eliminating oscillations in the reactive power flow.

The simplest control approach is to set the negative sequence current references to zero, which directly ensures balanced three phase currents. This strategy is referred to as Balanced Positive Sequence Current (BPSC).

If the objective is to eliminate the active power oscillations, the negative sequence current references can be calculated as a function of the voltage components and the positive sequence currents resulting from (3). As derived in [13], the negative sequence current references required for controlling constant active power (CAP) can be expressed as:

$$\mathbf{i}^{-*}_{CAP} = \begin{bmatrix} i_d^{-*} \\ i_q^{-*} \end{bmatrix}_{CAP} = \frac{-1}{(v_{o,d}^{+})^2 + (v_{o,q}^{+})^2} \cdot \begin{bmatrix} v_{o,d}^{+}v_{o,d}^{-} - v_{o,q}^{+}v_{o,q}^{-} & v_{o,q}^{+}v_{o,d}^{-} + v_{o,d}^{+}v_{o,q}^{-} \\ v_{o,q}^{+}v_{o,d}^{-} + v_{o,d}^{+}v_{o,q}^{-} & v_{o,q}^{+}v_{o,q}^{-} - v_{o,d}^{+}v_{o,d}^{-} \end{bmatrix} \begin{bmatrix} i_{o,d}^{+} \\ i_{o,q}^{+} \end{bmatrix} \quad (5)$$

A similar equation can be derived for ensuring constant reactive power (CRP) during unbalanced conditions [13]. The resulting current references can be expressed as:

$$\mathbf{i}^{-*}_{CRP} = -\mathbf{i}^{-*}_{CAP} \quad (6)$$

The negative sequence current references for the three defined cases can be easily generalized into a single control scheme as discussed in [13]. In the following, the case of balanced three phase currents is considered separately, while the cases of CAP or CRP are integrated into a single function, as shown in the upper part of

Fig. **4**.

Although these three strategies can be suitable for VSMs in grid-connected mode, they are mostly relevant for operation under strong grid conditions when the output currents of the VSM will not significantly influence the local voltage. Furthermore, these strategies are not necessarily directly applicable or suitable for operation in weak grids or in islanded mode with unbalanced loads.

Operation with negative sequence virtual impedance

The negative sequence currents can be defined by a negative sequence impedance in the same way as the positive sequence current references. Applying the same quasi-stationary equations for representing the negative sequence virtual impedance, the negative sequence current references can be expressed as:

$$\begin{aligned} i_d^{-*} &= \frac{\left(v_d^{-*} - v_d^-\right) r_v^- - \left(v_q^{-*} - v_q^-\right) \omega_{VSM} l_v^-}{\left(r_v^-\right)^2 + \left(\omega_{VSM} l_v^-\right)^2}, \\ i_q^{-*} &= \frac{\left(v_q^{-*} - v_q^-\right) r_v^- + \left(v_d^{-*} - v_d^-\right) \omega_{VSM} l_v^-}{\left(r_v^-\right)^2 + \left(\omega_{VSM} l_v^-\right)^2} \end{aligned} \quad (7)$$

Setting the negative sequence voltage references v_d^{-*} and v_q^{-*} to zero as shown in the middle of

Fig. **4**, results in a negative sequence current depending on the equivalent impedance, like in a regular synchronous machine. Indeed, the virtual resistance and inductance r_v^- and l_v^- for the negative sequence can be specified to different values than for the positive sequence.

However, this strategy would imply unbalanced currents in response to unbalanced voltages, depending on the virtual impedance and the equivalent grid impedance.

Operation with negative sequence voltage control

In case of operation in weak or islanded grids, the VSM could be capable of balancing the local voltages. Especially in islanded conditions, it could be required from the VSM to provide balanced voltages independently of any unbalances in the local load. Since the local load and/or grid impedance can change significantly, such local voltage balancing should be obtained by closed loop control. This can be implemented in several different ways, for instance by a controller directly providing the negative sequence voltage components as proposed in [17]. In this paper, an approach relying on the virtual impedance is preferred, to ensure that the current references can be easily limited in case of severe unbalanced conditions. Thus, two PI controllers are applied for providing the internal negative sequence voltage references to be applied in (7). The resulting control structure is also illustrated in the lower part of

Fig. **4**.

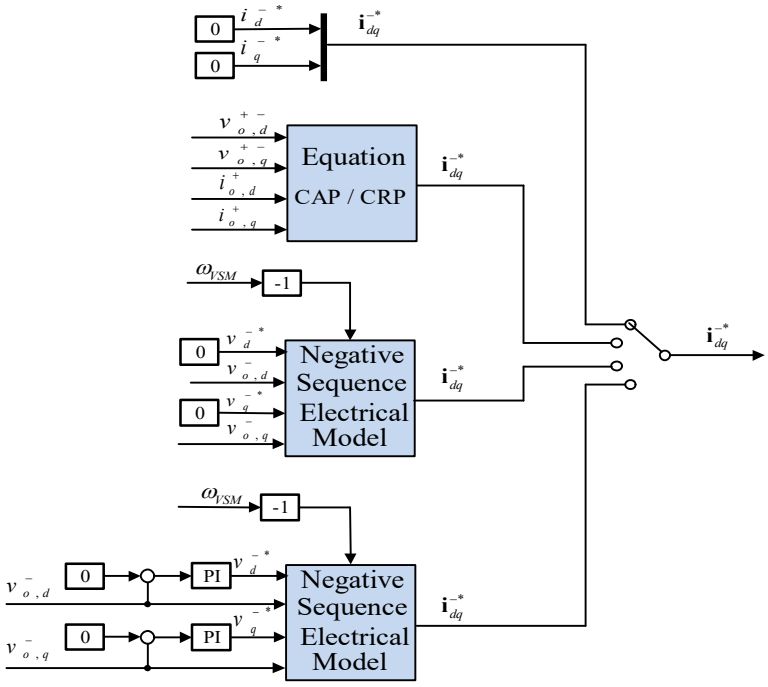

Fig. 4 Flexible selection of control objectives for the negative sequence current references

- Simulation Results

Time domain simulations in the Matlab/Simulink/ SimPowerSystems environment have been conducted to evaluate the performance and applicability of all the presented control strategies. A comprehensive set of results is presented in the following, to illustrate the operation in both grid-connected and islanded modes.

- *Case description*

Table 1 Parameters of the Investigated System Configuration

Parameter	**Value**	**Parameter**	**Value**
AC Voltage $V_{ll,g,n}$	400 V	Rated current	72 A
Rated angular frequency ω_n	2π50Hz	Primary filter inductance l_f , r_{lf}	0.08pu, 0.008pu
DC voltage V_{dcn}	686 V	Filter capacitance c_f	0.079 pu
Active damping k_{SOGI}, k_{AD}	√2 0.5 pu	Grid-side filter inductance l_g, r_g	0.2pu, 0.01pu
Current controller gains, kpc,kic	1.2 0.8	DSOGI-QSGs for sequence separation k_{SOGI}	√2
VSM Positive Seq. Impedance, r_v^+, l_v^+	0.01pu 0.2 pu	PLL PI controller, $k_{p,PLL}$, $k_{i,PLL}$	2, 70
VSM Negative Seq.Impedance, r_v^-, l_v^-	0.01 pu 0.2 pu	Negative sequence voltage control, $k_{p,NS}$, $k_{i,NS}$	0.1, 5
Virtual inertia Ta	10 s	VSM damping k_d	200 pu
Frequency droop k_ω	20 pu	Reactive power droop k_q	0 pu

The simulations are based on the system configuration from Fig. 1 with parameters given in Table 1. The performance of the investigated strategies is first studied in response to an unbalanced voltage sag. The inertial response is also verified for power and frequency transients under unbalanced grid voltages. Then, the transient resulting from islanding of a

small system that includes only the VSM and a local unbalanced resistive load is simulated. These results serve to illustrate which solutions can be suitable for islanded operation. The inertial response to changes in the load under unbalanced islanded operation is also evaluated.

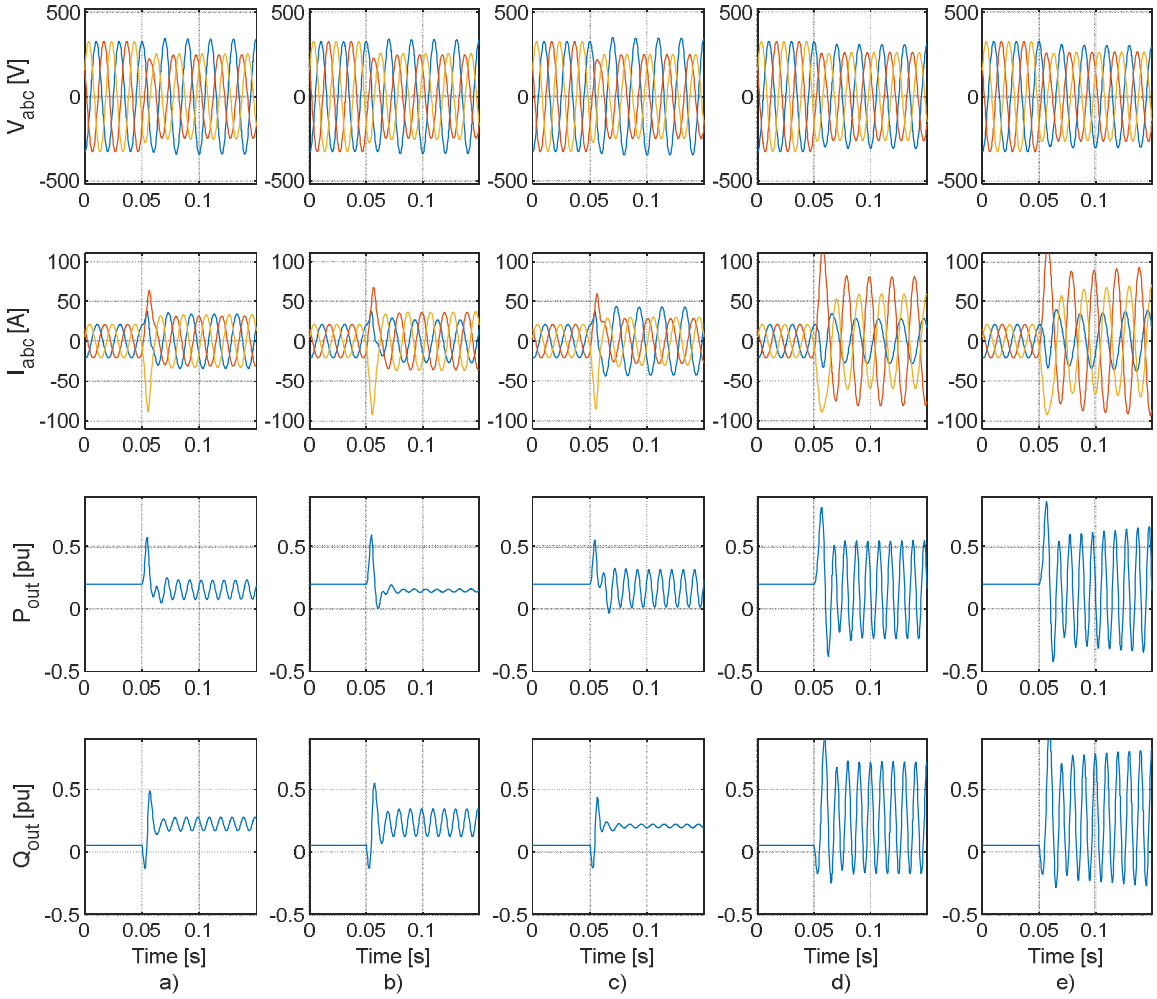

Fig. 5 Simulation results in grid-connected mode showing the transient response to an unbalanced voltage sag occurring at t=0.05, resulting in a grid voltage with 25% unbalance ($|V^-|/|V^+| = 0.2/0.8=0.25$). a) Balanced positive sequence currents b) Constant active power c) Constant reactive power, d) Negative sequence virtual impedance e) Negative sequence voltage controller.

- *Unbalanced operation in grid-connected mode*

As a first test, the CCVSM is exposed to an unbalanced voltage sag. The response in terms of currents and voltages as well as instantaneous powers is shown in Fig. , while a comparison of the average active power flow and the resulting virtual speed of the VSM is shown in Fig. 6. As shown in Fig. , an unbalanced voltage sag results in a transient drop of the active power and a significant change of reactive power due to the reduced amplitude of the positive sequence voltage.

The positive sequence voltage reference for the VSM is limited to a value close to 0.85 pu, as explained in section o to avoid excessive reactive power flow. The results in Fig. a) b) and c) also clearly show how the three cases with BPSC, CAP and CRP respond as expected. The case with a negative sequence virtual impedance results in higher and more unbalanced currents than the three first cases, and correspondingly higher oscillations in the active and reactive power flow. However, the unbalanced currents flowing through the grid-impedance is in this case helping to reduce the local unbalance in the voltage. When introducing the closed loop control for eliminating the voltage unbalance, the unbalance of the three phase currents is further increased as shown in Fig. e). A relatively slow response of the balancing controller can also be seen in the figure. The local voltage unbalance is finally eliminated by injecting negative sequence currents into the grid impedance but the maximum current amplitude among the phases depends on the voltage unbalance and the equivalent grid impedance. Therefore, this approach would not be generally applicable in strong grids with a low equivalent grid impedance.

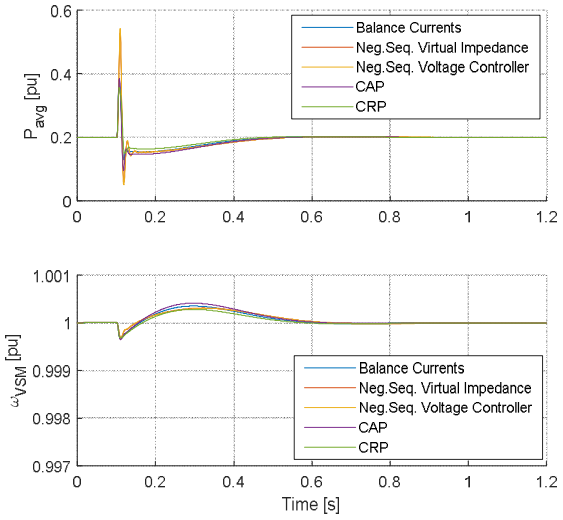

Fig. 6 Comparison of inertial response to an unbalanced voltage sag

As shown in Fig. 6 there are small differences in the initial transient of the average active power flow between the simulated cases, resulting from the different negative sequence currents, and this has a small influence on the VSM speed. After a transient determined by the inertia model, the power is controlled back to the reference value, and ω_{VSM} returns to the grid frequency of 1.0 pu for all the cases.

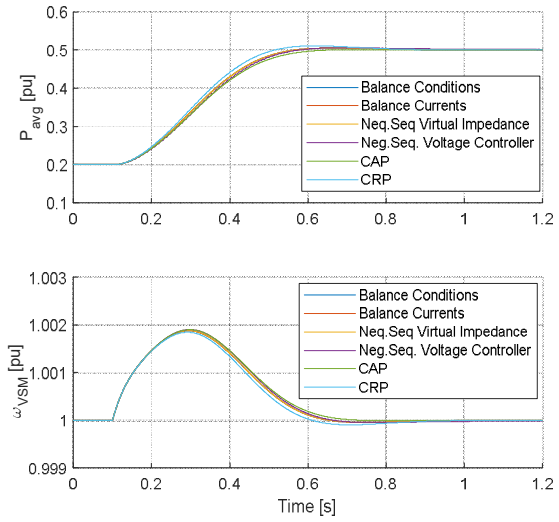

Fig. 7 Comparison of response to a step increase of 0.3 pu in the power reference at t= 0.1 s under unbalanced voltage conditions

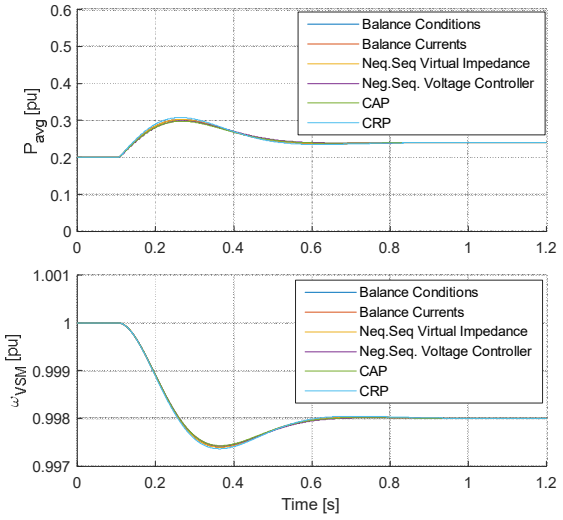

Fig. 8 Comparison of response to a step of −0.1 Hz (=0.002 pu) in the grid frequency at t = 0.1 s under unbalanced voltage conditions

To further evaluate the transient response of the evaluated control strategies, the CCVSM is exposed to a step in the active power reference of 0.3 pu and a step in the grid frequency of −0.002 pu, as shown in Fig. 7 and Fig. 8, respectively. As a point of reference, these figures also include a case with balanced grid voltages. The results show some minor differences in the average power during the transients, which results in corresponding differences in the VSM speed. However, these differences are very small, demonstrating that the influence from the negative sequence current control on the inertial dynamics of the VSM swing equation is limited when operating in grid-connected mode.

- *Transient response to islanding with local load*

The studied control strategies are exposed to an islanding transient by switching the breaker indicated in Fig. 1 from closed to open position. After disconnection from the grid, the converter is left to operate in islanded mode with an unbalanced local load with a total power demand of 0.5 pu at rated voltage. The unbalance is created by adding another load between phase *a* and *b* with half the impedance of the initial delta-connected load resistances. The response to the transient is shown in Fig. 9 for all the simulated cases. As clearly shown by the results in Fig. 9 a), b) and c), the cases where the negative sequence current references are directly specified to shape the power flow characteristics are not suitable for islanded operation. Indeed, all these three strategies are generating over-voltages in the phase with the lowest load. The case with balanced three phase currents is even increasing the amplitude of the local negative sequence voltage to 0.4 pu, while the case with constant active power is maintaining a negative sequence voltage in the range of 0.2 pu. The case with CRP is even resulting in an uncontrolled increase in the negative sequence voltage, and a significant increase in the total average load power due to the increased voltage, but without being able to eliminate the reactive power oscillations. Thus, even if operation with BPSC, CAP and CRP can be suitable for operation in strong grids, these control functions should be immediately disabled when transitioning into islanded mode.

The response to the islanding transient for the case with virtual impedance defining the negative sequence currents is shown in Fig. 9 d). In this case, the transient response to the islanding is smooth and fast, with the resulting negative sequence currents contributing to balancing of the load voltage. The resulting amplitude of the negative sequence voltage is then reduced to 0.04 pu. However, since the negative sequence currents are resulting from

the virtual impedance, they cannot fully compensate the unbalance caused by the load. Finally, Fig. 9 e) shows the results with the closed loop control for eliminating the voltage unbalance. As expected, this strategy is able to maintain balanced three phase voltages independently of the unbalance in the load resistance. Indeed, the negative sequence currents resulting from this control strategy in steady-state operation correspond to the currents that would result from feeding the load with a balanced three phase voltage source. It is also noted that both these strategies provide unbalanced currents to the local unbalanced load also before the islanding. Thus, the grid is (partially) relieved from supplying unbalanced currents to the unbalance local load.

A comparison of the response in average active power and virtual speed of the VSM after islanding with the unbalanced load is presented in Fig. 10. As shown in the figure, the cases with balanced currents or constant active power are not able to maintain the desired average voltage of the load, which is resulting in reduced power provided to the resistive load. Thus, the frequency droop control is also resulting in a higher steady-state frequency than when the load voltage is maintained close to the rated value. The case with constant reactive power is instead resulting in a significant increase of the load power and a corresponding reduction in the steady state frequency. This further confirms how this control strategy is unsuitable for operation in islanded mode.

The case with negative sequence voltage control results in the expected load power of 0.5 pu and a corresponding droop effect in the frequency. The results for the case with only a negative sequence virtual impedance are also very close to the case with closed loop balancing of the voltage.

The general trend of the results in Fig. 10 is confirmed by the results in Fig. 11, which shows the response to a change of the load resistance under unbalanced islanded operation. In this figure, the cases with constant active or reactive power are not included since the operation with these control strategies is clearly unacceptable. A case with the initial balanced load is also included as a point of reference. The figure shows how the case with balanced three phase currents results in a total average load close to the case with balanced loads, since no additional current is provided to the phases with increased load. As in Fig. 10, the load power and the steady-state frequency of the case with negative sequence virtual impedance is almost identical to the case with closed loop control of the voltage. Indeed, these two

strategies are the only cases providing reasonable performance for operation in islanded mode with unbalanced loads.

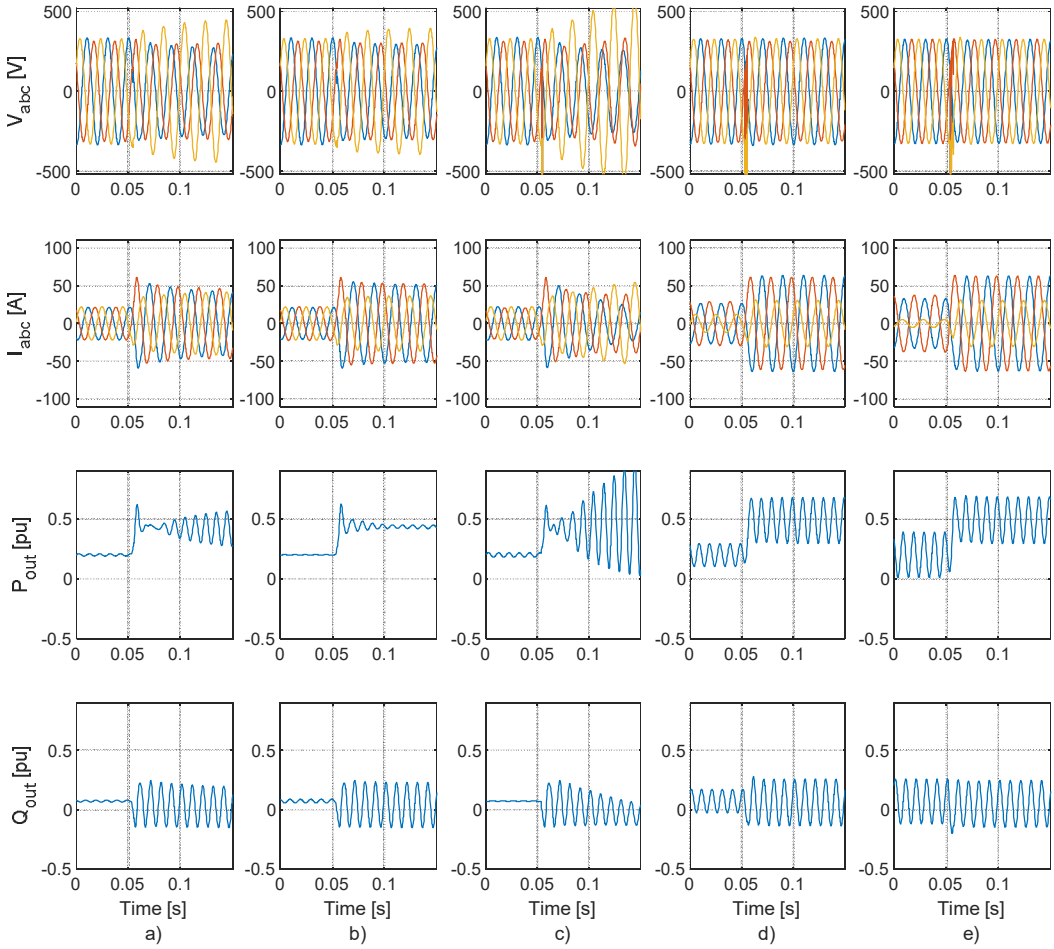

Fig. 9 Simulation results showing the transient response to sudden islanding with an unbalanced load at t=0.05 s a) Balanced currents b) Constant active power, c) Constant reactive power, d) Negative sequence virtual impedance c) Negative sequence voltage controller

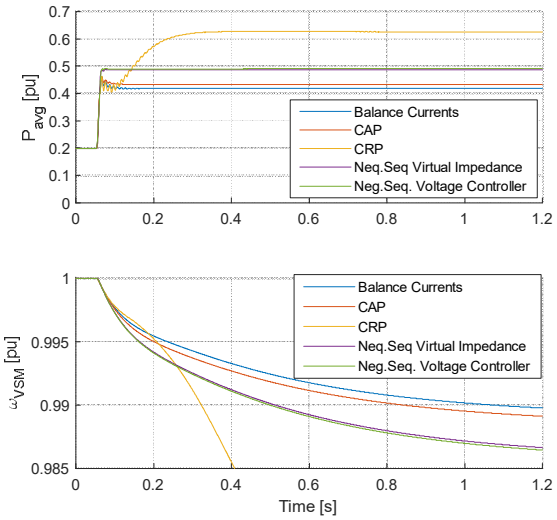

Fig. 10 Comparison of response to the transition from grid-connected operation to islanded mode with an unbalanced load

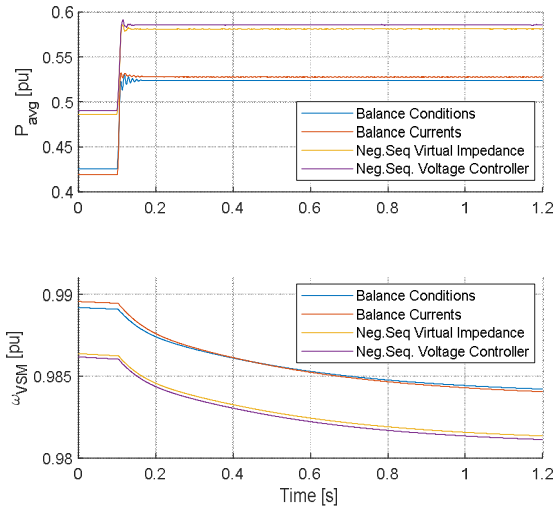

Fig. 11 Response to a step increase of the load by 0.1 pu under unbalanced conditions

- Conclusions

This paper has evaluated the options for operating a current controlled Virtual Synchronous Machine (CCVSM) under unbalanced conditions, and the resulting performance in both grid-connected and islanded modes. Five different strategies for controlling the negative sequence currents are identified, and their performance is assessed by time domain

simulations. The simulation results clearly show how the control strategies based on calculation of the negative sequence current references for shaping the power flow characteristics are only suitable for grid-connected operation. Thus, if any of these strategies are preferred for grid-connected operation, they should be immediately disabled in case of transitioning to islanded mode. Operation with a negative sequence virtual impedance results in a similar steady-state response to unbalances as would result from a synchronous machine and can ensure stable operation in both grid-connected and islanded operation. However, this approach will not fulfil any specific objectives of shaping the power flow characteristics or balancing of the voltage. Closed loop control of the negative sequence components for balancing the local voltages is suitable for islanded operation with unbalanced local loads. Although this approach also can be utilized for grid-connected operation in weak grids with high equivalent impedance, the controllers will saturate if the system is operated in a strong grid. Thus, there is no universal control strategy that will be suitable for all types of unbalanced operation. Instead, a flexible mechanism for choosing between different objectives depending on the operating conditions, as presented in this paper, can be useful. Further analysis should consider how to adapt the operation of the VSM to any grid-connected or islanded conditions by automatically selecting the proper objective for control of the negative sequence currents.

References

[1] H. Alrajhi Alsiraji, R. El-Shatshat, “Comprehensive assessment of virtual synchronous machine based voltage source converter controllers,” in IET Generation, Transmission, Distribution, vol. 11, no. 7, pp. 1762–1769, may 2017

[2] H. Bevrani, T. Ise, Y. Miura, “Virtual synchronous generators: A survey and new perspectives,” in *International Journal of Electric Power and Energy Systems*, vol. 54, pp. 244–254, January 2014

[3] S. D'Arco, J. A. Suul, "Virtual Synchronous Machines – Classification of Implementations and Analysis of Equivalence to Droop Controllers for Microgrids," in *Proceedings of IEEE PES PowerTech 2013*, Grenoble, France, 16-20 June 2013, 7 pp.

[4] H.-P. Beck, R. Hesse, "Virtual Synchronous Machine," in *Proc. of the 9th Int. Conf. on Electrical Power Quality and Utilisation*, Barcelona, Spain, 9-11 Oct. 2007, 6 pp.

[5] Q.-C. Zhong and G. Weiss, “Synchronverters: Inverters that mimic synchronous generators,” *IEEE Transactions on Industrial Electronics,* Vol. 58, No. 4, pp. 1259–1267, April 2011

[6] K. Sakimoto, Y. Miura, T. Ise, "Stabilization of a power system with a distributed generator by a virtual synchronous generator function," in *Proceedings of the 8th Int. Conf. on Power Electron. – ECCE Asia*, Jeju, Korea, 30 May- 3 Jun. 2011, 8 pp.

[7] P. Rodriguez, I. Candela, A. Luna, "Control of PV Generation Systems using the Synchronous Power Controller," in *Proceedings. of the 2013 IEEE Energy Conversion Congress and Expo.*, ECCE 2013, Denver, Colorado, USA, 15-19 Sept. 2013, pp. 993-998

[8] S. D'Arco, J. A. Suul, O. B. Fosso, "Small-signal modelling and parametric sensitivity of a Virtual Synchronous Machine in islanded operation," in *International Journal of Electric Power and Energy Systems*, Vol. 72, pp. 3-15, November 2015

[9] O. Mo, S. D'Arco, J. A. Suul, "Evaluation of Virtual Synchronous Machines with Dynamic or Quasi-stationary Machine Models," in *IEEE Transactions on Industrial Electronics*, Vol. 64, No. 7, pp. 5952-5962, July 2017

[10] M. Chen, X. Xiao, Ch. Y, Sh. Tao, "Flexible Power Control of Virtual Synchronous Generators Under Unbalanced Grid Voltage Conditions," in *Proceedings of the 2017 IEEE Energy Conversion Congress and Exposition*, ECCE 2017, Cincinnati, Ohio, USA, 1-5 October 2017, pp 2881-2888

[11] F. Li, G. Liu, K. Zhu, W. Wang, "An Improved Control Strategy of Virtual Synchronous Generator under Unbalanced Conditions", in *Proceedings of the 2018 IEEE 4th Southern Power Electronics Conference*, SPEC 2018, Singapore, 10-13 December 2018, 6 pp.

[12] W. Zhang, J. Rocabert, J. I. Candela, P. Rodriguez, "Synchronous power control of grid-connected power converters under asymmetrical grid fault," in *Energies*, Vol. 10, No. 7, 2017, 21 pp.

[13] T. Zheng, L. Chen, Y. Guo, Sh. Mei, "Comprehensive control strategy of virtual synchronous generator under unbalanced voltage conditions", *IET Generation, Transmission & Distribution, Vol. 12, No. 7, pp. 1621-1630, April 2018*

[14] T. Zheng, L. Chen, Y. Guo, S. Mei, "Flexible unbalanced control with peak current limitation for virtual synchronous generator under voltage sags" in Journal of Modern Power Systems and Clean Energy, Vol. 6, No. 1, pp. 61-72, January 2018

[15] H. Miao, F. Mei, Y. Yang, H. Chen, J. Zheng, "A Comprehensive VSM Control Strategy Designed for Unbalanced Grids", *Energies*, Vol. 12, No. 6, 2019, 17 pp.

[16] X. Zheng, C. Wang, S. Pang, "Injecting positive-sequence current virtual synchronous generator control under unbalanced grid," in *IET Ren, Power Gen.*, Vol. 13, No. 1, pp. 165-170, Jan. 2019

[17] X. Wu, J. Mei, B. Wang, D. Liang, Ch. Qin, J. Zong, "Unbalanced Loads Control Strategy for Virtual Synchronous Generator in Passive Network," in *Proc. of the 2019 IEEE Innovative Smart Grid Technologies Conference – Asia*, ISGT-Asia 2019, Chengdu, China, 21-24 May 2019, pp. 2063-2068

[18] P. Rodriguez, A. Luna, R. S. Muñoz-Aguilar, I. Etxeberria-Otadui, R. Teodorescu, F. Blaabjerg, "A Stationary Reference Frame Grid Synchronization System for Three-Phase Grid-Connected Power Converters Under Adverse Grid Conditions", *IEEE Transactions on Power Electronics*, Vol. 27, No. 1, pp. 99-112, January 2012

[19] P. Rodriguez A.V. Timbus, R. Teodorescu, M. Liserre, F. Blaabjerg, "Flexible Active Power Control of Distributed Power Generation Systems During Grid Faults", IEEE Transactions on Industrial Electronics, Vol. 54, No. 5, pp.2583-2592, October 2007

[20] S. D'Arco, J. A. Suul, O. B. Fosso, "Small-Signal Modeling and Parametric Sensitivity of a Virtual Synchronous Machine," in *Proceedings of the 18th Power Systems Computation Conference*, PSCC 2014, Wrocław, Poland, 18-22 August 2014, 9 pp.